

Probabilistic Assessment of Risk and Robustness of Large Span Timber Roofs

Ph.D. Dissertation
Simona Miraglia

Corso di Dottorato di Ricerca in
Ingegneria delle Costruzioni,
XXIV ciclo
Dipartimento di Ingegneria Strutturale
Università di Napoli "Federico II"
Via Claudio, 21 - 80125 Napoli
e-mail: simona.miraglia@gmail.com

Tutor: Coordinatore del corso:
Prof. L. Rosati Prof. L. Rosati

November, 2011

*"The most important questions of life are, for the most part,
really only problems of probability."*

Pierre Simon de Laplace

Acknowledgements

The develop of this dissertation could not have been possible without the guidance of my advisor Professor Luciano Rosati, who supported me and encouraged me throughout my academic program.

A special thank goes to Dr. Salvatore Sessa and Dr. Francesco Marmo, who advised me through the dissertation writing process, being always kindly helpful. They both support me a lot and mostly Salvatore had always to calm my fits of nerves.

I am also thankful to my colleagues Sergio Guarino and Severino Orlando for the nice office-time spent together.

This dissertation could also not have been written without the guidance of Prof. Daniel Straub, who was my host during my stay as visiting scientist at *Fachgebiet Risikoanalyse und Zuverlässigkeit* at *Technische Universität München*. He invested a lot of time teaching me as much he could do and encouraging me to do my best, always. I am grateful also to my colleague Philipp Dietsch from the *Lehrstuhl für Holzbau und Baukonstruktion* for advising me and working with me on this project and to Dr. Jochen Köhler of ETH-Zürich and Prof. John Sørensen of Aalborg University for the useful

advise.

I will always remember the nice time spent with my colleagues and friends within the *ERA Group* and the *Lehrstuhl für Massivbau* in München. Mostly, I am grateful to Dr. Giulio Cottone, Patty Papakosta, Johannes Fischer, Qamar Mahboob, Katrin Runtemund, Dr. Habil. Karl Breitung and the marvelous factotum of Lehrstuhl für Massivbau Frau Anneliese Spitzauer. Without Anlis I would have been totally lost. I am also thankful to my friend and flatmate Monika Shah for the nice time spent together. I will always remember all of them with love.

Finally, I am grateful to my family. They all supported my education and encouraged me.

Napoli, November 2011

Simona Miraglia

Contents

Introduction	1
1 Robustness and Risk Assessment	5
1.1 Timber Structural Problem	5
1.2 Cases of Structural Failures	7
1.2.1 Failures in Timber Structures	11
1.3 State of the art about timber analysis	12
1.4 Risk assessment approach advantages	15
1.5 The Structural Robustness	17
1.5.1 Robustness measure overview	23
2 Structural Reliability	31
2.1 The Structural Response	31
2.2 Deterministic Measure of Structural Reliability	33
2.3 Probabilistic Measure of Structural Reliability	34
2.4 Monte Carlo Direct Sampling	39
2.5 First Order Reliability Method (FORM)	41

CONTENTS

2.5.1	Transformation into the Standard Normal Space . . .	44
2.5.2	The Design Point: The H-L-R-F Algorithm	48
2.6	The Probability of Failure of a System of Components . . .	52
2.6.1	The Ditlevsen bounds	55
3	Structural Model	59
3.1	Large-Span Timber Roof Description	59
3.2	Timber deterministic design rules	66
3.3	Failure modes for a purlin	69
3.4	Failure modes for the beam	74
3.4.1	Limit state function for bending failure of the primary beam	75
3.4.2	Limit state function for tension perpendicular to the grain failure of the primary beam	76
3.4.3	Limit state function for shear failure of the primary beam	77
3.4.4	Limit state function for combined shear and tension perpendicular to the grain failure of the primary beam	79
3.5	Failure modes for large span roofs: system behavior	81
3.6	Quantifying Risk and Robustness of the timber roof system	84
3.6.1	Definition and metric of Risk	85
3.6.2	Definition of a probability based Robustness criterion	87
4	Timber Statistics	89
4.1	Timber Specific Weight/Density	90
4.2	Bending strength probability distribution and Isaksson Model	92

CONTENTS

4.2.1	Isaksson Model of bending strength	94
4.3	Strength perpendicular to the grain f_{t90} and f_{c90} : probability distribution	97
4.4	Compression f_{c0} and tensile stress f_{t0} strength in the direction of the grain: probability distribution	99
4.5	Tangential Strength: probability distribution	100
4.6	Extension of the Isaksson model for a joint spatial variability model of timber strength properties	103
4.7	Systematic Weaknesses	107
5	Load Statistics	109
5.1	Permanent Load Distribution	110
5.2	Snow Load Distribution	110
5.3	Shape Factor Distribution	116
6	Application	121
6.1	Purlin's analysis: probability integral for a simplified case .	122
6.2	Purlin's analysis (FORM, MCS)	126
6.2.1	First Order Reliability Method formulation for the purlin	126
6.2.2	Monte Carlo sampling for the analysis of the purlins	132
6.3	Primary beams analysis (FORM, MCS)	148
6.3.1	First Order Reliability Method formulation for the primary beam	148
6.3.2	Monte Carlo sampling for the analysis of the primary beams	165

CONTENTS

7	Structural Interaction	171
7.1	Numerical results for the roof system (MCS)	171
8	Conclusions	193
	Bibliography	196
A	The Fault Tree of the Failure Event	205
B	Computation of Ditlevsen bounds for a series system	209

List of Tables

1.1	Ratio between Young Modulus and Resistance.	6
1.2	Incidence of errors in building process by phase.	9
1.3	Causes of Error.	10
2.1	Coefficient of the polynomial approximation.	48
3.1	Dimensions and layout of the secondary system.	60
3.2	Characteristic values of the strength according to DIN338 [9]. . .	62
3.3	Dimensions of the primary beams.	64
3.4	Characteristic values of the strength for glulam from DIN14080 [11].	65
4.1	Parameters of the Normal distributions of the specific weight for the used timber class.	91
4.2	Parameters of the LogNormal distributions of the bending strength for the used timber class.	97
4.3	JCSS Correlation Matrix.	103
4.4	Timber material statistics for C24.	107
4.5	Timber material statistics for GL24c.	107

LIST OF TABLES

5.1	Parameters of the load distributions used.	120
6.1	Probability of Failure for the middle span of a simply supported purlin.	126
6.2	Probability of failure of a critical section j , $Pr(F_j(1yr) \bar{D})$ and corresponding reliability index β_j	130
6.3	Probability of failure of a critical section j , $Pr(F_j(1yr) \bar{D})$ and corresponding design point x^*	131
6.4	Probability of failure of one purlin.	131
6.5	Probability of failure of secondary system, $Pr(F_j(1yr) \bar{D})$ and corresponding Ditlevsen bounds.	132
6.6	Probability of biaxial bending failure of secondary system for $k_m = 1$	133
6.7	Probability of biaxial bending failure of secondary system for $k_m = 0.7$	134
6.8	$E[A_F F, \bar{D}]$ of secondary system for $k_m = 1$	134
6.9	Probability of biaxial bending failure of secondary system for $k_m = 1$ and with systematic weaknesses with rate $p = 1\%, 10\%, 30\%$	139
6.10	$E[A_F F, D]$ of secondary system for $k_m = 1$	140
6.11	$Pr(F)$ for the secondary system configurations for $Pr(D) = 1\%, 10\%$ and weakening rate of 30%	144
6.12	$Pr(A_F < 0.15 \cdot A_{roof} F)$ for the secondary system configurations for $Pr(D) = 1\%, 10\%$ and weakening rate of 30%	146

LIST OF TABLES

6.13 Risk as $E[A_F]$ for the secondary system configurations for $Pr(D) = 1\%, 10\%$ and weakening rate of 30%.	147
6.14 Risk $E[A_F]$ for the secondary system configurations for $Pr(D) = 1\%, 10\%$ and weakening rate of 30%.	147
6.15 Probability of failure of the most loaded section of the primary beam, $Pr(F_j(1yr))$ and corresponding reliability index β_j with the simply supported secondary elements.	152
6.16 Importance coefficients and values of the r.v. at design point x^* for the most loaded section of the primary beam with the simply supported secondary elements.	153
6.17 Probability of failure of the most loaded section of the primary beam, $Pr(F_j(1yr))$ and corresponding reliability index β_j with the continuous secondary elements.	154
6.18 Importance coefficients and values of the r.v at design point x^* for the most loaded section of the primary beam with the continuous secondary elements.	154
6.19 Probability of failure of the most loaded section of the primary beam, $Pr(F_j(1yr))$ and corresponding reliability index β_j with the lap-jointed secondary elements.	154
6.20 Importance coefficients and values of the r.v. at design point x^* for the most loaded section of the primary beam with the lap-jointed secondary elements.	155
6.21 Probability of bending failure of the most loaded primary beam respect to the three configurations, $Pr(F(1yr))$ and $Pr(F(50yr))$	155

LIST OF TABLES

6.22	Probability of bending failure of the system of six primary beams respect to the three configurations, $Pr(F(1yr))$ and $Pr(F(50yr))$	156
6.23	Probability of shear failure of the most loaded section of the primary beam, $Pr(F_j(1yr))$ and corresponding reliability index β_j with the simply supported secondary elements. . . .	158
6.24	Importance coefficients and values of the r.v. at design point x^* for the most loaded section of the primary beam with the simply supported secondary elements.	158
6.25	Probability of shear failure of the most loaded section of the primary beam, $Pr(F_j(1yr))$ and corresponding reliability index β_j with the continuous secondary elements.	159
6.26	Importance coefficients and values of the r.v. at design point x^* for the most loaded section of the primary beam with the continuous secondary elements.	159
6.27	Probability of shear failure of the most loaded section of the primary beam, $Pr(F_j(1yr))$ and corresponding reliability index β_j with the lap-jointed secondary elements.	159
6.28	Importance coefficients and values of the r.v. at design point x^* for the most loaded section of the primary beam with the lap-jointed secondary elements.	160
6.29	Probability of shear failure of the most loaded primary beam respect to the three configurations, $Pr(F(1yr))$ and $Pr(F(50yr))$.160	

LIST OF TABLES

6.30	Probability of shear failure of the system of six primary beams respect to the three configurations, $Pr(F(1yr))$ and $Pr(F(50yr))$	160
6.31	Probability of tension perp. failure of the most loaded section of the primary beam, $Pr(F_j(1yr))$ and corresponding reliability index β_j with the simply supported secondary elements.	162
6.32	Importance coefficients and values of the r.v. at design point x^* for the most loaded section of the primary beam with the simply supported secondary elements.	163
6.33	Probability of tension perp. failure of the most loaded section of the primary beam, $Pr(F_j(1yr))$ and corresponding reliability index β_j with the continuous secondary elements.	163
6.34	Importance coefficients and values of the r.v. at design point x^* for the most loaded section of the primary beam with the continuous secondary elements.	163
6.35	Probability of tension perp. failure of the most loaded section of the primary beam, $Pr(F_j(1yr))$ and corresponding reliability index β_j with the lap-jointed secondary elements.	164
6.36	Importance coefficients and values of the r.v. at design point x^* for the most loaded section of the primary beam with the lap-jointed secondary elements.	164
6.37	Probability of tension perp. failure of the of the system of six primary beams respect to the three configurations, $Pr(F(1yr))$ and $Pr(F(50yr))$	165

LIST OF TABLES

6.38	Probability of failure of the most loaded primary beam respect to the choosen limit state.	166
6.39	Probability of failure of the most loaded primary beam respect to bending failure when considering the splitting of section due to tension perp.	167
6.40	Probability of failure of the system of six primary beams respect to the choosen limit state.	169
6.41	Probability of bending failure for the system of six primary beams upon tension perp. failure.	169
7.1	Probability of Bending Failure for the primary beams system.	174
7.2	Probability of Shear Failure for the primary beams system.	175
7.3	Probability of Tension perp. Failure for the primary beams system.	175
7.4	Probability of Failure for combination of Shear and Tension Perp. for the primary beams system.	176
7.5	Probability of bending Failure for the purlin system.	176
7.6	Statistics of the percentage of area failed for the secondary system.	185
7.7	Statistics of the percentage of area failed for the primary system.	186
7.8	Statistics of the percentage of area failed for the roof system.	186
7.9	Risk for the secondary system, primary system and of the timber roof.	189

LIST OF TABLES

7.10 Robustness for the secondary system, primary system and
the timber roof. 189

7.11 Reliability, Risk and Robustness for the timber roof. 190

List of Figures

1.1	Wood cross section.	14
2.1	Time dependent reliability problem.	35
2.2	Failure Domain Ω_f	37
2.3	Transformation to the standard normal space for a single random variable (A. Der Kiureghian 2005).	44
2.4	l.s.f and β point in the standard normal space when two dimensions are considered (Straub 2010).	49
2.5	Polyhedral and convex safe set (O. Ditlevsen 2007).	55
3.1	Illustration of a typical large-span timber roof system (Dietsch and Winter 2010).	61
3.2	Geometry of the roof (Dietsch and Winter 2010).	61
3.3	Three investigated purlin configurations.	62
3.4	Pitched cambered glulam beam with a mechanically fixed apex.	64
3.5	Rectangular cross section subjected to biaxial bending.	71
3.6	A possible failure scenario for the three configurations.	73
3.7	Load scheme for the primary beam.	74

LIST OF FIGURES

3.8	Distribution of the bending stresses in the curved beam.	76
3.9	Tension perpendicular to the grain.	77
3.10	Effective section due to shrinkage cracks.	79
3.11	SIA-265 LSF for combined shear and tension perpendicular to the grain.	80
3.12	Consequences of beam bending failure on simply supported purlins.	82
3.13	Consequences of beam bending failure on continuous and lap- jointed purlins.	83
3.14	Cracks due to tension perpendicular to the grain in a glulam beam (Holzforschung, MPA-BAU TUM).	84
3.15	Consequences of beam displacement on continuous and lap-jointed purlins.	85
3.16	Flow chart of the failure analysis.	86
4.1	Plot of the p.d.f. and CDF of the specific weight γ	91
4.2	Variability of strength along a timber element.	93
4.3	Lengthwise variation of bending strength for Isaksson model (PMC- JCSS 2006).	95
4.4	Weibull distribution of the tension strength perpendicular to the grain for timber GL24c.	98
4.5	Compression strength perpendicular to the grain Normal proba- bility distribution.	99
4.6	Tension strength parallel to the grain lognormal probability dis- tribution.	101

LIST OF FIGURES

4.7	Compression strength parallel to the grain normal probability distribution.	102
4.8	Shear strength Lognormal probability distribution.	102
5.1	Plot of the p.d.f. and CDF for permanent load P	111
5.2	Recordings of meteorological variables and ground snow cover from November 2005 to March 2006 at the DWD met office station in Bad Reichenhall (DE) (U. Strasser 2008).	111
5.3	Spike train for the snow load on the ground.	113
5.4	Plot of the p.d.f. and CDF for snow load on the ground Q	116
5.5	Windward and lee side on a double pitched roof.	118
5.6	Mean and standard deviation of the shape factor for lee side.	118
5.7	Mean and standard deviation of the shape factor for windward side.	119
5.8	Plot of the pdf and CDF of Shape Factor C	120
6.1	Probability density function of M_R and M_S	125
6.2	Mean and Standard Deviation respect to time for $k_m = 1$	135
6.3	Mean and Standard Deviation respect to time for $k_m = 0.7$	135
6.4	Histogram of A_F given (F, \overline{D}) for $k_m = 1$	136
6.5	Histogram of A_F given (F, \overline{D}) for $k_m = 0.7$	136
6.6	CDF of A_F given (F, \overline{D}) for $k_m = 1$	137
6.7	CDF of A_F given (F, \overline{D}) for $k_m = 0.7$	138
6.8	Histogram of A_F given F, D for $k_m = 1$ and $p = 1\%$	140
6.9	Histogram of A_F given F, D for $k_m = 1$ and $p = 10\%$	140
6.10	Histogram of A_F given F, D for $k_m = 1$ and $p = 30\%$	141
6.11	CDF of A_F given (F, D) for $k_m = 1$ and $p = 1\%$	141

LIST OF FIGURES

6.12	CDF of A_F given (F, D) for $k_m = 1$ and $p = 10\%$	142
6.13	CDF of A_F given (F, D) for $k_m = 1$ and $p = 30\%$	142
6.14	CDF of A_F for $k_m = 1$ and $Pr(D) = 0.01$	145
6.15	CDF of A_F for $k_m = 1$ and $Pr(D) = 0.10$	145
6.16	Roof system configurations.	153
7.1	Mean and Standard deviation of the failed area for the simply supported purlins with redistribution 10%- 20%- 30%- 40%.	177
7.2	Mean and Standard deviation of the failed area for the beams with simply supp. purlins with redistribution 10-20-30-40%.	178
7.3	Mean and Standard deviation of the failed area for the continuous purlins.	178
7.4	Mean and Standard deviation of the failed area for the beams with continuous purlins.	179
7.5	Mean and Standard deviation of the failed area for the lap-jointed purlins.	179
7.6	Mean and Standard deviation of the failed area for the beams with lap-jointed purlins.	180
7.7	Histograms of the failed area for the simply supported purlins with redistribution 10-20-30-40%.	181
7.8	Histograms of the failed area for the beams with simply sup. purlins with redistribution 10-20-30-40%.	181
7.9	Histograms of the failed area for the continuous purlins.	182
7.10	Histograms of the failed area for the lap-jointed purlins.	182
7.11	CDF of the failed area for the simply supported purlins.	183

LIST OF FIGURES

7.12 CDF of the failed area for beams with simply supported purlins and redistribution 10-20-30-40%.	184
7.13 CDF of the failed area for the beams and continuous purlins. . .	184
7.14 CDF of the failed area for the beams and lap-jointed purlins. . .	185
7.15 CDF of the failed area for the roof system with simply supported purlins with redistribution 10%- 20%- 30%- 40%.	188
7.16 CDF of the failed area for the roof system with simply supported continuous and lap-jointed purlins with redistribution 40%. . . .	188
A.1 Event-Tree of Failure Event.	206

Introduction

During the past ten years, several collapses of wide span roofs occurred in Northern Europe under high snow loads, in some cases leading to fatalities [16]. Many of these roofs were composed by either solid or glulam timber elements. These failures can be attributed to design errors, lack of elements' quality or bad execution. In addition, failure can be caused by lack of maintenance or by unforeseen events that lead to a lower capacity (damage) or higher loads than expected. The failures are most likely to originate from errors made during the design phase and execution, while failures due to material deficiencies or maintenance are relatively uncommon, which was also found in an extensive study by Ellingwood [12].

In this context, attempts have been made to evaluate the robustness of wide span timber roofs [4, 7, 26]. These studies were performed within the framework of the COST action on performance and robustness of structures.

This study proposes an alternative approach: it aims to use a fully probabilistic assessment to investigate the behavior of large span timber roofs, with different purlin configurations, respect to reliability, robustness and

risk. The reason of this philosophy consists in the ambiguous definitions of structural robustness, compartmentalization and redundancy.

Generally, robustness of a structure is understood as the insensitivity to local failure and the avoidance of progressive collapse. This is a property of the structure itself, not dependent on possible causes of initial local failure [36]. Many authors [21, 37] relate robustness to structural redundancy, which requires static indeterminacy and the avoidance of progressive collapse, and [1] use the ratio between direct and indirect expected damage as a measure of robustness. This definition also includes the consequences of failure, and it requires direct or indirect computation of the risk.

In **Chapter 1** a review about the causes of structural collapse and the state of art concerning different approaches to measures structural robustness are presented, while **Chapter 2** introduces the theory of structural reliability methods used for the probabilistic assessment of risk and robustness of a large span timber roof.

The investigated structure is a simple but typical timber roof system. Similar roof structures are widely used for large-span roofs of sport-arenas, industrial factories or farm storage buildings. The behavior of the timber roof is investigated with respect to three different secondary system structural configurations for the secondary system (simply-supported, continuous and lap-jointed purlins). These configurations were also subject to a previous deterministic analysis of the system of primary elements (beams) and secondary elements (purlins) carried out by Dietsch et al. in [7].

The risk and robustness assessment of the three roof systems is performed by probabilistically considering all possible failure scenarios and all possible

combination of structural interaction among the components of both primary (beams) and secondary system (purlins). In **Chapter 3** the assumed failure mechanisms and the interaction among the components of the roof system are extensively described. In addition, referring to EC5 damage limit requirement, a probabilistic based measure for structural robustness is proposed. On the basis of deterministic failure mechanisms for timber elements, a fully probabilistic model of both loads and strength properties is used. The statistics of timber properties and loads are presented in **Chapter 4** and **Chapter 5** respectively.

The assessment of the secondary system accounts also for the possibility of systematic errors (which are modeled by weakened sections that occur randomly in the secondary structure), in order to investigate and compare the behavior of a system with compartmentalization (simply supported purlins) and a system with redundancy (continuous and lap-jointed purlins).

In **Chapter 6**, the probabilistic assessment of the secondary system (purlins) and primary system (beams) is done by means of Monte Carlo Simulations and First Order Reliability Method. In **Chapter 7** the assessment of the full roof system considering the structural interaction is presented. This interaction is modeled with an event tree that describes the consequences of the failure event according to different conditions.

An important result is the computation of the full distribution of the consequences, in terms of roof area failed, given a failure of the system. Indeed, this distribution can be interpreted as a measure of robustness.

Chapter 1

Robustness and Risk Assessment

During the past twenty years, several collapses of wide span roofs occurred in Northern Europe during the winter season under high snow loads, in some cases leading to fatalities [16]. Many of these roofs were built with timber elements (solid or glulam timber). These failures can be attributed to different reasons. Here a review of structural failures and the state of art about the structural robustness evaluation is described.

1.1 Timber Structural Problem

In the last decades the interest in a wider application of timber in structural design strongly increased. The main reason is the higher interest in the use

of sustainable and environmental friendly materials and in the wide field of architectural possibility that this flexible and charming material gives to designers.

Indeed, timber material is biologically produced in the growing tree and therefore biodegradable. For this reason, it is a high quality fiber composite material naturally designed to carry the loads acting on the tree (vertical load and wind) and to create maximum strength in the stressed directions [41].

Timber is also a very light and efficient material compared to the other structural material (see table 1.1).

Material	Young Modulus/Resistance
Concrete (C25-30, $f_{ck} \cong 25MPa$)	$\cong 1250$
Steel (Fe430, $f_t = 430MPa$)	$\cong 480$
Glulam ($BS11 \div BS18$)	$\cong 470$
Alluminium (alloy 7020, $f_t \cong 355MPa$)	$\cong 200$

Table 1.1: Ratio between Young Modulus and Resistance.

In addition, the production process of timber is highly optimized in order to have a cheap production with the smallest percentage of elements that do not fulfill the standard requirements. Therefore, timber is not only a cheaper material than concrete and steel, but it is also reliable and gives a great push to the evolution both of the production process of elements and joints and to design methods.

However, the non-homogeneity of the material, due to the presence of growth defects in the form of knots, zone of compressed wood, oblique fiber orientation and other growth characteristics, naturally created for the needs

1.2 Cases of Structural Failures

of the trees and differing according to the type of wood, reduce the strength significantly when the wood is used in other contexts [41]. Moreover, the presence of knots and other defects (rupture, compression zones, slope of grain, decay, bark pockets, wane and resin pockets) leads to a variability of the mechanical properties also inside small elements. For this reason, timber material design rules and methods are still elementary if compared to the design methods of the other structural materials and mostly timber is designed in linear elastic range.

1.2 Cases of Structural Failures

Despite the high level of knowledge reached by structural engineers in modeling the performance and the capacity of large and complex structural systems and the increasing development of computer tools and software able to simulate the behavior of advanced structures, the high number of structural collapses occurring in the last years is surprising.

During the winter season of 2005-2006, more than fifty roofs failed in Germany, Austria and Poland due to a large accumulation of the snow and some of them led also to fatalities. However, structures should be able to resist such high value of the load if properly designed according to modern codes. Indeed, structures are designed with the characteristic value of the snow load, normally chosen as the annual maximum value that can be exceeded in average only once every 50 years. Beside this, codes provide additional safety margins by adding load combination factors and resistance partial

safety factors, so that the structure should be able to withstand loads that exceed significantly the design load, unless the resistance is affected by design errors or deterioration.

Investigations about several of these failed structures showed that, except few cases, the failure was due to human errors in applying existing technology in the design and in the construction phase.

Ellingwood in [12] compiled results from a series of investigations during the years 1979- 1985 to identify where errors occur in the building process. This study was included and extended in the report TVBK of Lund University (Sweden) [16]. Some of the results from this paper together with new results are reported in table 1.2

The occurrence of errors are of the same order of magnitude for design/planning and construction respectively, with slightly higher frequency in the design phase; failures due to material deficiencies or maintenance are relatively uncommon. Furthermore, a previous statistical study of Allen (1976) indicates that only the 10% of the failure occurs due to stochastic variability in load and capacities, while the remaining 90% was due to design and construction errors including modeling and analysis errors. A similar European study done by Hauser (1979), showed that the 22% of the failure was caused by stochastic variability, but it was not indicated which percentage of the remaining 78% was due to design errors. The building phase, in which the damage occurred or was detected, was also reported in [16]:

- During construction 58%;

1.2 Cases of Structural Failures

Reference	Planning & Design [%]	Construction [%]	Utilization & Maintenance [%]	Other ^a [%]	Total [%]
CEB 157 (1893)	50	40	8	–	98
Matousek (1982)	45	49	6	–	100
Grunau (1979)	40	29 ^b	31	–	100
Raygaertz(1979)	49	22	29 ^b	–	100
Brand et al.(2005)	40	40	–	20	100
Taylor (1975)	36	12	–	–	–
Yamamoto et al.(1982)	36	43	21	–	100
Rackwitz et al.(1983)	46	30	23	–	99
Melchers et. al. (1983)	55	24	21	–	100
Fraczek (1979)	55	53	–	–	108 ^c
Allen (1979)	55	49	–	–	104 ^c
Hadipriono (1985)	19	27	33	20	99
Hauser (1979)	37	35	5	23	100
Gonzales (1985)	29	59	–	13	101 ^c

a: Includes cases where failure can not be associated with only one factor and may be due to several of them.

b: Building materials, environmental influences, service conditions.

c: Multiple errors for single failure case.

Table 1.2: Incidence of errors in building process by phase.

- During use 39%;
- During rebuild/deconstruction 3%.

This confirms the findings from other investigations that failures occur more frequently during the construction phase than later. For those failure cases where people were killed or injured, the percentage of cases occurring during construction is even higher (65-70 %). However, the fact that the error was detected in the construction phase does not necessarily imply that the error was initiated by inadequate construction methods.

In [12] also a classification of human errors was reported. Three basic types of errors can be identified:

- Errors of concept (stupidity, ignorance);
- Errors of execution (carelessness, forgetfulness, negligence);
- Errors of intention (venality, irresponsibility).

In table 1.3, derived from [12], the causes of human error are listed according to the three categories defined above.

Reference	Ignorance, negligence, carelessness [%]	Insufficient knowledge [%]	Mistakes [%]	Reliance on others [%]	Other [%]	Total [%]
Matousek (1982)	35	38 ^a	9	6	12 ^b	100
Melchers (1983)	24	52	8	2	13	99

a: Breaks down as insufficient knowledge 25%; underestimation of influences 13%.

b: Breaks down as unknown situation 4%; other sources 8%.

Table 1.3: Causes of Error.

1.2 Cases of Structural Failures

Furthermore, the first category can also include load cases not considered in the design, incorrect assumptions, incorrect analytical modeling, incorrect modeling of the interaction structure-foundation-soil or of the non-linear behavior in large-deformation behavior.

The second category includes also calculation or detailing errors, mistakes in reading drawings and specifications, defective workmanship.

The third category includes unwarranted shortcuts, use of lower quality material and acceptance of marginal workmanship in order to maintain construction schedules and save money.

1.2.1 Failures in Timber Structures

In [16] a review of the more probable cause of damage leading to a failure of a timber structure are:

- Inadequate behavior of the joints;
- Effects of moisture exposure;
- Poor durability performance;
- Inadequate bracing of structural system;
- Inadequate performance of material and products;
- Inadequate estimate of loads.

Inadequate consideration of load effects or underestimation of the actions are instead quite uncommon and are considered among the design errors.

Quite uncommon is also the use of inadequate quality of the wood material, even if deficiencies in the quality of the timber was observed in some cases, due to a too high occurrence of knots and too much irregular grains.

Mostly, the behavior of the connections appears to be critical and in the most cases of failure, errors in the construction of the joints were found. Moisture content variations are also often cause of shrinkage cracks development both around the cross section and in direction orthogonal to the grain due to moisture-induced stresses.

1.3 State of the art about timber analysis

Wood is a material "biologically produced" in the growing tree and it is a high quality fiber composite material. The wood cells are oriented predominantly in one direction that is the fiber direction or "grain" direction that is parallel to the longitudinal axis of the stem and also the strongest direction. Differently from other building materials the strength and the stiffness in the fiber direction are very large in relation to the weight of the material especially in traction.

In addition, timber is a non-homogeneous material, since it contains growth defects in the form of knots, zone of compressed wood, oblique fiber orientation and so on. Therefore, the mechanical behavior of the timber cannot be derived in a reliable way from the properties of clear wood. Moreover, the presence of knots and other defects (rupture, compression zones, slope of grain, decay, bark pockets, wane and resin pockets) is different according

1.3 State of the art about timber analysis

to each kind of wood.

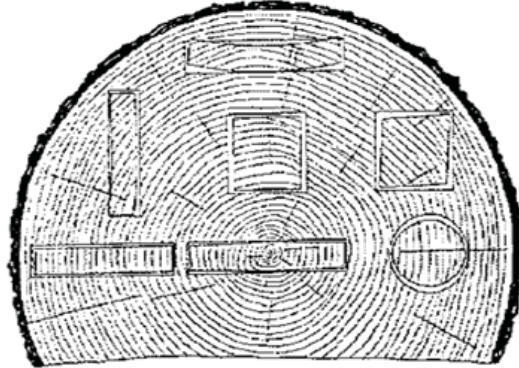
According to [10, 11, 14], the influence of defects is implicitly included in the strength value specified for the timber class and these values can only be applied if the stresses are determined by elastic theory.

The fact that the load-bearing capacity of timber is governed by the presence and characteristics of random growth defects means that the strength of timber elements also depends upon the size of the structural element itself and on the way in which it is loaded.

In structural application wood is generally used in form of *solid timber* and of *glulam*. Solid timber is directly cut and formed from wood pieces (see figure 1.1), while glulam elements are made from laminations of structural timber bonded together with adhesives mixed with the constituents or sprayed on their surfaces with application of heat and pressure. This production process removes partially the growth defect of "solid wood" or distributed them in the finished product in a way that the strength is less affected and the finite product is more uniform. For this reason and also because the locally weak sections of the laminations are able to redistribute stress to adjacent stronger sections, even if glulam timber is made from laminations of solid wood, the strength is significantly higher for glulam than for wood.

Both for solid timber and for glulam, structural design codes treat timber material as an homogeneous, orthotropic elastic material with one main axis in the fiber direction and with the same properties in all directions perpendicular to the main axis. An important difference is in the size-volume

Figure 1.1: Wood cross section.



effect. Elements made of solid timber have often small sections so that the volume effect is null, while glulam elements have often special shapes (e.g. curved or tapered) with thin and high cross sections so that size effect and also instability are more common.

Although the calculation method proposed in the codes is simplified because aims at "manual calculations", it is on the safe side. Only for very special structures it can be worth adopting a FEM model (either 2D or 3D), but the cylindrical orthotropy must be taken into account also according to the year ring growth pattern of the specific wood used.

However, timber elements are designed mostly in bending and because timber has a linear elastic fragile behavior when subjected to bending, a linear elastic analysis is sufficient to understand the global behavior of the structure. Therefore, it can be assumed an elastic linear behavior of the material with parameters corresponding to the mean values of the stiffness and resistance.

1.4 Risk assessment approach advantages

Generally, the connections are built as hinged joints, hence exhibiting a low stiffness, and this allows one to calculate and build the structure as statically determinate, with the exception of some special cases.

Differently from other structural materials, for timber structures it is important to define the service class according to the exposure to humidity. This condition changes strongly with the moisture content inside the wood and this percentage of humidity changes the resistance and the stiffness of the elements and leads to a faster degradation of the material due both to mechanical splitting and to mildew.

1.4 Risk assessment approach advantages

Safety of structure is a complex problem. Indeed, loads, material strength and model uncertainties are three fully random fields but, for practical reason, engineers are used to look at the behavior of structures in deterministic way, i.e. to assign a certain load capacity according to a specific demand computed from defined load parameters. If these load parameters were certain and we knew the maximum of all load configurations that can be experienced by the structure, it would be sufficient for the safety to design the structure in such a way that the limit situation is attained exactly for the maximal value load. This also implies that any kind of uncertainty, even on just one of the parameters affecting the behavior of the structure, e.g. geometry, material resistance, modeling and load parameters, will lead to an unsafe design.

A fully probabilistic structural analysis allows one to compute, by means of mechanical and mathematical model, the value of the probability that a structure behaves in a certain way when one or more parameters (such as mechanical properties, geometry and loads) are of random nature [6].

In this case, the mathematical model must define all the properties and parameters of the structure in terms of random variables with appropriate distribution.

In addition, the mathematical model has to describe the variables of the problem in a realistic way, being often supported by experimental studies, and also have to be operative i.e. suitable to solve engineering problems.

The probabilistic approach is obviously an extension of the deterministic one and has the big advantage of leading to understand the most likely behavior of the structure (e.g. which limit state is more likely to occur under the set of random variables considered) and to solve design decision problems related to the probabilistic structural analysis.

In the deterministic analysis, in fact, we assign the dimensions to the elements in order to achieve a certain behavior under a specific action and given a certain strength. This is equivalent to search for the event with a probability of one. Probabilistic analysis can be used to define which are the optimal properties and dimensions to be assigned to the structural elements, within all the probabilistically defined possibilities. This is equivalent to search for the minimum of the probability of occurrence of the failure event related to a specific behavior with respect to the probabilistically defined parameters of the problem, i.e. to search for the dimensions that assure the optimum related to a certain behavior.

1.5 The Structural Robustness

Because of the computational effort required by a fully probabilistic approach, the majority of outstanding national codes have introduced only a semi-probabilistic design approach, where all the variables are assumed to be Normal random variables.

1.5 The Structural Robustness

Robustness is one of the fundamental issues and necessary properties for structural systems.

As reported in modern codes and technical literature, it is indicated as an important requirement for structural design. Mostly after the collapse of the Ronan Point Building in 1968, where the consequences were unacceptable compared to the initial damage, and the collapse of the World Trade Center, robustness became object of a renewed interest. This is also because the advance in building technology and technique allow one to realize advanced types of structures and so that the consequences of a structural collapse may exceed the mere rebuilding costs by orders of magnitudes including also fatalities.

However, the meaning of robustness is often not clear and leaves space for several interpretation, but it is reasonable to confirm that robustness is strongly related to internal structural characteristics such as redundancy, ductility and joint behavior characteristics, but also to the consequences of structural collapse.

The Robustness of a structure is generally meant to be the *insensitivity to*

local failure and to progressive collapse. This means that it must be read as a property of the structure itself and it is independent from possible causes of initial local failure [36]. In this sense Robustness must not be confused with the definition of collapse resistance given in EC1, i.e. as insensitivity to accidental circumstances which are represented by low probability events and unforeseeable incidents. Collapse resistance is a property of the structure but it is influenced by both structural features and causes of possible failure. Moreover robustness is related to the insensitivity of *key elements* to failure. A key element is defined as a limited part of the structure whose possible failure implies a failure of the entire structure or of a significant part of it [37]. It is also strongly dependent on the specific scenario of events (trigger-failure-event) over a complex series of intermediate events involving more localized damages which finally led to collapse. In this scenario, the magnitude of the consequences depends not only on internal structural characteristics but may be even more pronounced depending on passive and active measures for damage reduction and detection as well as possible nonconformities with design assumptions due to a bad quality of execution, design errors and/or lack of maintenance.

The requirement for robustness is defined both in EN1990-EC0: Basis of Structural Design and in EN1991-EC1: Accidental actions. The EC0 establish the principle for robustness, the EC1 provides methods and criteria for the design of a robust construction against *identified accidental actions* and *unidentified actions*. Precise definitions are available in the following European codes:

1.5 The Structural Robustness

- ISO 22111 (ISO 2007b): Ability of a structure (or part of it) to withstand events (like fire, explosion, impact) or consequences of human errors, without being damaged to an extent disproportionate to the original cause;
- Eurocode 0 (CEN 2002): The ability of a structure to withstand events like fire, explosions, impact or the consequences of human error, without being damaged to an extent disproportionate to the original cause;
- SIA 260 (SIA 2004): Ability of a structure and its members to keep the amount of deterioration or failure within reasonable limits in relation to the cause.

However, the previous definitions are all similar and relate the robustness to the consequences of a certain event (failure or damage) as already discussed. In Eurocode EN 1990:2002 (CEN 2002), the basic requirement to robustness is given in clause 2.1 4(P): *A structure should be designed and executed in such a way that it will not be damaged by events such as explosion, impact and the consequences of human errors to an extent disproportionate to the original cause.*

Given a certain exposure, the structure can have a local damage and it may survive or (a substantial part) may collapse due to:

- Exposures which could be unforeseen, unintended effects and defects (incl. design errors, execution errors and unforeseen degradation) such as unforeseen action effects, incl. unexpected accidental ac-

tions, unintended discrepancies between the structure's actual behavior and the design models, unintended discrepancies between the implemented project and the project material, unforeseen geometrical imperfections, unforeseen degeneration;

- Local damage due to exposure (direct consequence of exposure);
- Total (or extensive) collapse of the structure following the local damage (indirect consequence of exposure);

In this definition it is clear that robustness is especially related to precautions to prevent/reduce the indirect consequences in case of extensive collapse associated with a local damage due to exposure.

It must also be noted that the system behavior is very important in robustness assessment. This is a consequence of the fact that primary criteria in building design codes are related to achieve a sufficient reliability of components (sections). It should also be noted that redundancy in systems is closely related to robustness. In principle, redundant system are believed to be more robust than non-redundant systems - but this is not always the case as illustrated by the failures of the Siemens Arena and the Bad Reichenhall Ice Arena, see [16, 19, 43].

Moreover the current design codes and design procedures are based on actions and resistances defined statistically on the basis of empirical data. The choice of an allowable probability of failure is reflected in the computation of actions and resistance using probabilistic methods and it is implicit in the choice of partial safety factors and series of load combination schemes. In this way the code lead to a uniform safety level, but all these assumption

1.5 The Structural Robustness

can fail in the case of progressive collapse for three main reasons [36]:

- Current design codes are based on the consideration of local and not global failure (check of cross section and stability); on the contrary, the global safety, i.e. the safety against the collapse of the entire system, is function of the safety of all the elements to local failure (response of the system to local failure). This means that for non-robust structures the uniform safety level of the single elements does not lead to the same safety level of the system and to a safe design;
- Current design methods do not take into account the lower probability events and this cannot be done for non-robust structures because they are more sensible to local failure due to unforeseeable loads;
- Current design methods require a specification of an admissible probability of failure (or structural safety level) because the target failure probabilities of probabilistic design codes are usually derived by calibration with previous deterministic codes and without considering any impact on people;

The Danish Code of Practice for the Safety of Structures and probabilistic modeling of the timber material is now the base for the Probabilistic Model Code (PMC) of Joint Committee for Structural Safety and according to the first one a structure has to be designed in such a way to be in agreement at least with one of the following criteria:

- Demonstrating that those parts of the structure essential for the safety (key elements) have only little sensitivity with respect to un-

intentional loads and defects;

- Demonstrating a load case with *removal of a limited part of the structure* in order to document that an extensive failure of the structure will not occur if a limited part of the structure fails;
- Demonstrating sufficient safety of key elements, such that the entire structure with one or more key elements has the same reliability as a structure where robustness is documented by the previous condition.

However, both Eurocode and PMC do not provide any specific criterion for quantify the level of robustness. For this reason, robustness is often identified with the *structural redundancy*, that can be defined as the availability of multiple load-carrying elements or multiple load paths which can bear additional loads in case of failure of some elements, avoiding in this way progressive collapse. That means that in case of failure of one or more elements, the structure is able to redistribute the loads avoiding the global failure of the structure, but this property is not necessary related to the static indeterminacy but rather depends on the geometry of the structure and the property of single elements.

Important aspects related to robustness are defined in [36, 12]:

- Key Elements: exterior columns and walls should be capable of spanning two or more stories without bucking, columns should be designed to withstand blast pressure etc;
- Progressive Collapse: it is characterized by a disproportion in size between a triggering event and the resulting collapse [36]. According to

1.5 The Structural Robustness

[12] progressive collapse of a building is a catastrophic partial or total failure that follows from an initiation event that causes local damage and cannot be absorbed by the inherent continuity and ductility of the building structural system;

- Redundancy: Incorporation of redundant load paths in the vertical load carrying system;
- Ductility: Structural members and member connections have to maintain their strength through large deformations (deflections and rotations) so the load redistribution(s) may take place.

1.5.1 Robustness measure overview

A measure of robustness it is needed for evaluation, comparison, optimization and regulation of the robustness of a structure [37]. If a quantitative measures is defined, critical elements can be identified and also different structural configurations can be compared. In order to regulate robustness, quantification is required. Minimum values of robustness can be defined in standards and design guidelines generally or according to the type of structure and depending on the significance and exposure of the building [38]. We can allocate robustness measure into two categories:

- behavior-based measures;
- structural attributes.

The behavior based measure are often related to the response of a structure to an assumed initial local failure and require non-linear analysis of

the structural response. For this reason they are usually not considered a realistic measure to which a code can refer to.

Stiffness-based index (Starossek-Haberland 2009)

A simple method to measure structural robustness is to compute the static-stiffness matrix of the structural system after the removal of one structural element or a connection and compare it with the stiffness of the intact system:

$$R_s = \min_j \frac{K_j}{\det K_0}. \quad (1.1)$$

Where R_s is the stiffness-matrix-based robustness index, K_0 is the active stiffness of the intact system and K_j is the active stiffness of the system upon the removal of the element j or the connection j . This index has values in the interval $[0, 1]$, with the upper bound indicating an intact system and the zero value indicates a complete lack of robustness.

However, it was shown that only a low correlation between the decrease of capacity due to the removal of an element and the corresponding robustness R_s exists. Therefore this measure seems to be not very effective, although simple.

1.5 The Structural Robustness

Damage-based index (Starossek-Haberland 2009)

Given the definition of robustness in terms of insensibility to local failure, a measure related to the extension of the damage, upon a certain trigger event, can be suggest.

$$R_d = 1 - \frac{p}{p_{lim}}. \quad (1.2)$$

Where R_d is the damage-based robustness measure, p is the maximum extent of additional damage (maximum damage progression) caused by the assumed initial damage i_{lim} and p_{lim} is an acceptable damage progression. This index has values in the interval $[0, 1]$, with the upper bound indicating the optimal robustness. This is a more general measure and the damage can be considered both in terms of structural damage (mass, volumes, floor areas) and in terms of costs (repair, delay, service interruption).

Energy-based index (Starossek-Haberland 2009)

Energy-based approaches is based on the comparison between the energy released by the initial failure and the energy required for a collapse progression.

$$R_e = \max_j \frac{E_{r,j}}{E_{s,k}}. \quad (1.3)$$

Where R_e is the energy-based robustness measure, $E_{r,j}$ the energy released by the initial failure of a structural element j and available for the

damage of the next structural element k , $E_{s,k}$ is the energy required for the failure of the next structural element k .

This measure does not have value restrictions: values between zero and one are acceptable, while negative values indicate progressive collapse.

Energy-based index may be difficult to use because the determination of the energy release is not easy and can be both under and over estimated. In addition, the energy released by the initial failure of the structural element is composed of several parts and depends on the failure mechanism. For structures that have a tendency for a pancake-like or domino-like collapse, the dominant portion of the energy will be kinetic energy converted from the potential energy of the collapsing structural elements and a numerical estimate can be done, but in case of other types of collapse, the energy release can only be determined through a comprehensive structural analysis.

Risk-based index (Baker-Schubert-Faber 2008)

Backer et al. suggest a risk-based robustness index that takes into account also for the direct and indirect causes of a failure by measuring the fraction of total system risk resulting from direct consequences. This is motivated by the concept that a robust system is considered to be a system where indirect risks do not contribute significantly to the total system risk.

$$I_R = \frac{Risk_{dir}}{Risk_{dir} + Risk_{ind}}. \quad (1.4)$$

1.5 The Structural Robustness

Where $Risk_{dir}$ are the direct consequences associated with local component damage (that might be considered proportional to the initiating damage) and $Risk_{ind}$ are the indirect consequences associated with subsequent system failure (that might be considered disproportional to the initiating damage).

The index has values in the interval $[0, 1]$. If $I_R = 1$ there are not indirect consequences to the failure event and the system is considered to be robust. If $I_R = 0$ all the risk is in the indirect consequences.

However, this index is a measure of relative risk due to indirect consequences and it can lead to a high value of the index also in presence of a large direct risk respect to the indirect risk. In this case the system should be rejected on the base of reliability criteria. Moreover, the optimal system is the one which has the minimum risk. This implies that the definition of a robustness index by equation is not always fully consistent with a full risk analysis, but can be considered as a helpful indicator based on risk analysis principles. It is noted that since the direct risks typically are related to code based limit states, they can generally be estimated with higher accuracy than the indirect risks.

In addition, the exposure is an important factor in risk-based assessment and therefore it can be useful to introduce an index conditioned on the exposure.

$$I_{R|exposure} = \frac{Risk_{dir|exposure}}{Risk_{dir|exposure} + Risk_{ind|exposure}}. \quad (1.5)$$

Reliability-based index (Frangopol et al. 1990)

In [15, 17] a probabilistic measure for robustness is associated to redundancy of the structure and consequently to the robustness.

$$R_I = \frac{P_{F,damaged} - P_{F,intact}}{P_{F,intact}}. \quad (1.6)$$

Where the $P_{F,damaged}$ is the probability of the failure event F for the damaged structural system and $P_{F,intact}$ is the probability of failure of the intact structural system. The index takes values between zero and infinity, with smaller values indicating larger robustness.

As related redundancy factor it can also be written in equivalent way as:

$$\beta_R = \frac{\beta_{intact}}{\beta_{intact} - \beta_{damaged}}. \quad (1.7)$$

Where β_{intact} is the reliability index of the intact structural system and $\beta_{damaged}$ is the reliability index of the damaged structural system. The index takes values between zero and infinity, with larger values indicating larger robustness.

Deterministic robustness index (ISO 2007a)

The RIF-index (Residual Index Factor) is a specific deterministic robustness measure used in the offshore structure. The RIF index is also called Damage Strength Ratio and it is a measure of the effect of the failure of the element j on the structural capacity, where the failure is defined as a

1.5 The Structural Robustness

full loss of functionality of the structure.

$$RIF_i = \frac{RSR_{fail,i}}{RSR_{intact}}. \quad (1.8)$$

Where the RSR_{intact} and $RSR_{fail,i}$ are the Reserve Strength Ratio of the intact structure and of the structure upon the removal-failure of component i respectively. The RIF takes values between zero and one, with larger values indicating larger robustness.

The RSR is defined as the ratio

$$RSR = \frac{R_c}{S_c}. \quad (1.9)$$

Where R_c denotes characteristic values of the base shear capacity of an offshore platform (typically a steel jacket) and S_c is the ultimate design load corresponding to collapse.

Chapter 2

Structural Reliability

Hereby the basis of structural reliability methods will be introduced.

The *Structural Reliability* concerns with the *computation and prediction of the probability of limit state violation for an engineered structural system at any stage during its life*, [28]. The violation of Ultimate Limit State is a rare event, as we can observe in everyday life, because very few structures collapse or require to be repaired suddenly.

2.1 The Structural Response

The response of a structure to a certain load event depends on the type and magnitude of the load as much as on the strength and stiffness of the structure itself. The response can be considered satisfactory only according to defined requirements. Safety requirement are usually the safety level

against structural collapse or limitation of damage or serviceability criteria. Typical limit state requirements are defined according to three level for the safety of the structural response:

- Ultimate , identified by the collapse of the structure or a part of it including events like rupture, progressive collapse, plastic mechanisms, instability, fatigue, deterioration etc.;
- Damage, often included in the collapse event and includes excessive cracking, inelastic deformation etc.;
- Serviceability, disruption of use due to excessive deflection, vibrations, local damages etc.

To predict the probability of violation of a certain limit state means to predict the probability of occurrence of this special event. This measure can be obtained only through an assessment that considers completely all the uncertainties of the variables of the problem.

The use of *safety factors* and *load factors*, that is commonly introduced in all the modern structural codes, is a conservative but only *deterministic* measure of safety. This because these factors lead to use a conservative value of the variables upon which it is assumed to be no uncertainly.

2.2 Deterministic Measure of Structural Reliability

As described before the traditional measure of safety introduce deterministic factors on resistance R and loads S in order to assign to them a value that is conservative and on which it is assumed to be no uncertainly. These factors can be applied on the strength (*safety factors*) or on the actions (*load factor*).

Safety factor are usually applied on the strength and are introduced in elastic stress analysis as a reducing factor:

$$\sigma_{lim,i} = \frac{\sigma_{u,i}}{F}. \quad (2.1)$$

The reducing factor F is applied directly on the ultimate stress strength and is usually selected on the basis of experimental observations, practical experience economical issues etc. and is always imposed by the code committee. This limit is equivalent to define an admissible stress limit and therefore is valid only in linear elastic field analysis that is well known to be far from the usual stress state analysis.

Load factor is a safety factor applied on the loads Q and developed for being used in the plastic theory of structures. Commonly, it is defined as the amplification factor λ that must be applied to the set of loads acting on the structure in service condition to led the structure to failure.

Given a certain limit state function, the collapse-failure occur when the external work function L_e of the loads λQ exceeds the internal work function

L_i of all plastic resistance R_p (plastic moments etc).

$$L_i(R_p) \leq L_e(\lambda Q). \quad (2.2)$$

The *Partial Safety Factor* approach applies partial factors both to resistance and loads. Commonly the load partial safety factor differs from load to load in order to take into account the different variability and uncertainty associated to the different nature of the load. According to the definition of plastic collapse given in Eq.2.2 we can rewrite the PVW (Eq. 2.3) .

$$L_i(\varphi R_p) \leq L_e \left(\sum_{j=1}^n \gamma_j \cdot Q_j \right). \quad (2.3)$$

However, these measures of safety fail in invariance because they depend on the defined limit state function and how loads and resistance are defined.

2.3 Probabilistic Measure of Structural Reliability

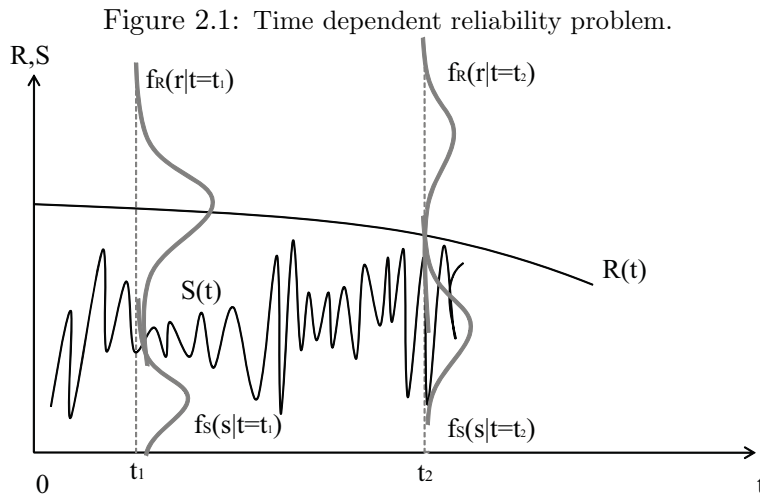
The full probabilistic measure of the safety of a structural element is defined as the *probability of the failure event*. This can be computed only by considering randomness in time and space of both loads and resistance.

Loads due to natural phenomena (snow, wind, earthquake...) occur with randomness in time and in space. The randomness in time can be considered in terms of *return period* defined as the expected time between two

2.3 Probabilistic Measure of Structural Reliability

successive statistically independent events, where the event can be related also to a certain threshold to be exceeded. This means that the time between events is a random variable (r.v.). The magnitude of each event is also uncertain and so must be defined as r.v. with a certain probabilistic distribution (in terms of probability density function or cumulative density function).

Also resistance and geometric property can be defined in terms of a probabilistic distribution. In addition, the structural resistance changes with time, due to deterioration phenomena, while loads have the tendency to increase. For this reason, the probability density functions f_S and f_R of the loads S and resistance R become wider and flatter with time and also the mean value of S and R changes with time (see figure 2.1).



When the resistance R is not strongly changing in time and the load

S is applied many times in a defined time interval $[0, T]$ as single time-varying load, it can be assumed that R is constant and S acts as a single load following a certain probability distribution (usually an extreme value distribution as Gumbel or Frechet), neglecting the time-dependency.

In this case the *limit state function* (l.s.f.) $g(r, s)$, where (R, S) is the vector of basic random variables of the problem, can be defined as in Eq. 2.4.

$$g(r, s) = R - S \leq 0. \quad \text{or} \quad g(r, s) = \frac{R}{S} \leq 1. \quad (2.4)$$

This is also known as the general structural reliability problem for component failure events.

By definition, the failure event F corresponds to the event Eq. 2.5

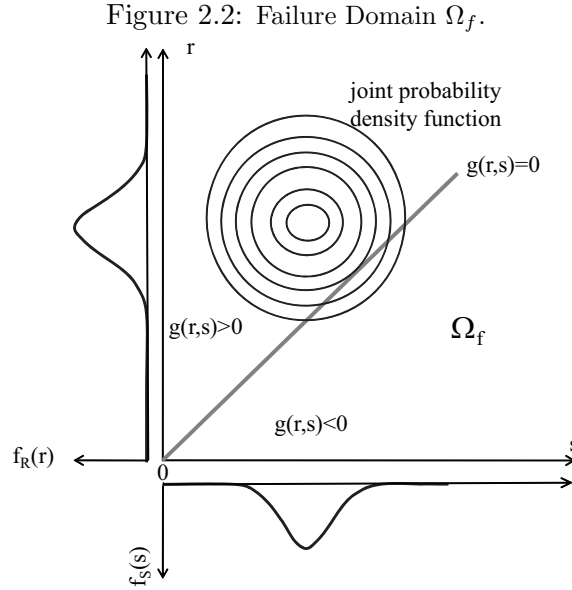
$$F = \{g(r, s) \leq 0\}. \quad (2.5)$$

and the probability of failure is therefore

$$P_r(F) = P_r(g(r, s) \leq 0). \quad (2.6)$$

where $\{g(r, s) \leq 0\} = \Omega_f$ is the failure domain in the space of the r.v. R and S . The probability of failure is the probability of (r, s) taking a value within the failure domain Ω_f . The $P_r(F)$ can be computed by integrating the joint probability density function of (r, s) , denoted by $f_{RS}(r, s)$ over Ω_f (see figure 2.2).

2.3 Probabilistic Measure of Structural Reliability



The $P_r(F)$ is given by the following integral:

$$P_r(F) = \int_{\Omega_f} f_{RS} dr ds. \quad (2.7)$$

When R and S are independent $f_{RS}(r, s) = f_R(r)f_S(s)$ where $f_R(r)$ and $f_S(s)$ are the marginal density function of R and S . The integral becomes:

$$P_r(F) = \int_{-\infty}^{+\infty} \int_{-\infty}^{s \geq r} f_R(r)f_S(s) dr ds. \quad (2.8)$$

For R and S statistically independent, we can reduce this integral of one order using the property of *convolution integral*.

The definition of cumulative distribution function for a vector of r.v. \mathbf{X} for $x \geq y$ is provided by:

$$F_X(x) = P_r(X \leq x) = \int_{-\infty}^x f_X(y) dy. \quad (2.9)$$

This allow us to rewrite the probability integral for independent R and S as

$$P_r(F) = P_r(g(r, s) \leq 0) = \int_{-\infty}^{+\infty} F_R(x) f_S(x) dx. \quad (2.10)$$

Where $F_R(x)$ is the probability that $R \leq x$ and the $f_S(x)$ represents the probability of S to assume values in the range $[x, x + \Delta x]$ for $\Delta x \rightarrow 0$.

Generally, the r.v. of the problem R and S are not independent. In addition, the analytical solution of this integral often does not exist and also the numerical integration has computation times that increase exponentially with the number of dimensions. Therefore, to solve the probability integral when the number of random variables is larger than 3 to 5 is possible only in approximated way.

All structural reliability methods aim at solving the probability integral, but all of these methods are approximations, and each method has its own advantages and disadvantages, which make them suitable for different applications. There are three way of solving this multi-dimensional integral:

- direct integration (solution possible in only few special cases);
- numerical integration with Monte Carlo sampling;
- Transform the integrand into a multi-normal joint probability density function for which the solution is already known.

2.4 Monte Carlo Direct Sampling

A simple, intuitive general and often powerful method for solving structural reliability problems is Monte Carlo Simulation (MCS), which is a general method for analyzing functions of random variables. MCS proceeds by artificially generating samples from the distribution of the input variables and then evaluating the functions $g(r, s)$, for each sample value separately. In this way, a set of samples of the function value $g(r, s)$ are generated, which can be evaluated using statistical methods.

A powerful but approximated method in the case of a non-linear limit state function with non-Normal random variables, proceeds by transforming all random variables into Normal random variables and then approximating the limit state function by a linear (first-order polynomial) function. This approach is known as the First-Order Reliability Method (FORM) and is founded on the principle, that the limit state function $g(r, s)$ can be directly evaluated by a first- order Taylor series expansion around the performance point that is calculate by means of a line-search based algorithm (HLRF). These methods will be described in the following.

2.4 Monte Carlo Direct Sampling

Monte Carlo method is a simulation technique. It consists in the generation of a large number of samples to observe the result of the sequence of experiments/samples. For any structural reliability problem it is possible to define the random variables (r.v.) to model both the property of the elements and the loads, and to assign a limit state function $g(\mathbf{X})$, where

\mathbf{X} is the vector of the r.v, according to the failure mechanism.

By generating a number N of sample of the vector of random variables \mathbf{X} , the limit state function is evaluated at each realization x_i and if the limit state is violated, the element is considered *failed*. This experiment is repeated for the set of N samples and the probability of failure can be approximated by the ratio between the number of experiments in which $g(\mathbf{X}) \leq 0$ and the total number of experiments N .

$$P_r(F) = \frac{\sum_{i=1}^N I_i [g(X_i) \leq 0]}{N}. \quad (2.11)$$

Where $I_i [g(\mathbf{X}_i) \leq 0]$ is the indicator function at sample i equal to 1 if $g(X_i) = 0$.

The number of total sample N is related to the accuracy we want to achieve. The MCS gives us an estimation of the solution and the value of the probability computed with MCS converges to the true one only if $N \rightarrow \infty$. Therefore we can associate to this estimate a mean value and an upper and lower bound of confidence.

We can evaluate mean and variance of the estimated probability with Eqs. 2.12 and 2.13

$$E [P_r(F)] = \frac{\sum_{i=0}^N I_i}{N}. \quad (2.12)$$

$$\text{VAR} [P_r(F)] = \frac{\sum_{i=0}^N \text{VAR} [I_i]}{N^2} = \frac{\text{VAR} [I]}{N} = \frac{P_r(F) - P_r(F)^2}{N}. \quad (2.13)$$

The confidence interval is defined as the interval that has the p_c probability of containing the true value of the $P_r(F)$. The probability of failure

2.5 First Order Reliability Method (FORM)

estimated with MC is computed as sum of N r.v. and this sum will converge asymptotically to the Normal distribution for $N \rightarrow \infty$. By assuming the $P_r(F)$ having the Normal distribution with parameters $E[P_r(F)]$, $\text{VAR}[P_r(F)]$, the confidence interval can be computed as

$$p_c = E[P_r(F)] \mp \sqrt{\text{VAR}[P_r(F)]}. \quad (2.14)$$

2.5 First Order Reliability Method (FORM)

In the field of component reliability problem, the probability of failure of a component corresponds to a certain reliability index. The FOR-Method is an approach with high computational efficiency, developed mostly at TU München in the '70 and '80 by Prof. Rackwitz and his research group. This method allows to compute the reliability index β and the design point \mathbf{u}^* . In addition, the reliability index is an invariant safety measure and for this reason FORM is a very important method.

First some definitions need to be given. Let's assume both resistance R and loads S as normal distributed and that the limit state function can be written as $g(r, s) = R - S$. With this expression, the limit state function g represents a safety margin, also normal distributed, with mean and variance fully defined by the well-known addition rule of Normal r.v. (see Eqs. 2.15 and 2.16).

$$\mu_g = \mu_R - \mu_S. \quad (2.15)$$

$$\sigma_g^2 = \sigma_R^2 - \sigma_S^2. \quad (2.16)$$

The probability of failure, as defined in the previous section is

$$\begin{aligned} P_r(F) &= Pr(g(r, s) \leq 0) = \Phi\left(\frac{0 - \mu_g}{\sigma_g}\right) = \\ &= \Phi\left(\frac{0 - (\mu_R - \mu_S)}{\sqrt{\sigma_R^2 - \sigma_S^2}}\right) = \\ &= \Phi(-\beta). \end{aligned} \quad (2.17)$$

Where $\beta = \mu_g/\sigma_g$ is the well-known *reliability index* or *safety index*. If both standard deviation of R and S become smaller, the β becomes larger (safety increases) and the probability of failure decreases, while if the difference between the mean values of R and S decreases the probability of failure increase.

The design point is commonly defined as the point on the limit state function-surface, defined by a realization of the r.v. \mathbf{X}^* , that is the most likely point that leads to failure. It will be shown that the β index corresponds to the design point \mathbf{u}^* in the space of the standard normal variables, and that \mathbf{u}^* represents also the nearest point of the l.s.f. to the origin of the standard normal space.

If the limit state function is linear and the r.v. are all Normal distributed the probability of failure is simply given by the Eq. 2.5. Commonly, the l.s.f. g is not linear and the r.v. are not Normal distributed. In this case

2.5 First Order Reliability Method (FORM)

a first order approximation of the l.s.f. is needed and the r.v. must be transformed into Standard Normal Variable. In this way the optimization problem of searching for the most likely point corresponding to failure of the component can be solved into the space of the Standard normal variable, because we have an isometric multidimensional space with a linear failure surface and statistically independent r.v..

Transforming the r.v. into the standard normal space, the probability integral can be equivalently written as:

$$\begin{aligned} Pr(F) &= Pr g(x) \leq 0 = \int_{g(x)} f(x) dx = \\ &= Pr G(u) \leq 0 = \int_{G(u)} \varphi(u) du. \end{aligned} \quad (2.18)$$

The first order approximation of the l.s.f. $g(\mathbf{X})$ (or equivalently of $G(\mathbf{U})$) is usually done by a Taylor series expansion respect to the vector of r.v. \mathbf{X} (or \mathbf{U}) and around a point \mathbf{x}_0 (or \mathbf{u}_0) of the l.s.f, cut at the first order (Eq. 2.19).

$$g(\mathbf{X}) \approx g(x_0) + \sum_{i=1}^n \frac{\partial g(X)}{\partial x_i} (X_i - x_{0,i}) |_{x=x_0}. \quad (2.19)$$

Obviously, the accuracy of the solution depends on the choice of the approximation point x_0 and on the formulation of the l.s.f..

Hasofer and Lind in [20] proposed to perform the Taylor expansion around the design point x^* .

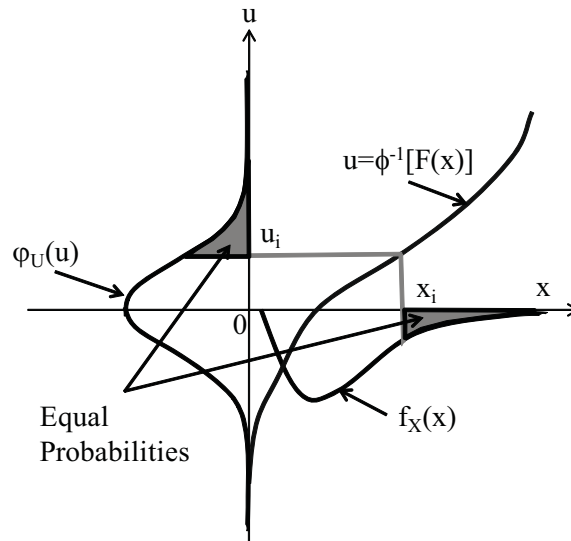
Rackwitz and Friessler in [32] extended the procedure to non-Normal distributed r.v. and developed an efficient algorithm to find the design point.

2.5.1 Transformation into the Standard Normal Space

Let \mathbf{X} be the vector of r.v. of the problem and \mathbf{U} the vector of uncorrelated Gaussian r.v. corresponding to each variable x_i into the standard normal space as shown in figure 2.3.

The transformation $U = T(X)$ is defined in Eq. 2.20.

Figure 2.3: Transformation to the standard normal space for a single random variable (A. Der Kiureghian 2005).



$$T : F_X(\mathbf{x}) = F_U(T(\mathbf{x})) . \tag{2.20}$$

2.5 First Order Reliability Method (FORM)

Where F_x is the joint *Cumulative Density Function* (CDF) of the r.v. \mathbf{X} and F_u is the standard Multi-Normal CDF that can be computed from the standard Normal CDF as $F_U(u) = \prod_{i=1}^n \Phi(u_i)$.

If the r.v. \mathbf{X} are statistically independent Normal distributed r.v., we have that $F_X(x) = \prod_{i=1}^n F_{x_i}(x_i)$ and the transformation T has the form given in Eq. 2.21.

$$T : u_i = \Phi^{-1} [F_{x_i}(x_i)], \quad i = \dots, n. \quad (2.21)$$

The inverse of the transformation of Eq.2.21 is given in Eq. 2.22.

$$T^{-1} : x_i = F_{x_i}^{-1} [\Phi(u_i)], \quad i = \dots, n. \quad (2.22)$$

If the r.v. \mathbf{X} are Normal distributed but statistically dependent, the joint Normal distribution is fully defined by the vector \mathbf{M}_x of the mean values, the diagonal matrix \mathbf{D}_x of the standard deviations and by the correlation matrix \mathbf{R}_{xx} . Calling \mathbf{L} the lower triangular matrix obtained by Choleski decomposition of \mathbf{R}_{xx} , i.e. $\mathbf{L}\mathbf{L}^T = \mathbf{R}_{xx}$, the transformation T and its inverse in this case are:

$$T : \mathbf{u} = T(\mathbf{x}) = \mathbf{L}^{-1}\mathbf{D}^{-1} (\mathbf{x} - \mathbf{M}_x). \quad (2.23)$$

$$T : \mathbf{x} = T^{-1}(\mathbf{u}) = \mathbf{M}_x + \mathbf{D}\mathbf{L}\mathbf{u}. \quad (2.24)$$

Commonly, in structural reliability problems, not all the r.v. of the vector \mathbf{X} are Normal distributed, but this variables can still be described in

the Standard Normal Space though the property of Gaussian Copulas: *for jointly Normal distributed random variables, the joint distribution is fully described by the marginal distributions and the correlation matrix.*

In addition, a set of r.v. \mathbf{X} , with their marginal distribution $F_{x_i}(x_i)$ and correlation coefficients ρ_{ij} , are defined to be *Nataf* distributed if their marginally transformed r.v. \mathbf{U} in the standard normal space are jointly Normal distributed.

Der Kiureghian and Liu in [5] demonstrated that the correlation coefficients ρ_{ij} and $\rho_{u,ij}$ of the two sets of r.v. \mathbf{X} and \mathbf{U} are related through the expression in Eq. 2.25, where $\rho_{u,ij}$ is the correlation coefficient between u_i and u_j and $\phi_2(u_i, u_j, \rho_{u,ij})$ is the bivariate normal pdf of the couple of r.v. u_i and u_j .

$$\rho_{ij} = \int_{-\infty}^{+\infty} \int_{-\infty}^{+\infty} \left(\frac{x_i - \mu_i}{\sigma_i} \right) \left(\frac{x_j - \mu_j}{\sigma_j} \right) \phi_2(u_i, u_j, \rho_{u,ij}) du_i du_j. \quad (2.25)$$

It can be noted that the standard normal variable u_i is related to the variable x_i through the expression 2.26.

$$u_i = \frac{x_i - \mu_i}{\sigma_i} \quad (2.26)$$

Moreover, from the property of the correlation coefficient ρ_{ij} , the following equivalence is valid:

$$\rho_{ij} = \int_{-\infty}^{+\infty} \int_{-\infty}^{+\infty} u_i u_j \cdot \phi_2(u_i, u_j, \rho_{u,ij}) du_i du_j =$$

2.5 First Order Reliability Method (FORM)

$$\begin{aligned}
 &= E[u_i, u_j] = \\
 &= \frac{\text{COV}[x_i, x_j]}{\sigma_i \sigma_j}. \tag{2.27}
 \end{aligned}$$

The correlation matrix $\{\rho_{u,ij}\}$ can be computed from the known ρ_{ij} iteratively with the Eq. 2.27, but this procedure is computationally inefficient. In [5], an empirical polynomial approximation of the factor $N_{ij} = \rho_{u,ij}/\rho_{ij}$ can be found. The expression of the polynomial approximation is given in Eq. 2.28, where V_a and V_b are the coefficients of variation (c.o.v.) of the couple of r.v. (a, b) considered, $r_{f_a f_b}$ is the correlation coefficient in the origin space and $a, b, c, d, e, f, g, h, k, l$ are the coefficients of the polynomial approximation.

$$\begin{aligned}
 N = a + b \cdot V_a + c \cdot V_a^2 + d \cdot r_{f_a f_b} + e \cdot r_{f_a f_b}^2 + f \cdot r_{f_a f_b} \cdot V_a + \\
 + g \cdot V_b + h \cdot V_b^2 + k \cdot r_{f_a f_b} \cdot V_b + l \cdot V_a \cdot V_b. \tag{2.28}
 \end{aligned}$$

This polynomial expression depends mostly on the coefficient of variation of the origin marginal distributions of each couple of rv (a, b) and their marginal distribution. The coefficients of the polynomial are listed according to the type of marginal distributions.

For the distribution type used in this dissertation, the coefficients are defined in table 2.1.

Finally the correlation matrix between each couple of Nataf distributed r.v. is given in Eq.2.29.

$$\mathbf{R}_{\mathbf{U}\mathbf{U}} = \{N_{ij}; \rho_{ij}\}. \quad (2.29)$$

V_a	V_b	$N(V_b, V_a)$
N	N	1
LN	LN	$\frac{\text{Ln}(1+r_{f_a f_b} \cdot V_a \cdot V_b)}{r_{f_a f_b} \sqrt{\text{Ln}(1+V_a^2)\text{Ln}(1+V_b^2)}}$
N	LN	$\frac{V_b}{\sqrt{\text{Ln}(1+V_b^2)}}$
N	W	$1.031 - 0.195 \cdot V_a + 0.328 \cdot V_a^2$
LN	W	$1.031 - 0.011 \cdot V_a + 0.22 \cdot V_a^2 + 0.052 \cdot r_{f_a f_b} + 0.002 \cdot r_{f_a f_b}^2 + 0.005 \cdot r_{f_a f_b} \cdot V_a - 0.21 \cdot V_b + 0.35 \cdot V_b^2 - 0.174 \cdot r_{f_a f_b} \cdot V_b + 0.009 \cdot V_a \cdot V_b$

Table 2.1: Coefficient of the polynomial approximation.

N: Normal Distribution.

LN: Lognormal Distribution.

W: Weibull Distribution.

2.5.2 The Design Point: The H-L-R-F Algorithm

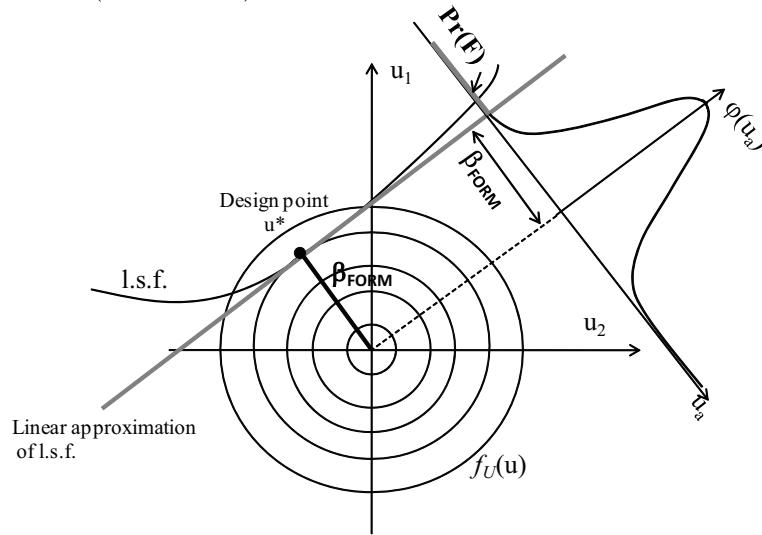
Once the l.s.f. has been linearized and the r.v. \mathbf{X} of the problem transformed into Standard Normal variables, in order to find the design point \mathbf{u}^* we use the line search based algorithm of Hasofer-Lindt-Rackwitz-Fissler.

The linearization of the l.s.f. in \mathbf{u}^* means that we are approximating the l.s.f. in \mathbf{u}^* with its tangent. This means also that the probability integral

2.5 First Order Reliability Method (FORM)

$P_r(g(x) \leq 0)$ is approximated by $P_r(G_U(u) \leq 0)$ (see figure 2.4).

Figure 2.4: l.s.f and β point in the standard normal space when two dimensions are considered (Straub 2010).



Here the main steps of HLRF Algorithm are summarized.

The HLRF algorithm consists in an iterative gradient based procedure to evaluate the l.s.f. in a set of points until the convergence to the optimal solution (*design point*) inside the space of the Standard normal Variables. First it is needed to set the start point of the iteration at the origin of the standard normal space $\mathbf{U}_0 = \emptyset$. To start the step-algorithm the gradient $\nabla g(\mathbf{U}_0)$ of the limit state function g is evaluated at the start point and then the displacement vector between the point \mathbf{U}_0 and the first point \mathbf{U}_1 of the algorithm is evaluated with the expression 2.30.

$$d_1 = \left[\frac{G(U_0)}{\|\nabla G(U_0)\|} + \alpha_0 U_0 \right] \alpha_0^T - U_0. \quad (2.30)$$

where α_0 is the row vector of the gradient components (with changed sign) as computed with the Eq.2.31 and normalized respect to the norm of the gradient of the limit state function $G(U)$. The vector α_0 represents a measure of the weight/importance of each component on the solution:

$$\alpha_0 = -\frac{\nabla G(U_0)}{\|\nabla G(U_0)\|}. \quad (2.31)$$

The new point of the step algorithm is computed as in Eq. 2.32

$$U_1 = U_0 + d_1. \quad (2.32)$$

By generalizing the Eqs.2.30 and 2.31, the next steps of the algorithm are computed with Eqs. 2.33 and 2.34.

$$d_{i+1} = \left[\frac{G(U_i)}{\|\nabla G(U_i)\|} + \alpha_i U_i \right] \alpha_i^T - U_i. \quad (2.33)$$

$$\alpha_i = -\frac{\nabla G(U_i)}{\|\nabla G(U_i)\|}. \quad (2.34)$$

The iteration process is computed until the components of the displacement vector d_i are smaller than a certain error ε : $|d_i| \leq \varepsilon$. This corresponds to minimize the distance of the design point u^* to the origin of the standard normal space.

The design point \mathbf{U}^* is therefore defined in Eq. 2.35, with the constraint

2.5 First Order Reliability Method (FORM)

that $G_U(u) = 0$, i.e u^* belongs to the surface defined by the l.s.f. G .

$$\mathbf{U}^*: \beta_{FORM} = \min \sqrt{(\mathbf{U} - \mathbf{M}_x)^T \mathbf{R}_{UU}^{-1} (\mathbf{U} - \mathbf{M}_x)}. \quad (2.35)$$

The reliability index is in this way equal to the length of the vector that defines the position of \mathbf{U}^* into the standard normal space (Eq. 2.36).

$$\beta_{FORM} = \sqrt{|\mathbf{U}^*|}. \quad (2.36)$$

2.6 The Probability of Failure of a System of Components

In the case of a system of m components, the system has m ways to fail. Mathematically, we have m limit state surfaces that intersect pair wise in the space of the r.v. leading to sets of singular points, which are points at which the limit-state surface is not differentiable.

Generally, two kind of system can be defined:

- *Series system*, if the failure of one component i leads to the failure of the system (weakest link)

$$F_s = \bigcup_{i=1}^m F_i \quad (2.37)$$

.

- *Parallel systems*, if all the components must fail to have the total failure of the system

$$F_p = \bigcap_{i=1}^m F_i \quad (2.38)$$

.

Any system can be generally represented both as a series system of parallel systems and as a parallel system of series systems, where the failure event F is defined as:

$$F = \bigcup_{i=1}^m \left(\bigcap_{j=1}^i F_j \right) \text{ or } F = \bigcap_{i=1}^m \left(\bigcup_{j=1}^i F_j \right). \quad (2.39)$$

2.6 The Probability of Failure of a System of Components

For example, a statically determined structure can be modeled as series system of elements, because the failure of one element leads the system to lose its load carrying capacity, while a statically indeterminate structure can have several failure modes and several of the single failure modes do not occur unless several structural elements have failed [6].

For an equally correlated system with correlation coefficient ρ and where each component has the reliability index β_i , we can define the safety margin for each component i in Eq. 2.40:

$$M_i = (a \cdot u_i + b \cdot v) + \beta_i. \quad (2.40)$$

Where a and b are constant parameters of the distribution of the safety margin and are equal to $a = \sqrt{(1 - \rho)}$ and $b = \sqrt{\rho}$.

It follows that the covariance between safety margins M_i and M_j of the components i and j is defined as $\text{COV}[M_i, M_j] = b^2 = \rho$ with $M_i \sim N(\beta_i, 1)$.

For a parallel system the probability of failure is given by the intersection between failure events, as given in the expression 2.41.

$$\begin{aligned} F_p &= \bigcap_{i=1}^m F_i = \bigcap_{i=1}^m \left\{ \alpha_i^T \cdot u + \beta_i \leq 0 \right\} = \\ &= \bigcap_{i=1}^m \{z_i \leq -\beta_i\} = \Phi_m(-\beta, \mathbf{R}) = \\ &= \prod_{i=1}^m \Phi_i \left(\frac{-\beta_i - \sqrt{\rho} \cdot v_i}{\sqrt{\rho}} \right). \end{aligned} \quad (2.41)$$

Where $\Phi_m(-\beta, \mathbf{R})$ is the m-variate standard normal CDF evaluated at the threshold β and with correlation matrix \mathbf{R} .

This allows one to compute the probability of failure with the integral Eq. 2.42.

$$P_r(F_p) = \int_{-\infty}^{\infty} \phi(\mathbf{v}) \left[\prod_{i=1}^m 1 - \Phi_i \left(\frac{-\beta_i - \sqrt{\rho} \cdot \mathbf{v}_i}{\sqrt{1-\rho}} \right) \right] d\mathbf{v}. \quad (2.42)$$

For a series system the probability of failure is given by the union of failure events as in Eq. 2.43.

$$\begin{aligned} F_s &= \bigcup_{i=1}^m F_i = \bigcup_{i=1}^m \left\{ \alpha_i^T \cdot u + \beta_i \leq 0 \right\} = \\ &= \bigcup_{i=1}^m \{z_i \leq -\beta_i\} = 1 - \bigcap_{i=1}^m \{z_i > -\beta_i\} = 1 - \bigcap_{i=1}^m \{z_i \leq \beta_i\} = \\ &= 1 - \Phi_m(\beta, \mathbf{R}) = \\ &= 1 - \prod_{i=1}^m 1 - \Phi_i \left(\frac{\beta_i - \sqrt{\rho} \cdot \mathbf{v}_i}{\sqrt{\rho}} \right). \end{aligned} \quad (2.43)$$

The probability of failure is finally given by integral in eq. 2.44.

$$P_r(F_s) = \int_{-\infty}^{\infty} \phi(\mathbf{v}) \left[1 - \prod_{i=1}^m 1 - \Phi_i \left(\frac{\beta_i - \sqrt{\rho} \cdot \mathbf{v}_i}{\sqrt{1-\rho}} \right) \right] d\mathbf{v}. \quad (2.44)$$

Obviously, if all the components have also the same reliability index, the productorial in the Eq. 2.42 and Eq. 2.44 becomes a power of m .

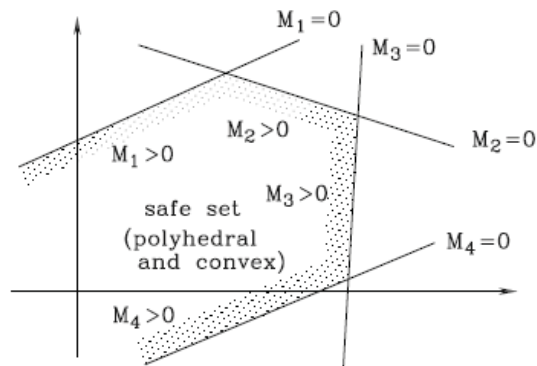
2.6 The Probability of Failure of a System of Components

For the case of non-equicorrelated system of components with different reliability indexes, several algorithms to compute the integral of the m-variate standard normal CDF can be found in the literature (see Genz [18], Joanni [23], Kang-Song [25]).

2.6.1 The Ditlevsen bounds

As described in the previous section, the probability of failure for a general system on m components, each with its linear safety margin M_i , can be described by a convex polyhedral safe domain (see figure 2.5), where each M_i represents an hyperplane. The set of safety margins are jointly normal distributed and when the M_i are almost plane and the β_i assumes large positive values, the computation of the m-dimensional normal distribution function $1 - \Phi_m(\beta, \mathbf{R})$ leads to small probability.

Figure 2.5: Polyhedral and convex safe set (O. Ditlevsen 2007).



By calling I_A and indicator function equal to 1 if $M_i > 0$ and null if $M_i < 0$, the indicator function for the safe set is equal to the productorial of the I_{s_i} safe sets of all the m components (see Eq. 2.45).

$$I_s = I_{s1} \cdots I_{sm}. \quad (2.45)$$

Let's consider the expression in Eqs. 2.46 and 2.47.

$$1 - I_s = 1 - I_1 \cdots I_m = 1 - I_1 + I_1 \cdot (1 - I_2) + \\ + I_1 I_2 \cdot (1 - I_3) + \cdots + I_1 I_2 I_3 \cdots I_m \cdot (1 - I_m). \quad (2.46)$$

$$I_1 \cdots I_m = \begin{cases} = \max \left\{ 1 - \sum_{j=1}^i (1 - I_j), 0 \right\} \\ \leq I_j, \text{ if } j < i \end{cases} \quad (2.47)$$

In Eq.2.47 the inequality is obvious. The equality assumes value equal to 1 only if all $I_j = 1$, and the unity value represents the maximum possible value. By substituting Eq. 2.47 in Eq. 2.46, Eqs. 2.48 and 2.49 are obtained.

$$1 - I_s = 1 - I_1 + \sum_{i=2}^m \left[\max \left\{ (1 - I_i) \left(1 - \sum_{j=1}^{i-1} (1 - I_j) \right), 0 \right\} \right]. \quad (2.48)$$

$$1 - I_s \leq 1 - I_1 + \sum_{i=2}^m [(1 - I_i) \min \{I_1, I_2, \dots, I_{i-1}\}] = \\ = 1 - I_1 + \sum_{i=2}^m [(1 - I_i) (1 - \max \{I_1, I_2, \dots, I_{i-1}\})] =$$

2.6 The Probability of Failure of a System of Components

$$= \sum_{i=1}^m (1 - I_i) - \sum_{i=2}^m \max_{j < i} \{(1 - I_i)(1 - I_j)\}. \quad (2.49)$$

From Eqs.2.48 and 2.49 it is straightforward to derive the following expression for the indicator function for the complementary set to the safe set I_s

$$I_f = 1 - I_s = \begin{cases} = I_{f1} + \sum_{i=2}^m \left[\max \left\{ I_{fi} - \sum_{j=1}^{i-1} (I_{fi} I_{fj}), 0 \right\} \right] \\ \leq \sum_{i=1}^m [I_{fi} - \sum_{i=2}^m \max_{j < i} \{I_{fi} I_{fj}\}] \end{cases} \quad (2.50)$$

By assuming that the expectation of a random indicator function I_A is the same as the probability $P(A)$ of the event A, from Eq.2.50, the Ditlevsen probability inequalities valid for an arbitrary probability distribution can be derived.

$$I_f \begin{cases} \geq P(F_1) + \sum_{i=2}^m \left[\max \left\{ P(F_i) - \sum_{j=1}^{i-1} (P(F_i \cap F_j)), 0 \right\} \right] \\ \leq \sum_{i=1}^m [P(F_i) - \sum_{i=2}^m \max_{j < i} \{P(F_i \cap F_j)\}] \end{cases} \quad (2.51)$$

With the definition of generalized reliability index as $\beta = -\Phi^{-1}[P(F)]$, it is formally assigned a normal distribution to the space of input variables, such that this normal distribution has the same second-moment representation of the vector of input variables \mathbf{X} . Therefore the expression in Eq.2.51 gives a valid bounds to the reliability index by setting $P(F) = \Phi(-\beta)$ and $P(F_i \cap F_j) = \Phi_2(-\beta_i, -\beta_j; \rho_{ij})$, for $j = 1, \dots, m$.

Chapter 3

Structural Model

Large-span timber roofs are realized by primary and secondary elements in a rectangular arrangement. Secondary structures are either realized as statically determinate or indeterminate systems. The latter are often preferred since they feature a more efficient bending stress distribution and enable load distribution in case of a local damage, but they might also facilitate progressive collapse. The primary elements are usually simply supported beams, usually realized with a shape which is optimized with regard to bending stresses.

3.1 Large-Span Timber Roof Description

The investigated structure is a simple but typical timber roof system (figure 3.1). The structural system, shown in figure 3.2, is exemplary for common

structural designs for large-span roofs of sport-arenas, industrial factories or farm storage buildings. The roof covers an area of $lxw = 30.0m \times 20.0m$ and is supported by 6 primary pitched cambered beams at a distance $e=6.0m$. The secondary elements (purlins) are mounted on the primary elements, which feature a pitch angle of 10° .

Three different configurations of the secondary system are studied: (a) purlins designed as simply supported elements; (b) purlins designed as continuous beams; (c) purlins designed as lap-jointed beams (figure 3.3). This system has been already subject to a previous deterministic analysis (Dietrich and Winter 2010 [7]).

The purlins are realized with timber grade C24, with dimensions summarized in table 3.1 and characteristic value of the strength in table 3.2. The distance between the purlins e_p is selected to achieve a utilization factor between 0.9 and 1, calculated according to [14]. The resulting values of e_p for different configurations are given in table 3.1.

Configuration	distance [m] e_p [mm]	width [mm]	height [mm]
Simply Supported (a)	1.0	100	200
Continuous (b)	1.2	100	200
Lap-Jointed (c)	1.6	100	200

Table 3.1: Dimensions and layout of the secondary system.

Usually, structural timber sections have a high ratio $h/b \geq 2$ in order to achieve a high capacity in the vertical plane, due to the fact that timber elements are mostly loaded in bending. This leads also to a sensitivity to lateral buckling, but the dimension chosen here are still in a range that is

3.1 Large-Span Timber Roof Description

Figure 3.1: Illustration of a typical large-span timber roof system (Dietsch and Winter 2010).

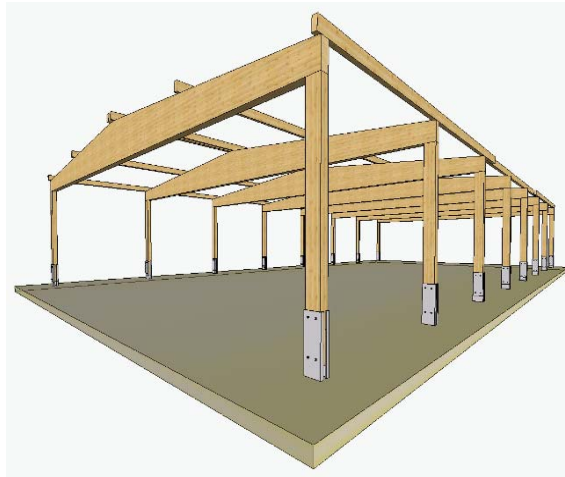
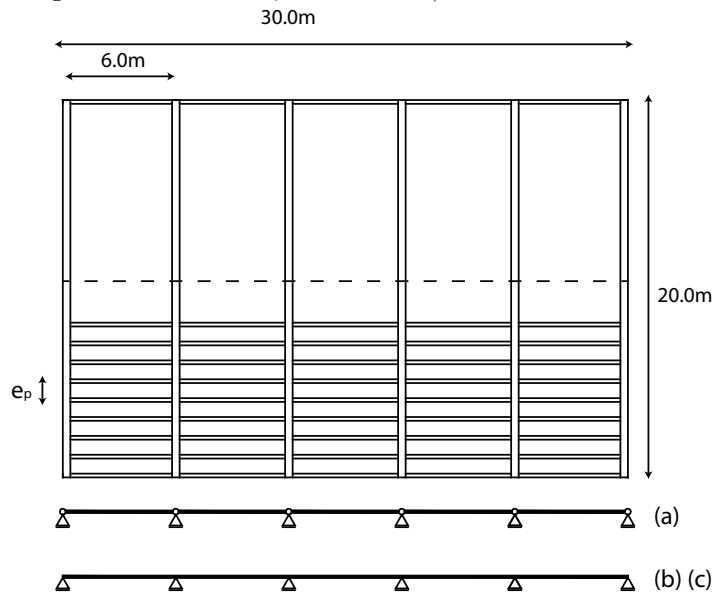


Figure 3.2: Geometry of the roof (Dietsch and Winter 2010).



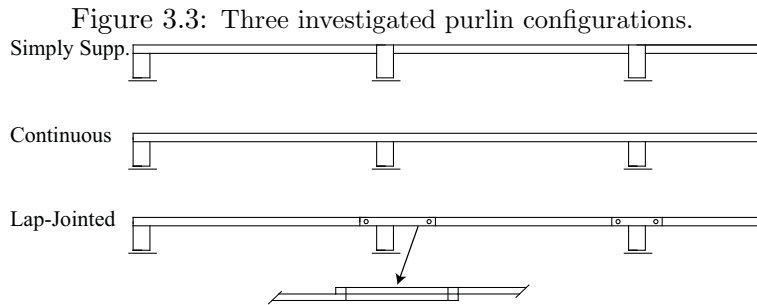


Table 3.2: Characteristic values of the strength according to DIN338 [9].

		Nadelholz														Laubholz						
		C14	C16	C18	C20	C22	C24	C27	C30	C35	C40	C45	C50	D18	D24	D30	D35	D40	D50	D60	D70	
Festigkeitseigenschaften (in N/mm ²)																						
Biegung	$f_{m,k}$	14	16	18	20	22	24	27	30	35	40	45	50	18	24	30	35	40	50	60	70	
Zug in Faserrichtung	$f_{t,0,k}$	8	10	11	12	13	14	16	18	21	24	27	30	11	14	18	21	24	30	36	42	
Zug rechtwinklig zur Faserrichtung	$f_{t,90,k}$	0,4	0,4	0,4	0,4	0,4	0,4	0,4	0,4	0,4	0,4	0,4	0,4	0,6	0,6	0,6	0,6	0,6	0,6	0,6	0,6	
Druck in Faserrichtung	$f_{c,0,k}$	16	17	18	19	20	21	22	23	25	28	27	29	18	21	23	25	26	29	32	34	
Druck rechtwinklig zur Faserrichtung	$f_{c,90,k}$	2,0	2,2	2,2	2,3	2,4	2,5	2,6	2,7	2,8	2,9	3,1	3,2	7,5	7,8	8,0	8,1	8,3	9,3	10,5	13,5	
Schub	$f_{v,k}$	3,0	3,2	3,4	3,6	3,8	4,0	4,0	4,0	4,0	4,0	4,0	4,0	3,4	4,0	4,0	4,0	4,0	4,0	4,5	5,0	
Steifigkeitseigenschaften (in kN/mm ²)																						
Mittelwert des Elastizitätsmoduls in Faserrichtung	$E_{0,mean}$	7	8	9	9,5	10	11	11,5	12	13	14	15	16	9,5	10	11	12	13	14	17	20	
5 %-Quantil des Elastizitätsmoduls in Faserrichtung	$E_{0,05}$	4,7	5,4	6,0	6,4	6,7	7,4	7,7	8,0	8,7	9,4	10,0	10,7	8	8,5	9,2	10,1	10,9	11,8	14,3	16,8	
Mittelwert des Elastizitätsmoduls rechtwinklig zur Faserrichtung	$E_{90,mean}$	0,23	0,27	0,30	0,32	0,33	0,37	0,38	0,40	0,43	0,47	0,50	0,53	0,63	0,67	0,73	0,80	0,86	0,93	1,13	1,33	
Mittelwert des Schubmoduls	G_{mean}	0,44	0,5	0,56	0,59	0,63	0,69	0,72	0,75	0,81	0,88	0,94	1,00	0,59	0,62	0,69	0,75	0,81	0,88	1,06	1,25	
Rohdichte (in kg/m ³)																						
Rohdichte	ρ_k	290	310	320	330	340	350	370	380	400	420	440	460	475	485	530	540	550	620	700	900	
Mittelwert der Rohdichte	ρ_{mean}	350	370	380	390	410	420	450	460	480	500	520	550	570	580	640	650	660	750	840	1080	
ANMERKUNG 1 Die oben angegebenen Werte für die Zug-, Druck- und Schubfestigkeit, das 5 %-Quantil des Elastizitätsmoduls, der Mittelwert des Elastizitätsmoduls rechtwinklig zur Faserrichtung und der Mittelwert des Schubmoduls wurden mit den in Anhang A angegebenen Gleichungen berechnet.																						
ANMERKUNG 2 Die tabellierten Eigenschaften gelten für Holz mit einem bei 20 °C und 65 % relativer Luftfeuchte üblichen Feuchtegehalt.																						
ANMERKUNG 3 Es kann sein, dass Bauholz der Klasse C45 und C50 nicht immer zur Verfügung steht.																						
ANMERKUNG 4 Die charakteristischen Werte für die Schubfestigkeit werden entsprechend EN 408 für Holz ohne Risse angegeben. Die Auswirkung von Rissen sollte in Bemessungsnormen behandelt werden.																						

3.1 Large-Span Timber Roof Description

insensitive to buckling.

The purlins in the three configurations have the same section, while the distance between the axis of the purlins is chosen so that the utilization factor according to EC5 [14] is in the range $0.9 < \eta < 1$. The resulting distances e_p between purlins are: a) 1.0m, b) 1.2m and c) 1.6m as in table 3.1.

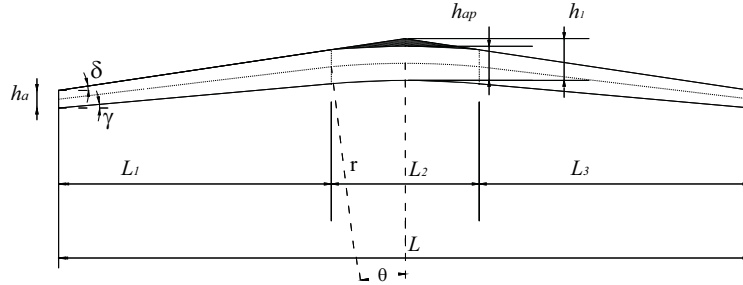
It is assumed that the connection between purlins and primary beams is realized with constraint that behaves like an hinge (angle-iron with bolts or screws). The joints are not modeled in this dissertation, therefore some assumption need to be stated. The joints are assumed intact and with a different capacity according to the the three different configurations.

The three static configurations chosen are the most common one. In addition, the simply supported configuration can be preferred because it is easy to build and assures a certain degree of compartmentalization, given that each element is independent, but it's more expensive due to the higher number of elements and connections to build. The continuous configuration allow to use a lower number of elements, but the cost are affected by the quality control of the finger joint made to obtain a unique purlin to cover the entire length. The Lap-jointed configuration is often preferred for the lower cost of building. In fact, the doubling of the section across the support allows also to have a slightly bigger section where the bending moment is higher.

The primary beams are made of glued laminated (glulam) timber of grade GL24c and feature the shape shown in Figure 3.4. The correspond-

ing dimensions are listed in table 3.3.

Figure 3.4: Pitched cambered glulam beam with a mechanically fixed apex.



Geometrical parameters	Size
Span L [m]	20
Span L_1 [m]	7.866
Span L_2 [m]	4.268
Span L_3 [m]	7.866
distance e [m]	6.0
Width b [mm]	180
Heigth at the support h_a [mm]	600
Heigth at the support h_{ap} [mm]	1163
Angle upper edge δ	10
Angle lower edge γ	6
Inner radius r [m]	20
Lamella thickness t [mm]	32

Table 3.3: Dimensions of the primary beams.

The choice of a special shape is motivated by the wide length of the element so that the dimension are strongly influenced by the serviceability check (displacement check) and by local shape effect on the stress distribution (e.g. tension perpendicular to the grain).

3.1 Large-Span Timber Roof Description

Table 3.4: Characteristic values of the strength for glulam from DIN14080 [11].

Festigkeitsklasse von Brettschichtholz		GL 20c	GL 22c	GL 24c	GL 26c	GL 28c	GL 30c	GL 32c
Biegefestigkeit	$f_{m,g,k}$	20	22	24	26	28	30	32
Zugfestigkeit	$f_{t,0,g,k}$	14	17	18	18,5	19,5	20	20
	$f_{t,90,g,k}$	0,5						
Druckfestigkeit	$f_{c,0,g,k}$	17,5	21	22,5	23	24	25	25
	$f_{c,90,g,k}$	2,5						
Schubfestigkeit (Schub und Torsion)	$f_{v,g,k}$	3,5						
Rollschubfestigkeit	$f_{r,g,k}$	1,2						
Elastizitätsmodul	$E_{0,g,mean}$	9 000	10 000	11 000	11 500	12 500	12 500	13 000
	$E_{90,g,mean}$	300						
Schubmodul	$G_{g,mean}$	650						
Rollschubmodul	$G_{r,g,mean}$	65						
Rohdichte	$\rho_{g,k}$	340	350	370	380	390	390	400
	$\rho_{g,mean}$	370	390	400	410	420	420	430

The timber GL24c is a composite of strength-graded wood laminations, which are flat wise glued together. In this case, the external laminations correspond to the class C24 and the internal one to class C16 (see table 3.4). In fact, in bending condition only the external laminations are subjected to high stresses so that a higher class of timber is needed, while for the shear or tension perpendicular to the grain the strength resistance is quite similar in all classes of timber depending only on the grain density (see table 3.4). The use of composite glulam allows to optimize further the costs and material use and it also enables members with varying cross-sections. All the strength values refer to a moisture content of 12%, i.e. to a relative humidity of 65% at 20C.

3.2 Timber deterministic design rules

Wood is a cellular composite material and the micro-structure of the wood cells rules the characteristic anisotropic behavior of the material. Therefore, the density is the single most important physical characteristic of wood because the strength depends from the density of the cells.

The water content also has influence on the mechanical properties. The anisotropic shrinkage caused by the drying process can cause distortions. In order to avoid distortions, the finite timber product is subjected to a strong quality control. In addition, the moisture content influences the strength. Generally, bending strength is higher than both compression and tensile strength. However, the bending behavior at failure depends on moisture content. In bending at low moisture content, failure is governed by areas in high tension. At high moisture content the failure is governed by areas of high compression. The failure governed by tensile areas is more dangerous because it exhibits a brittle behavior, while compression failure can be characterized by an extensive yielding behavior due to creases.

Both EC5 [14] and DIN1052 [10] define three use classes according to moisture condition of timber. Service class 1 shows higher compression strength than tensile strength for a given quality of wood.

Class 1 timber will fail always in brittle way and therefore only a linear distribution of stresses can be assumed in design. Class 1 is characterized by values of moisture content not bigger than 65% at 20C.

Timber of service class 2 shows a brittle failure behavior for low quality wood and a ductile behavior for high quality wood. Class 2 is character-

3.2 Timber deterministic design rules

ized by values of moisture content not bigger than 85% at 20C.

Service class 3 timber shows a lower strength in compression than in tension for all quality levels of timber. The bending failure starts with creases of compressed wood and as the bending moment increases, the neutral axes moves to the tensile region giving a large zone of the cross section in compression. Class 3 is characterized by values of moisture content bigger than 85% at 20C.

The Italian code reference for timber structure is the "N.I.CO.LE" design rules, but it is mostly an agreement on the design rules of EC5 adapted to the Italian conditions. However, most of the engineers refer always to EC5 [14], to the German code DIN1052 (2008) [10] and to the Swiss Code SIA265 [34].

As other building materials, timber design rule refer to two limit state design condition: ultimate limit state and serviceability.

The limit state condition for design is an essential condition and assures a certain strength level according to design load within an acceptable safety margin. The ultimate state can be both the collapse and an exceeding level of damage or danger for the people, but also the loss of stability, exceeding deformation, joint failure and kinematic conditions.

Serviceability condition of design assures a good serviceability condition during the life-time of the structure by giving a certain limit to the deformations under service loads. In addition, exceeding deformations can change the load condition of the structure and therefore the safety margin at limit state condition can change.

The aim of limit state design is to get a probability of exceeding the limit state assigned that is low enough for the structure in relation to the type of the structure (large-span roof, building, art-work), to the impact of the structure use (importance) and to life-cycle assigned.

The limit state design condition consists in fulfilling the requirement in Eq. 3.1.

$$S_d = \gamma_f \cdot S_k \leq \frac{R_k \cdot K_{mod}}{\gamma_m} = R_d. \quad (3.1)$$

S_d is the design action (e.g. bending moment, axial force) on the section object of the check, i.e. the highest action possible defined as the action with the probability of being exceeded of 5%. S_k is the characteristic value of the action with 5% fractile computed under the assumption of linear elastic structural behavior. γ_f is the load safety factor as defined in (see Eq.2.3 of section 2.2). R_d is the design strength of the section, i.e. the smallest strength defined as the strength value associated to the probability of 99.5% to be exceeded. R_k is the characteristic value of the strength defined as the 5% fractile value and computed according to the real behavior of the structure. γ_m is a safety factor that counts for the uncertainty of strength. K_{mod} is a coefficient that counts for the duration of the load and for environmental conditions.

In the computations, it will be assumed a value of 1 both for the factors K_{mod} , due to the assumption of load acting for a short interval of time, and for the γ because in reliability analysis a full probabilistic analysis is done and therefore no safety factor is needed.

3.3 Failure modes for a purlin

The evaluation of Eq. 3.1 is needed for any possible load condition. Therefore, in the code the load value is defined as combination of the loads. The load combination for ultimate limit state is defined in Eq.3.2.

$$S_d = \gamma_g \cdot G_k + \gamma_q \cdot \left[Q_{1k} + \sum_{i=2}^n \psi_{0i} \cdot Q_{ik} \right]. \quad (3.2)$$

In Eq. 3.2, G_k is the characteristic value of dead load, Q_{1k} is the characteristic value of the action to which the load combination refers to, Q_{ik} is the characteristic value of the independent action i among the action n . The factors γ_g and γ_q are the partial safety factors for dead load G and the action Q , and ψ_{0i} are the factors for combining of the loads Q_{ik} according to ultimate state. Usually the factors ψ_{0i} are assumed equal to 0.7.

The load combination for serviceability state is defined in Eq.3.3.

$$S_d = G_k + \psi_{11} \cdot Q_{1k} + \sum_{i=2}^n (\psi_{2i} \cdot Q_{ik}). \quad (3.3)$$

In Eq.3.3, the load combination coefficient ψ_{11} is equal to 1 for rare conditions, is 0 for permanent conditions and a values that changes according to the use of the structure for frequent condition (see [14]). The coefficient ψ_{2i} is equal to ψ_{0i} for rare conditions, while it changes according to the use of the structure for frequent and permanent conditions.

3.3 Failure modes for a purlin

According to the three assumed static configurations, the roof secondary elements are mostly subjected to a combination of bending moments. For

the special case of the lap-jointed purlins the computation of the bending moment is done without considering the change of the moment of inertia for the section coupling length across the joints. This is verified to be more conservative. Only in the section bending check, the change of the moment of inertia is considered in order to know if the section is really failed or not. This is possible because it is assumed that the two parts in the lap-joint connection are fully bonded.

The behaviour of the element in bending is assumed to be brittle with a linear distribution of the strain until failure, that means that when a section inside of the element is failed the entire element is considered to be failed (weakest link).

An important assumption is that no torsional stiffness is considered between the purlins that are next to each other, so that there isn't any collaboration in carrying the load, but each element carries just a load proportional to its area of influence.

For this analysis, only the bending failure mode is considered, shear failures, buckling failures and failures of joints are neglected, since in this case the bending failure is the main failure mechanism.

Bending failure at cross-section j is described by the limit state function in Eq. 3.4.

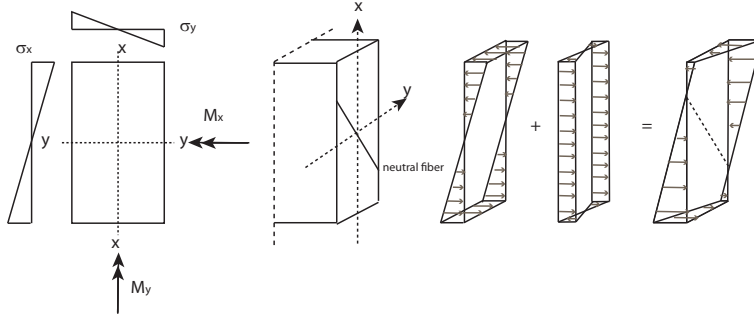
$$g_j = 1 - \max \left\{ \left(\frac{M_{Sx,j}}{M_{Rx,j}} + k_m \frac{M_{Sy,j}}{M_{Ry,j}} \right), \left(k_m \frac{M_{Sx,j}}{M_{Rx,j}} + \frac{M_{Sy,j}}{M_{Ry,j}} \right) \right\}. \quad (3.4)$$

$M_{Si,j}$ denotes the bending moment and $M_{Ri,j}$ denotes the bending capacity at cross section j in direction i (two-axial stress field shown in figure 3.5)

3.3 Failure modes for a purlin

due to the roof inclination of 10°). This limit state function represents a linear approximation of the resistance domain in the elastic stress-deformation field given in the EC5 [14]. The coefficient k_m takes into account the stress

Figure 3.5: Rectangular cross section subjected to biaxial bending.



distribution and the not homogeneity of the material. The failure in biaxial bending does not occur always for the highest stress at the corner of the rectangular section, as for the homogeneous materials and so the coefficient k_m is introduced. For rectangular sections k_m is equal to 0.7.

Several authors [4, 26, 27, 42] introduce a correction factor in the limit state function to account for the approximation made by this failure criterion. Since we believe that further investigation is necessary to better understand this factor, it is omitted in this study.

The bending moments are given in Eqs. 3.5 and 3.6.

$$M_{Sx,j} = a_{x,j} \cdot [C \cdot Q + G \cdot a_{cs} + P]; \quad (3.5)$$

$$M_{Sy,j} = a_{y,j} \cdot [C \cdot Q + G \cdot a_{cs} + P]; \quad (3.6)$$

The load coefficients $a_{x,j}$, $a_{y,j}$ depend on the structural configuration (a-b-c) and the location j along the longitudinal axis; a_{cs} is the cross section area of the purlins; the remaining variables are random variables describing the loads:

- Snow load on the ground Q;
- Shape factor C (snow load on the roof);
- Timber specific weight G;
- Permanent load P.

The bending capacities in Eqs. 3.5 and 3.6 are described by Eqs. 3.7 and 3.8.

$$M_{Rx,j} = R_j \cdot \frac{2I_x}{d_y}. \quad (3.7)$$

$$M_{Ry,j} = R_j \cdot \frac{2I_y}{d_x}. \quad (3.8)$$

Where R_j is the bending strength at cross section j , I_x and I_y are the inertia of the section and d_x, d_y are the width and depth of the purlins. The resistance of the elements is computed neglecting any time-dependency of the property of the material.

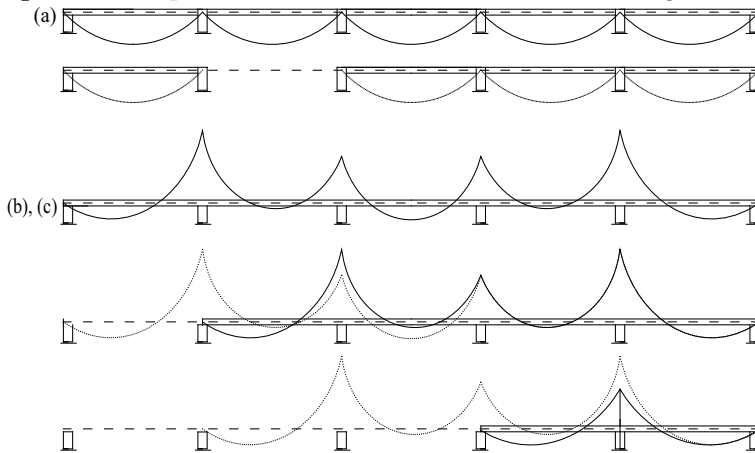
Each purlin is evaluated at discrete cross sections at distances of 0.5m along its longitudinal axis, based on the approximate distance between weak sections (e.g. knots) in the timber [27, 41].

Failure at a section j occurs when $g_j \leq 0$, where g_j is defined by Eq. 3.4.

3.3 Failure modes for a purlin

The purlin is modeled as a series system, that means that any failure of a section leads to failure of the purlin. Failure of a purlin leads to changes in the static scheme for configurations (b) and (c). Therefore, upon failure of one or more sections, the coefficients $a_{lx,j}$ and $a_{ly,j}$ in Eqs. 3.7 and 3.8 are recalculated and all sections are then evaluated with these values. In this way, the possibility of progressive failures is accounted for. This is illustrated in Figure 3.6.

Figure 3.6: A possible failure scenario for the three configurations.

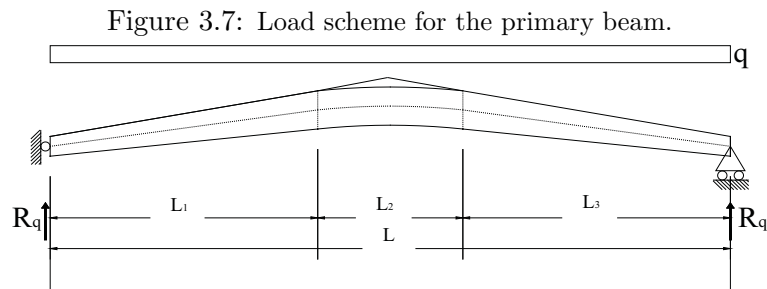


Furthermore, failure of the secondary system F is defined as the failure of one or more purlins. Therefore, also the roof is considered failed, when any of the discrete elements fail. This is justified by considering that the failure of an element will be detected immediately and corrective actions will be taken upon failure of one element.

3.4 Failure modes for the beam

The primary system is realized with glulam beams of special shape in order to cover a large span. The load on the beams consists of the vertical forces from the secondary elements (purlins) and the self weight of the beams. This load is modeled as a uniformly distributed load on the beam (see figure 3.7).

In the ultimate limit state condition, the glulam beam of figure 3.4 can



be subject to four failure mechanisms:

- Failure due to bending;
- Failure due to tension stresses perpendicular to the fibers in the curved section (inside the length L_2 of Figure 3.4);
- Failure due to shear across the support region;
- Failure due to a combined effect of tension perpendicular to the grain and shear stresses.

To evaluate the performance of the primary system, each beam is evaluated at discrete cross-sections at distances of 0.5m along its longitudinal axis,

3.4 Failure modes for the beam

based on the approximate distance between weak sections (e.g. knots) in the timber [27, 41]. Failure at a cross section j is described by limit state functions (l.s.f.) $g_{x,j}$, where index x identifies the failure mode. Failure mode x occurs in section j when $g_{x,j} \leq 0$.

3.4.1 Limit state function for bending failure of the primary beam

The l.s.f. for bending failure is defined as:

$$g_{b,j} = 1 - \frac{\sigma_{b,j}}{f_{b,j}} = k_j \frac{M_j}{k_r f_{b,j} b h_j^2 / 6}. \quad (3.9)$$

where $\sigma_{b,j}$ is the maximum tensile stress in the cross-section due to bending, $f_{b,j}$ is the bending resistance of section j , M_j is the bending moment in section j , b is the width and h_j is the height of the section.

The factor k_r takes into account the strength reduction due to bending of the laminates during the production and is here equal to 1. The coefficient $k_j \leq 1$ accounts for the non-linear distributions of stresses in the cross-section (figure 3.8).

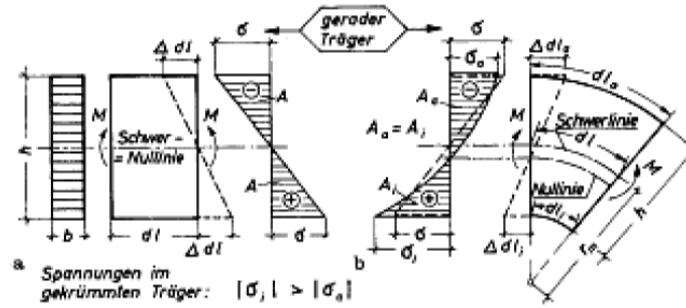
k_r is here defined as in [10, 14]:

$$k_j = \begin{cases} 1 + 4 \tan^2 (\delta - \gamma) & \text{if } j \in L_1, L_3; \\ 1 + 0.35 \left(\frac{h_{ap}}{r} \right) + 0.6 \left(\frac{h_{ap}}{r} \right)^2 & \text{if } j \in L_2 \end{cases}. \quad (3.10)$$

In Eq. 3.10, δ , γ , h_{ap} and r are geometrical parameters (see figure 3.4).

Due to the height of the section ($h \geq 600mm$ for glulam [10, 14]), the vol-

Figure 3.8: Distribution of the bending stresses in the curved beam.



ume effect in bending (height effect) is here neglected.

3.4.2 Limit state function for tension perpendicular to the grain failure of the primary beam

The limit state function for failure due to tension stresses perpendicular to the grain, which is relevant only for the curved sections of the beam, is given by:

$$g_{t90,j} = 1 - \frac{\sigma_{t90,j}}{f_{t90,j} k_{dis} k_{vol}}. \quad (3.11)$$

In 3.11, $f_{t90,j}$ is the tension strength perpendicular to the grain. The coefficient k_{dis} accounts for the shape and k_{vol} accounts for the volume effect of the beam. It is $k_{dis} = 1.4$ for double tapered and curved beams and $k_{vol} = \left(\frac{V_0}{V}\right)^{0.2}$ for glulam timber beams, with reference volume $V_0 = 0.01m^3$ [14]. The tension $\sigma_{t90,j}$ at the section j is computed according to Blumer

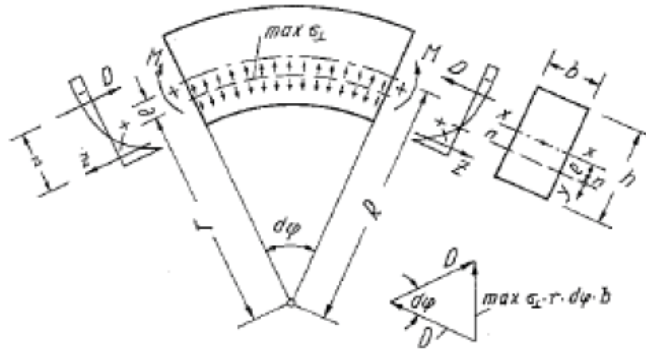
3.4 Failure modes for the beam

formulation [2]:

$$\sigma_{t90,j} = \frac{M_j}{bh_{ap}e} \left[\text{Ln} \left(\frac{\beta - \frac{e}{h_{ap}}}{\beta - 0.5} \right) + \frac{h_{ap}}{r} \left(\frac{e}{h_{ap}} - 0.5 \right) \right]. \quad (3.12)$$

In the expression above, it is $\beta = R/h_{ap}$, $r = h/\text{Ln} \left(\frac{\beta+0.5}{\beta-0.5} \right)$ and $e = R - r$ (see figure 3.4). R is the curvature radius with respect to the center of the section, b is the section width, h_{ap} is the beam height at apex (see Figure 3.9).

Figure 3.9: Tension perpendicular to the grain.



3.4.3 Limit state function for shear failure of the primary beam

The limit state function for shear failure in section j is defined as:

$$g_{v,j} = 1 - \frac{\tau_{v,j}}{f_{v,j}}. \quad (3.13)$$

In Eq. 3.13, $\tau_{v,j}$ is the maximum shear stress and $f_{v,j}$ is the shear strength in section j .

In the straight sections of the beam ($j \in L_1, L_3$) the maximum shear stress follows the Jourawski law for rectangular sections, while in the curved sections ($j \in L_2$), the stress along the depth is computed according to Blumer [2].

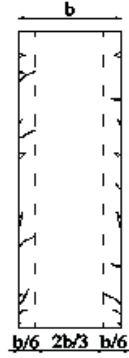
$$\tau_{v,j} = 1.5 \frac{V_j}{A_j}, \quad j \in L_1, L_3. \quad (3.14)$$

$$\begin{aligned} \tau_{v,j} = & \left[(1.5 - 6e^2) + (3.13e + 0.5e^2 - 12.5e^3) \frac{h_{ap}}{R} + \right. \\ & \left. + (-0.693 - 0.565e - 0.438e^2 + 223e^3) \left(\frac{h_{ap}}{R} \right)^2 + \right. \\ & \left. + 0.346 \left(\frac{h_{ap}}{R} \right)^3 \right] \frac{V_j}{K_{cr} b h_{ap}}, \quad j \in L_2. \end{aligned} \quad (3.15)$$

In Eqs.3.14 and 3.15, V_j is the shear at section j , b is the beam width, h_{ap} is the beam height at apex, e is the depth of the neutral fiber and the factor k_{cr} (see [14]) takes into account the reduction of the section due to shrinkage cracks at the vertical side faces of the cross section. k_{cr} is taken as 2/3 (see figure 3.10).

3.4 Failure modes for the beam

Figure 3.10: Effective section due to shrinkage cracks.



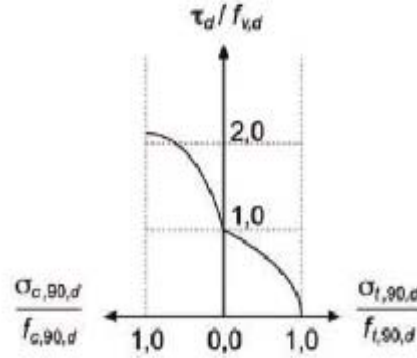
3.4.4 Limit state function for combined shear and tension perpendicular to the grain failure of the primary beam

The maximum values of shear stress and tension perpendicular to grain stress occur both in the central region of the cross section and the combined effect of these stresses can lead to a brittle sudden failure. This failure can be modeled by general resistance criteria [30]. There are several definition for this limit state surface (Haber-von Mises, Norris, Tsai and Wu as reported in [30]), but both the EC5 and DIN don't consider the combination of this two states. Here, the l.s.f. given in the Swiss Code [34] for modeling the combined failure mode is used. It is defined in 3.16 and figure 3.11.

$$g_{vt90,j} = 1 - \left\{ \left(\frac{f_{c90,j} + \sigma_{t90,j}}{f_{c90,j} + f_{t90,j}} \right)^2 + \right.$$

$$+ \left(\frac{\tau_{v,j}}{f_{v,j}} \right)^2 \left[1 - \left(\frac{f_{c90,j}}{f_{c90,j} + f_{t90,j}} \right)^2 \right] \}. \quad (3.16)$$

Figure 3.11: SIA-265 LSF for combined shear and tension perpendicular to the grain.



In Eq. 3.16, $f_{c90,j}$ and $f_{t90,j}$ are the strength in compression and tension perpendicular to the grain, $f_{v,j}$ is the shear strength of the section j and $\sigma_{t90,j}$ is the maximum tension stress at the section j according to Eq. 3.12. Even if both failure mechanisms for tension perpendicular to the grain and combined shear and tension perpendicular to the grain do not directly lead to global failure, these phenomena must be considered in the structural model as damage/deterioration events due to the loading process of the structure. These failure mechanisms cause the splitting of the cross section of the beam due to the propagation of a crack either from the supports (shear) or from the mid-span inside the curved region $j \in L_2$ (tension perp.). Because the maximum shear as well as tension perpendicular to grain stresses occur in the central region of the cross section, it is reasonable to consider that the cross section is divided in two parts over a certain

3.5 Failure modes for large span roofs: system behavior

length of the beam, once one of these two mechanisms arises. This leads to a lower bending capacity of the beam and to a higher vertical displacement under the load (lower elastic stiffness). This additional displacement has an effect on the secondary system load condition.

3.5 Failure modes for large span roofs: system behavior

The roof system is modeled as a series system of two subsystem: primary system (beams) and secondary system (purlins). System failure will occur when at least one primary or secondary element fails in bending.

The secondary system is considered to be failed when the purlins can no longer support the tertiary system in at least one location (i.e. when the roof "comes down"). It is then assumed that upon such a failure the structure will be closed and necessary actions will be taken (e.g. repairs, retrofitting).

The primary system is considered failed when at least one section of one beam is failed in bending. Upon bending failure of a primary beam, a percentage of the load acting on the beam will be transferred to the adjacent beams, due to the reserve capacity of the purlins and the connections. This effect occurs even if the beam is collapsing and can lead to progressive collapse of the roof due to this additional load transfer. This redistribution can reach a total value of 50% but also the 100% according to the connection details (ductility and plasticity reserve of the steel bolt and screws)

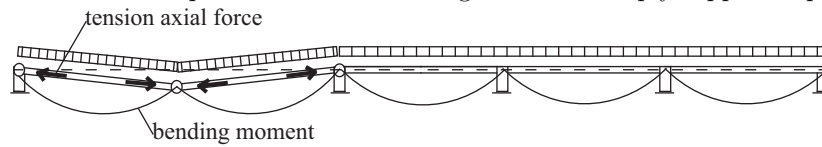
and to the "real" resistance of the purlins. This effect is included in the model by redistributing a percentage of the load carried by the failed beam to each of the adjacent beams. The primary system is then checked again with the new load configuration.

This simple model is applied independently of purlin configuration, but with a different redistribution factor. The applied redistribution factor is equal to 40% on each beam for the statically indeterminate configurations (continuous and lap-jointed purlin) for a total of 80%, while in the case of the statically determinate configuration this redistribution can vary strongly. Therefore, in the latter case the redistribution is assumed to vary inside the interval 10% and 40% on each beam.

In addition, failure of primary beams corresponds to a loss of support for the secondary system. For the statically determinate purlin configuration, failure of a beam will lead to longitudinal tension stresses in the purlins, because the failed beam will essentially hang on the purlins (see figure 3.12). In this case, combined bending and tension failure of the purlins is checked.

The new limit state function is defined in Eq. 3.17

Figure 3.12: Consequences of beam bending failure on simply supported purlins.



$$g_j = \min \left\{ 1 - \left(\frac{T_{S,j}}{N_{R,j}} + \frac{M_{Sx,j}}{M_{Rx,j}} + k_m \frac{M_{Sy,j}}{M_{Ry,j}} \right) \right\};$$

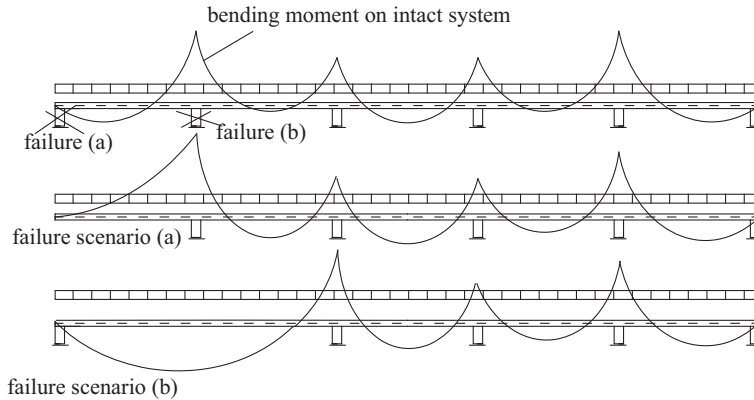
3.5 Failure modes for large span roofs: system behavior

$$1 - \left(\frac{T_{S,j}}{N_{R,j}} + k_m \frac{M_{Sx,j}}{M_{Rx,j}} + \frac{M_{Sy,j}}{M_{Ry,j}} \right) \} \quad (3.17)$$

$T_{S,j}$ is the additional tension force and $N_{R,j}$ the tensional capacity of the purlin at the section j .

For the statically indeterminate purlin configurations (b and c as shown in figure 3.3), failure of a beam will lead to a significant increase of bending demand in the purlins, which will almost certainly lead to failure of the purlins and consequently to system failure (see Figure 3.13). Failures of

Figure 3.13: Consequences of beam bending failure on continuous and lap-jointed purlins.



the primary beams due to shear and tension perpendicular to the grain will not directly lead to system failure. They can, however, lead to reduced bending capacity of up to 50% and thus facilitate bending failures of the beams. Mostly, the exceeding tensions perpendicular to the grain, inside the curved sector, cause the splitting of the grain (see figure 3.14).

In addition, these mechanisms lead to a loss of stiffness and therefore to a change in the load on the secondary elements (additional displacement of

Figure 3.14: Cracks due to tension perpendicular to the grain in a glulam beam (Holzforschung, MPA-BAU TUM).



the support). For the statically determinate purlins, the displacement of the support does not change the static condition and has no consequences. For statically indeterminate purlin configurations, the effect of the loss of stiffness in the primary beam is modeled by a displacement of the support of 100mm. This effect is included in the system assessment. When secondary elements fail in bending, the system will fail. Failures of secondary elements have no effect on the primary system, and, therefore, can be considered separately in the analysis.

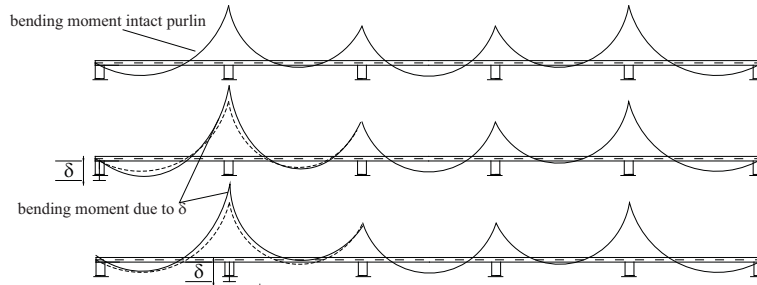
Figure 3.16 summarizes the analysis of the roof system.

3.6 Quantifying Risk and Robustness of the timber roof system

The results of numerical simulations will be used to assess robustness and risk of the chosen roof system. To compare risk and robustness of the three

3.6 Quantifying Risk and Robustness of the timber roof system

Figure 3.15: Consequences of beam displacement on continuous and lap-jointed purlins.



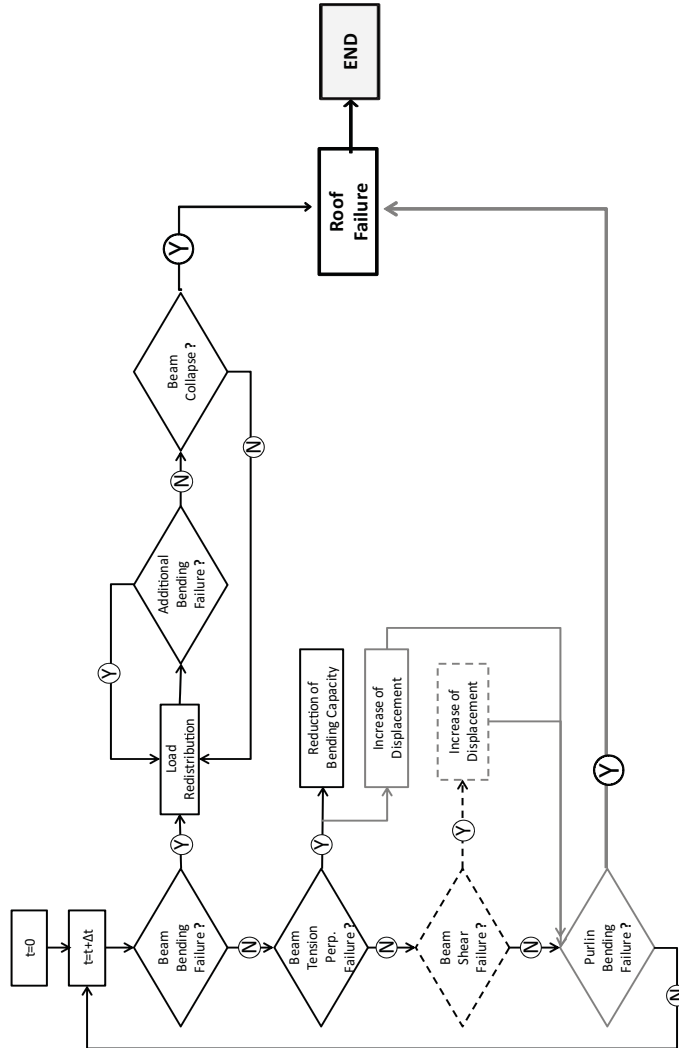
structural configurations of timber roofs, quantitative definitions of these characteristics are required. The definitions of measures for risk and robustness are provided in the following.

3.6.1 Definition and metric of Risk

Risk is generally defined as expected adverse consequences [22]. Consequences of a roof failure include fatalities, injuries, costs of repair or replacement of the structure and economical losses due to unavailability of the structure. Without making any assumptions on the use of the structure, a reasonable approximation for the consequences of a failure is to consider them as being proportional to the area of the roof that fails, A_F .

Let α be the proportionality factor that takes into account the use of the structure, the importance, people capacity and economical value. The risk can be defined as:

Figure 3.16: Flow chart of the failure analysis.



3.6 Quantifying Risk and Robustness of the timber roof system

$$E[\alpha A_F] = \alpha [A_F]. \quad (3.18)$$

where $E[\]$ is the expectation operation. For the purpose of comparing the pure structural behavior of the three different configurations of roof system, at this stage the factor α is neglected. The risk is therefore computed as the expected value of the area failed (see Eq.3.19) once the probability density function (pdf) $f_{A_F}(a)$ is defined.

$$E[A_F] = \int_0^{A_{roof}} a \cdot f_{A_F}(a) da. \quad (3.19)$$

3.6.2 Definition of a probability based Robustness criterion

As described already in section 1.5, structural robustness is generally understood as the ability of a structure (or of some part of it) to have a limited damage in case of failure due to unforeseen loads or damages. Therefore, the structural robustness is related to the behavior of the structure in terms of consequences to a failure or damage event.

Many authors [21, 37] relate robustness only to structural redundancy, which requires static indeterminacy and the avoidance of progressive collapse. Baker et al. [1] use the ratio between direct and indirect expected damage as a measure of robustness. This definition also includes the consequences of failure, and it requires computation of the risk (direct and indirect). The main idea is to achieve an optimal solution between additional cost to increase robustness and the reduction of failure consequences.

Therefore only a probabilistic approach can lead to the solution that fulfill this requirement (optimal solution)[3].

A criterion of evaluation of structural robustness is hereby proposed. It is based on the damage limit requirement reported in EN 1991-1-7 [13], which includes a damage limit requirement for floors: a failure should not lead to a failed area that exceeds the minimum between $100m^2$ and the 15% of the total area. This limit has been established for multi-stored frame buildings rather than single-stored, large-span structures. However, the limit of 15% is here adopted as a probability-based "robustness criterion" by converting it in a probabilistic measure: we calculate the probability that the failed area will be smaller than 15% of the total area, given a failure with the expression in Eq.3.20 (see also [29]).

$$\Pr [A_F < 15\% | F] = \int_0^{0.15 \cdot A_{roof}} f_{A_F|F}(a) da. \quad (3.20)$$

where $f_{A_F|F}$ is the conditional pdf of the failed roof area given a failure of the roof. Since the 15% threshold is somewhat arbitrary, the full conditional distribution of the failed area is also provided for assessing robustness.

Chapter 4

Timber Statistics

The natural growing process of wood determines the characteristics of timber material. Mostly, the dimension and density of wood cells is the interpretation key of timber behavior. In addition, the load bearing capacity of timber is governed by the presence and characteristics of natural growing defects that occur randomly inside the trees. This implies that the strength of timber elements also depends upon the size of the structural element and on the load condition.

Strength properties of structural timber are determined by direct testing of timber elements with standard procedures according to the stress state. Assuming that the theory of elasticity is valid, bending strength, compression, tension and shear capacity of timber elements are referred to the global behavior of an entire element and not to the material itself. In addition, according to [10], the influence of defects is implicitly included in the strength value specified for timber class and they can only be applied

if the stresses are determined by elastic theory.

For a fully probabilistic modelling of timber mechanical properties, the probabilistic model code (PMC) of Joint Committee for Structural Safety (JCSS) is adopted and herein described.

4.1 Timber Specific Weight/Density

All properties of wood material depend on the density of wood cells. The density does not vary strongly among the different wood species, but it is sensitive to temperature and relative humidity. The classification of both [10, 14] are based on the bending strength and this classification assigns to each class its density together with the other parameters. The values listed in [10, 14] refer to a temperature of $20 \pm 2^\circ$ humidity of $65 \pm 5\%$.

However, the variation of the density inside an element is very small.

In addition, the production process is strictly controlled, so that there isn't any variation of the geometrical dimensions. Therefore, the variation of the self weight of the element depends only on the variation of the specific weight.

The PMC [24] considers the timber specific weight Normal distributed with a small c.o.v. (10%) for both solid and glulam elements.

For the assessed structure, the parameters of the Normal distribution of timber specific weight γ for purlins and beams are listed in table 4.1 and the CDF and pdf of Normal distribution are reported in Eqs. 4.1 and 4.2.

4.1 Timber Specific Weight/Density

Timber class	μ_γ	σ_γ	c.o.v.	γ_k
Solid Timber C24	4.2	0.42	0.10	3.52
Glulam Timber GL24c	4.0	0.40	0.10	3.34

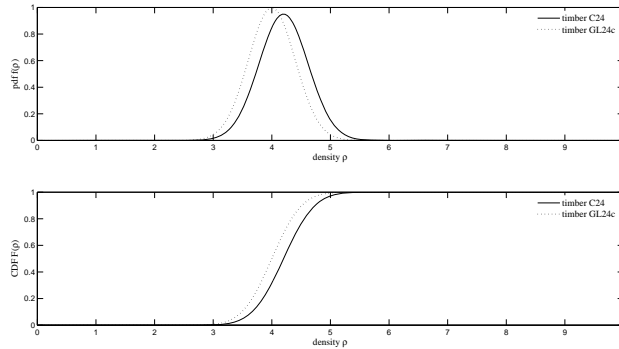
Table 4.1: Parameters of the Normal distributions of the specific weight for the used timber class.

$$f_\gamma(\gamma) = \frac{1}{\sigma_\gamma \sqrt{2\pi}} \exp \left[-\frac{1}{2} \left(\frac{\gamma - \mu_\gamma}{\sigma_\gamma} \right)^2 \right]. \quad (4.1)$$

$$F_\gamma(\gamma) = \Phi \left(\frac{\gamma - \mu_\gamma}{\sigma_\gamma} \right). \quad (4.2)$$

In Figure 4.1 the pdf and cdf of Eqs. 4.1 and 4.2 are plotted.

Figure 4.1: Plot of the p.d.f. and CDF of the specific weight γ .



In Eq. 4.2 the quantity Φ is defined as the integral of the Standard Normal Distribution (Eq. 4.3) respect to the standard variable $u = \frac{\gamma - \mu_\gamma}{\sigma_\gamma}$ for which there is no closed-form solution but only a numerical solution.

$$\Phi(u) = \int_{-\infty}^u \frac{1}{\sigma_P \sqrt{2\pi}} \exp\left[-\frac{1}{2}u^2\right] du. \quad (4.3)$$

4.2 Bending strength probability distribution and Isaksson Model

Despite the dishomogeneity of timber material, current code and engineering design methods consider timber as an homogeneous material in order to apply simplified design methods. In reality, due to the presence of defects, timber strength is not constant inside an element but depends both on the size (length) and on the load condition.

Generally, timber consists of single and/or clusters of defects (weak zones) distributed throughout zone of free-defect wood (clear wood). Therefore, it is commonly assumed that the strength along an element (inside the clear wood) is constant except within the section in which a defect occurs [27, 30, 41].

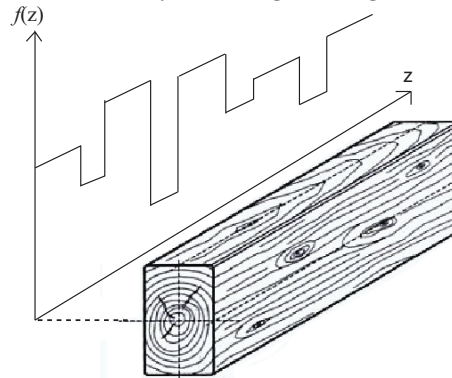
Due to the variability of the strength along the element (see figure 4.2) and the uncertainty about the distribution of the weak zones, strength of the weak zones is here described by stochastic variables. The distances between weak zones can be modeled as exponential distributed [24] or Gamma distributed [27].

By assuming the weak zones as Poisson distributed, the realization z_{ij} of the position of the weak zone j inside the element i occur according to the exponential distribution with mean value of $1/\lambda$. The JCSS [24] gives the

4.2 Bending strength probability distribution and Isaksson Model

value of $1/\lambda = 0.48m$ only for Norway spruce. In [41], Isaksson estimates the length of the weak zones in about $0.15m$ for both Norway spruce and Radiata Pine.

Figure 4.2: Variability of strength along a timber element.



Here, a discretized spatial model is used. Referring to data reported in [27, 41], timber elements (beams and purlins) are here divided into sections of $0.5m$ length and it is assumed that within each of these sections, one weak zone is present. This corresponds to fix a deterministic occurrence of weak zones.

The PMC of JCSS provides also a strength modification factor α for taking into account the deterioration of the material mechanical property due to duration of the load effects. The α coefficient depends on the exposure, load duration classes, different service classes (s.c.) and on the expected moisture content (m.c.) of the timber (s.c. 1, 2, 3 is associated with m.c. $< 12\%$, $< 20\%$, $> 20\%$). At this stage of assessment, duration of load is neglected and therefore the α coefficient is set to unity for sc1 (short load

duration).

Both purlins and beams of the assessed roof system are subjected mostly to bending moments. Therefore, the Isaksson model of bending strength can be used [24, 41]. The Isaksson model takes into account the variability of the bending strength at different locations. The model is described in the details in the section 4.2.1.

However, for the analysis of the considered roof system, it is required to have a joint model of the timber strength properties at different locations (sections) within a beam. This is not provided by the Isaksson model. Therefore, a generalization of the model is proposed and described in section 4.6.

4.2.1 Isaksson Model of bending strength

The Isaksson model of bending strength is based on the previous model of Riberholt (as reported in [41]) and supported by an extensive experimental study. The main idea is to consider that timber is composed of weak zones connected by segments of clear wood.

The main model assumption are here listed.

- Timber is composed of short weak zones connected by sections of clear wood;
- Weak zones correspond to knots or clusters and they are randomly distributed in space;
- Failure occurs only in the middle of the weak zones;

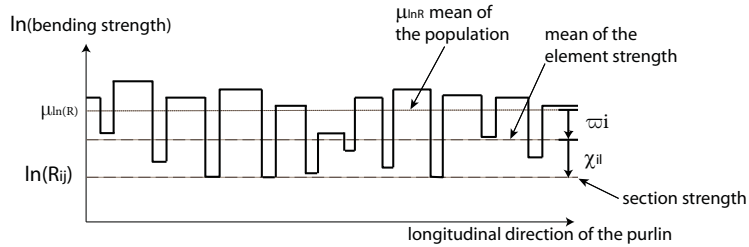
4.2 Bending strength probability distribution and Isaksson Model

- Strengths of the weak zones are correlated random variable;
- The correlation between weak sections is independent from the distance between the sections within the same element.

The bending strength of timber elements is modeled as a r.v. with lognormal distribution, then the variability within and between members is modeled according to Eq.4.4. Figure 4.3 shows the path of bending strength along a timber element.

$$\text{Ln}(f_{b_{ij}}) = \mu_{\text{Ln}(f_b)} + \varpi_i + \chi_{ij}. \quad (4.4)$$

Figure 4.3: Lengthwise variation of bending strength for Isaksson model (PMC-JCSS 2006).



The quantities in figure 4.3 and Eq.4.4 are here defined:

- $\mu_{\text{Ln}(f_b)}$ is the mean value of the logarithmic distribution of the strength of all sections in all components;
- ϖ_i is the difference between the logarithm of the mean strength of the sections within a component i and $\mu_{\text{Ln}(f_b)}$; ϖ_i is Normal

distributed with mean value equal to zero and standard deviation

$$\sigma_{\varpi_i} = \sqrt{0.4 \cdot \sigma_{\text{Ln}(f_b)}};$$

- χ_{ij} is the difference between the strength weak section j in the member i and the value $\mu_{\text{Ln}(f_b)} + \varpi_i$; χ_{ij} is Normal distributed with mean value equal to zero and standard deviation $\sigma_{\varpi_i} = \sqrt{0.6 \cdot \sigma_{\text{Ln}(f_b)}}$;
- ϖ_i and χ_{ij} are statistically independent.

According to Eq.4.4, the bending strength $f_{b,ij}$ of a particular section j within the component i is lognormal distributed with a standard deviation according to Eq.4.5.

$$\sigma_{\text{Ln}(f_b)}^2 = \sigma_{\varpi}^2 + \sigma_{\chi}^2. \quad (4.5)$$

In Eq. 4.5, σ_{ϖ} is the standard deviation between members, σ_{χ} is the standard deviation between sections within a member and $\sigma_{\text{Ln}(f_b)}$ is the standard deviation of the whole sample of weak sections and members.

From this model, it follows that the logarithm of bending strengths $\text{Ln}(f_{b,ij})$ of the cross sections $j = 1, \dots, n_j$ within a component i are correlated Normal random variables with correlation coefficient according to Eq. 4.6.

$$\rho_{\text{Ln}(f_b)} = \frac{\sigma_{f_{b,i}}^2}{\sigma_{f_{b,i}}^2 + \sigma_{f_{b,j}}^2} = \frac{\sigma_{f_{\varpi_i}^2}}{\sigma_{\varpi^2} + \sigma_{\chi^2}}. \quad (4.6)$$

For the timber class used in the analysis the parameters of the lognormal distributions are listed in table 4.2.

4.3 Strength perpendicular to the grain f_{t90} and f_{c90} : probability distribution

Timber class	μ_{f_b}	$\mu_{Ln(f_b)}$	$\sigma_{Ln(f_b)}$	c.o.v.	$f_{b,k}$
Solid Timber C24	36.97	3.58	0.246	0.25	24
Glulam Timber GL24c	31.00	3.42	0.149	0.15	24

Table 4.2: Parameters of the LogNormal distributions of the bending strength for the used timber class.

4.3 Strength perpendicular to the grain f_{t90} and f_{c90} : probability distribution

Tensile stress perpendicular to the grain is a commonly a severe stress condition for glulam cambered members. Indeed, the fracture perpendicular to the grain is a brittle mechanism and the strength in direction perpendicular to the grain is strongly dependent on the size of the element (volume effect) and also on the orientation and size of the annual growth rings.

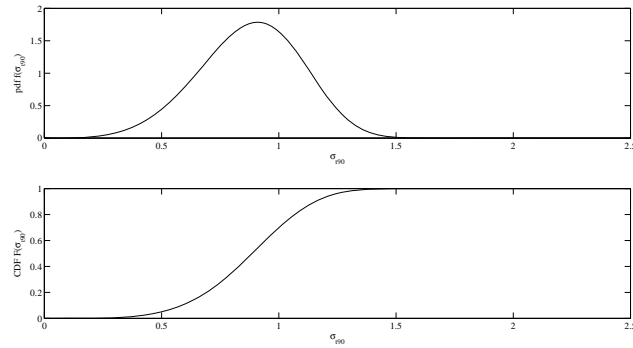
Due to the brittle nature of this fracture mechanism the PMC of JCSS indicates that an extreme value distribution of minima is a suitable probabilistic distribution for the tensile strength in direction perpendicular to the grain. Therefore the Weibull distribution into two parameters is here used. In Eqs. 4.7 and 4.8 the Weibull CDF and pdf are reported. The distribution defined in Eqs. 4.7 and 4.8 is plotted in figure 4.4 for timber GL24c.

$$F_{f_{t90}}(s_t) = \exp \left[- \left(\frac{f_{t90}}{a_s} \right)^k \right] \text{ for } f_{t90} \geq 0. \quad (4.7)$$

$$f_{f_{t90}}(f_{t90}) = \frac{k}{a_s} \left(\frac{f_{t90}}{a_s} \right)^{k-1} \exp \left[- \left(\frac{f_{t90}}{a_s} \right)^k \right] \text{ for } f_{t90} \geq 0. \quad (4.8)$$

The expressions in Eqs. 4.7 and 4.8 are defined only for positive parameters a_s and k . For glulam GL24c the parameters are $a_s = 0.961$ and $k = 4.542$.

Figure 4.4: Weibull distribution of the tension strength perpendicular to the grain for timber GL24c.



The fracture for compression perpendicular to the grain occur with big plastic displacements and the wood cells pressed until the cracking of the fibers inside the rings. The stress-strain relationship has in this case a shorter linear elastic range and a wider plastic range.

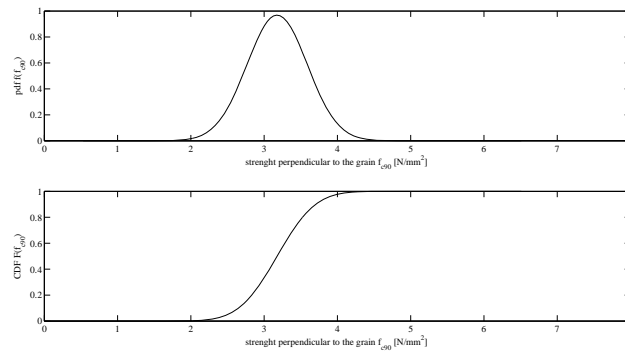
The PMC suggests the use of a Normal distribution for the compression strength perpendicular to the grain. In Eqs. 4.9 and 4.10 the Normal CDF and pdf defined for timber GL24c are reported and then plotted in figure4.5.

$$F_{f_{c90}}(f_{c90}) = \Phi\left(\frac{f_{c90} - \mu_{f_{c90}}}{\sigma_{f_{c90}}}\right). \quad (4.9)$$

4.4 Compression f_{c0} and tensile stress f_{t0} strength in the direction of the grain: probability distribution

$$f_{f_{c90}}(f_{c90}) = \frac{1}{f_{c90}\sqrt{2\pi}} \exp \left[-\frac{1}{2} \left(\frac{f_{c90} - \mu_{f_{c90}}}{\sigma_{f_{c90}}} \right)^2 \right]. \quad (4.10)$$

Figure 4.5: Compression strength perpendicular to the grain Normal probability distribution.



4.4 Compression f_{c0} and tensile stress f_{t0} strength in the direction of the grain: probability distribution

The behavior of timber in traction and compression is different. In tensile stress condition, timber shows a stress-strain behavior that is linear elastic until the limit condition. In compression stress condition, timber shows a linear elastic behavior with a small plasticity and a softening branch after the elastic limit.

The PMC suggests to use a lognormal distribution for tensile strength and a Normal distribution for the strength in compression. In Eqs. 4.11, 4.12 and Eqs. 4.13, 4.14 respectively, the CDF and pdf of the lognormal distri-

bution of tensile strength parallel to the grain and the Normal distribution of compression strength parallel to the grain are reported. The path of the two strength distributions are shown in figures 4.6 and 4.7

$$F_{f_{t0}}(f_{t0}) = \Phi\left(\frac{\text{Ln}f_{t0} - \mu_{\text{Ln}f_{t0}}}{\sigma_{\text{Ln}f_{t0}}}\right). \quad (4.11)$$

$$f_{f_{t0}}(f_{t0}) = \frac{1}{f_{t0}} \frac{1}{\sigma_{\text{Ln}f_{t0}} \sqrt{2\pi}} \exp\left[-\frac{1}{2} \left(\frac{\text{Ln}(f_{t0}) - \mu_{f_{t0}}}{\sigma_{\text{Ln}f_{t0}}}\right)^2\right]. \quad (4.12)$$

$$F_{f_{c0}}(f_{c0}) = \Phi\left(\frac{f_{c0} - \mu_{f_{c0}}}{\sigma_{f_{c0}}}\right). \quad (4.13)$$

$$f_{f_{c0}}(f_{c0}) = \frac{1}{\sigma_{f_{c0}} \sqrt{2\pi}} \exp\left[-\frac{1}{2} \left(\frac{f_{c0} - \mu_{f_{c0}}}{\sigma_{f_{c0}}}\right)^2\right]. \quad (4.14)$$

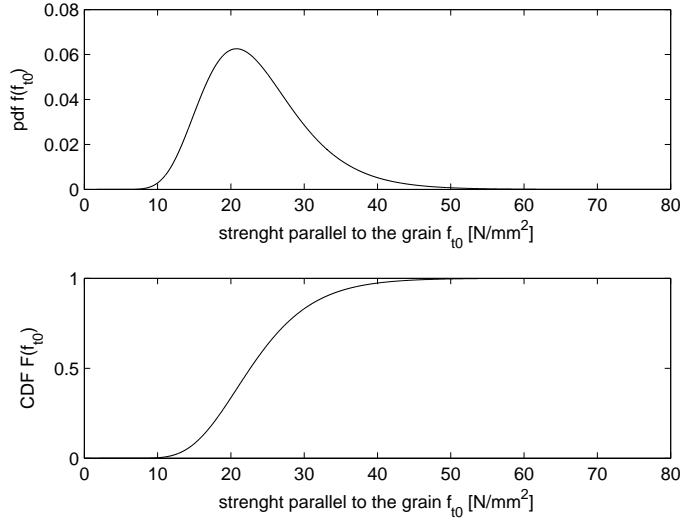
4.5 Tangential Strength: probability distribution

Due to the anisotropy of wood material, the behavior of timber under shear load depends on the orientation of the fibers inside the section. Indeed, when the action is applied in the direction parallel to the grain, a slope of fibers is also possible, differently from the case of shear acting in direction orthogonal to the grain. The shear strength depends positively on density of fibers and negatively on moisture content and temperature.

According to PMC, a lognormal distribution is chosen to model the variability of the shear strength. The cdf and pdf are reported in Eqs. 4.15 and 4.16 respectively. In figure 4.8 the pdf and cdf of the lognormal distribution

4.5 Tangential Strength: probability distribution

Figure 4.6: Tension strength parallel to the grain lognormal probability distribution.



of the shear strength for timber GL24c is plotted.

$$F_{f_v}(f_v) = \Phi\left(\frac{f_v - \mu_{f_v}}{\sigma_{f_v}}\right). \quad (4.15)$$

$$f_{f_v}(f_v) = \frac{1}{f_v} \frac{1}{\sigma_{f_v} \sqrt{2\pi}} \exp\left[-\frac{1}{2} \left(\frac{\ln(f_v) - \mu_{f_v}}{\sigma_{\ln f_v}}\right)^2\right]. \quad (4.16)$$

Figure 4.7: Compression strength parallel to the grain normal probability distribution.

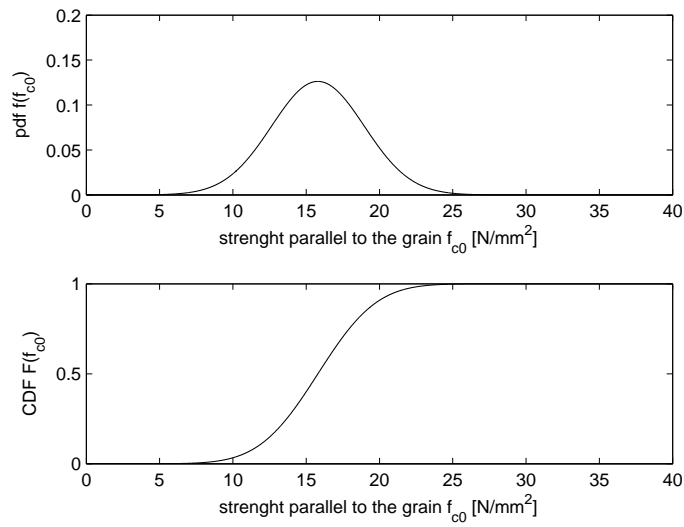
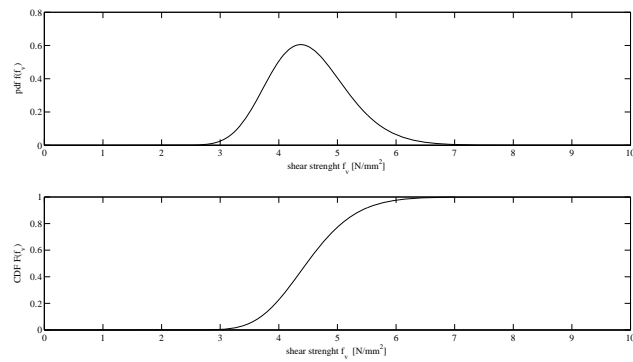


Figure 4.8: Shear strength Lognormal probability distribution.



4.6 Extension of the Isaksson model for a joint spatial variability model of timber strength properties

4.6 Extension of the Isaksson model for a joint spatial variability model of timber strength properties

The approach of Isaksson model is suitable to be applied also to other strength characteristics. However, the cross-correlation among different material properties at different locations in the element is not described by the Isaksson model. This motivates the extension of the model as proposed in the following. Correlation among the material properties must be taken into account. This correlation is mainly due to the fact that most mechanical properties depend on the density of wood cells and therefore on the specific weight. The PMC [24] provides correlation factors among the material properties within one section, which are used in this study and are shown in table 4.3. This correlation matrix applies to both solid and glulam timber.

Σ_{XX}	γ_{ij}	$f_{b,ij}$	$f_{v,ij}$	$f_{t0,ij}$	$f_{t90,ij}$	$f_{c90,ij}$
γ_{ij}	1	0.6	0.6	0.6	0.4	0.8
$f_{b,ij}$	0.6	1	0.6	0.6	0.4	0.6
$f_{v,ij}$	0.6	0.4	1	0.6	0.6	0.4
$f_{t0,ij}$	0.6	0.4	0.6	1	0.2	0.4
$f_{t90,ij}$	0.4	0.4	0.6	0.2	1	0.4
$f_{c90,ij}$	0.8	0.6	0.4	0.4	0.4	1

Table 4.3: JCSS Correlation Matrix.

The subscript ij indicates that the correlation matrix of Table 4.3 refers to the property of the section j within the element i . Commonly, material properties among different elements are uncorrelated, because each compo-

ment is manufactured independently. On the contrary, material properties among different sections within one component are correlated r.v. and the correlation among them should be taken into account for a more realistic model.

Here, a joint probabilistic model of multiple strength properties at varying locations within one element is proposed. This model has two special cases:

- Multiple properties at the same location must have the correlation coefficient matrix defined in table 4.3;
- Values of the same material property at different locations must have a dependence that is described by the Isaksson model.

The model can therefore be seen as a generalization of both the Isaksson model and the correlation model of the PMC.

Let $X_{a_{ij}}$ and $X_{b_{ik}}$ be two different material properties at locations j and k in element i . Since material properties among different elements are uncorrelated, it is sufficient to consider only a single element i and therefore the index i will be omitted in the following.

Let's define for each X_{a_j} and X_{b_k} , for $j = 1, \dots, n_j$ and $k = 1, \dots, n_j$, the corresponding standard Normal random variables U_{a_j} and U_{b_k} . They are related by the marginal transformations in Eqs. 4.17 and 4.18.

$$X_{a_j} = F_{X_a}^{-1} [\Phi (U_{a_j})]. \quad (4.17)$$

$$X_{b_k} = F_{X_b}^{-1} [\Phi (U_{b_k})]. \quad (4.18)$$

4.6 Extension of the Isaksson model for a joint spatial variability model of timber strength properties

In Eqs. 4.17 and 4.18, $F_{X_a}^{-1}$ and $F_{X_b}^{-1}$ are the inverse cumulative distribution functions (CDF) of X_{a_j} and X_{b_k} and Φ is the standard Normal CDF. Let's define U_{a_j} as the sum of two uncorrelated random variables, Λ_a and Ψ_{a_j} (Eq.4.19).

$$U_{a_j} = \Lambda_a + \Psi_{a_j}. \quad (4.19)$$

Λ_a is Normal distributed with zero mean and variance $\sigma_{\Lambda_a}^2 = 0.4$. Ψ_{a_j} is Normal distributed with zero mean and variance $\sigma_{\Psi_a}^2 = 0.6$.

Since the two r.v. are uncorrelated, it follows that U_{a_j} has zero mean and variance $\sigma_{\Lambda_a}^2 + \sigma_{\Psi_a}^2 = 1$. Similarly, for the property b the same law can be defined (Eq.4.20) .

$$U_{b_j} = \Lambda_b + \Psi_{b_j}. \quad (4.20)$$

To represent the correlation between the different material properties, it is required that Λ_a and Λ_b are correlated with correlation coefficient r_{ab} . Furthermore, Ψ_{a_j} and Ψ_{a_k} are also correlated with r_{ab} when $j = k$; for $j \neq k$ they are uncorrelated.

The value of r_{ab} must be selected to give a correlation coefficient between the two material properties at the same location j , X_{a_j} and X_{b_j} , equal to the one provided by correlation coefficient matrix of PMC, (see table 4.3).

Let ρ_{ab} denote this target correlation coefficient.

The correlation coefficient between U_{a_j} and U_{b_j} is therefore given in Eq.4.21.

$$r_{U_{a_j}U_{b_j}} = \text{COV} [U_{a_j}, U_{b_j}] = \sigma_{\Lambda}^2 r_{ab} + \sigma_{\Psi}^2 r_{ab} = r_{ab}. \quad (4.21)$$

Since U_{a_j}, U_{b_j} are related to X_{a_j}, X_{b_k} through the marginal transformations provided in Eqs.4.17 and 4.18, the relation between $r_{U_{a_j}U_{b_j}}$ and ρ_{ab} is described by the Nataf transformation, see (Der Kiureghian and Liu [5]). Therefore, r_{ab} is obtained as in Eq. 4.22.

$$r_{ab} = r_{U_{a_j}U_{b_j}} = c_{ab} \cdot \rho_{ab}. \quad (4.22)$$

The coefficient c_{ab} in Eq.4.22 is the transformation coefficient of the Nataf distribution, which depends on the marginal distributions of X_{a_j} and X_{b_j} .

The joint distribution among X_{a_j} and X_{b_k} for any values of $j = 1, \dots, n_j$ and $k = 1, \dots, n_j$ is at this stage fully defined. To verify that this model reduces to the Isaksson model, when considering only one property, i.e. when $a = b$, it is enough to notice that the marginal transformation of Eqs. 4.17 and 4.18 for the case of the lognormal distribution is defined as in Eq.4.23.

$$X_{a_j} = \exp \left(\mu_{\text{Ln}X_a} + U_{a_j} \sigma_{\text{Ln}X_a} \right). \quad (4.23)$$

In Eq. 4.23, $\mu_{\text{Ln}X_a}$ and $\sigma_{\text{Ln}X_a}$ are the parameters of the lognormal distribution. The substitution of Eq. 4.19 in Eq. 4.23 provides Eq. 4.24.

$$X_{a_j} = \exp \left(\mu_{\text{Ln}X_a} + \Lambda_a \sigma_{\text{Ln}X_a} + \Psi_{a_j} \sigma_{\text{Ln}X_a} \right). \quad (4.24)$$

4.7 Systematic Weaknesses

This is identical to the Isaksson model of Eq.4.4, since $\mu_{\text{Ln}X_a} = \mu_{\text{Ln}f_b}$, $\Lambda_a \sigma_{\text{Ln}X_a} = \varpi_i$ and $\Psi_{a_j} \sigma_{\text{Ln}X_a} = \chi_{ij}$.

Finally in table 4.4 and 4.5 a short review of the timber material statistics is given.

C24	r.v.	Distribution	μ	σ	c.o.v.	$value_k$
Specific Weight [kN/m^3]	γ_{ij}	Normal	4.2	0.42	0.10	3.52
Bending Strength [N/mm^2]	$f_{b_{ij}}$	Lognormal	36.97	9.24	0.25	24
Tension parallel to the grain [N/mm^2]	$f_{t0_{ij}}$	Lognormal	23.6	7.08	0.30	14
Compression parallel to the grain [N/mm^2]	$f_{c0_{ij}}$	Normal	15.8	3.16	0.20	21

Table 4.4: Timber material statistics for C24.

GL24c	r.v.	Distribution	μ	σ	c.o.v.	$value_k$
Specific Weight [kN/m^3]	γ_{ij}	Normal	4.0	0.40	0.10	3.34
Bending Strength [N/mm^2]	$f_{b_{ij}}$	Lognormal	31.0	4.65	0.15	24
Shear Strength [N/mm^2]	$f_{v_{ij}}$	Lognormal	4.52	0.68	0.15	3.5
Tension perpendicular to the grain [N/mm^2]	$f_{t90_{ij}}$	2-p Weibull	0.848	0.21	0.25	0.5
Compression perpendicular to the grain [N/mm^2]	$f_{c90_{ij}}$	Normal	3.177	0.412	0.10	2.5

Table 4.5: Timber material statistics for GL24c.

4.7 Systematic Weaknesses

In order to study the behavior of the three different structural configurations for the secondary structure when also *systematic errors* are present,

a probabilistic model for these errors needs to be defined.

Systematic errors are caused, or indirectly induced, by human errors or unforeseeable complex conditions. Therefore, systematic errors can be modeled as random events related to their possible causes, then in relation to the causes, systematic events can induce common failure in the form of single points of failure or the progressive failure in a redundant system.

Due to their nature, no probabilistic models of such errors exist. Therefore, in this dissertation a model will be proposed as purely hypothetical with the aim only to compare the performance of the different structural configurations. The event that systematic errors are present is denoted by D .

It is here assumed that systematic errors D can occur as design errors, manufacture error (wrong cross section, wrong strength grade) or execution errors (production, execution of holes in the joints, finger joints etc.), leading to significant reductions in bending strength locally, e.g. at the finger joints. The occurrence of these weak sections is modeled by a Bernoulli process with rate $p = 0.30$. The bending strength of the secondary element at the weak sections, $f_{b,D}$, is modeled by a lognormal distribution whose mean value is reduced by 20% compared to the intact sections. The c.o.v. of $f_{b,D}$ is identical to the one of the intact element.

Chapter 5

Load Statistics

A full probabilistic assessment requires the definition of the statistics of the loads acting on the structure. Several descriptions of the probability distributions (p.d.f and CDF) to be used can be found in the literature.

Hereby, the probabilistic model of the loads is based on the Probabilistic Model Code of the Joint Committee of Structural Safety [24].

The most severe load condition is given by the snow load, because it has the highest variability. Self weight and permanent load have a very low variability. The probabilistic load of the self weight will be described together with the timber strength characteristics because they all depend strongly on the density of wood cells.

5.1 Permanent Load Distribution

The definition of loads is based on the previous deterministic study of the Timber Chair of TUM [7]. The permanent load P is given by the weight of the roofing and in [7] it is quantified in $0.4kN/m^2$ as mean value. According to [24] the permanent load is assumed to be Normal Distributed with mean value $\mu_P = 0.4kN/m^2$ and coefficient of variation (c.o.v.) equal to 0.1. The Normal distribution of mean value μ_P and standard deviation σ_P is defined by the pdf in Eq. 5.1, the CDF in Eq. 5.2 and inverse in Eq. 5.3.

$$f_P(p) = \frac{1}{\sigma_P \sqrt{2\pi}} \exp \left[-\frac{1}{2} \left(\frac{p - \mu_P}{\sigma_P} \right)^2 \right]. \quad (5.1)$$

$$F_P(p) = \Phi \left(\frac{p - \mu_P}{\sigma_P} \right). \quad (5.2)$$

$$F_P^{-1}(p) = \Phi^{-1} \left(\frac{p - \mu_P}{\sigma_P} \right). \quad (5.3)$$

In figure 5.1 the p.d.f. and CDF of permanent load P are plotted.

5.2 Snow Load Distribution

Snowfalls occur during the winter season as sequence of events with a duration that changes with the climatic region and with the altitude (see figure 5.2 from [39]).

5.2 Snow Load Distribution

Figure 5.1: Plot of the p.d.f. and CDF for permanent load P.

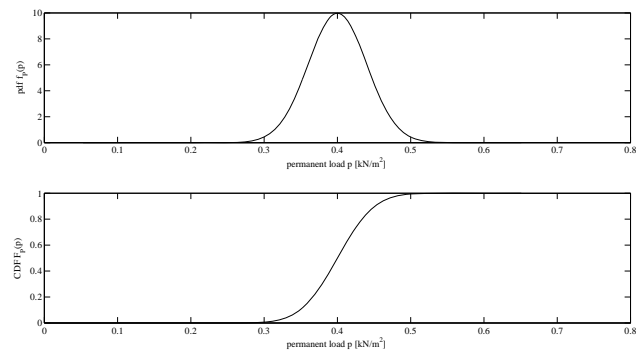
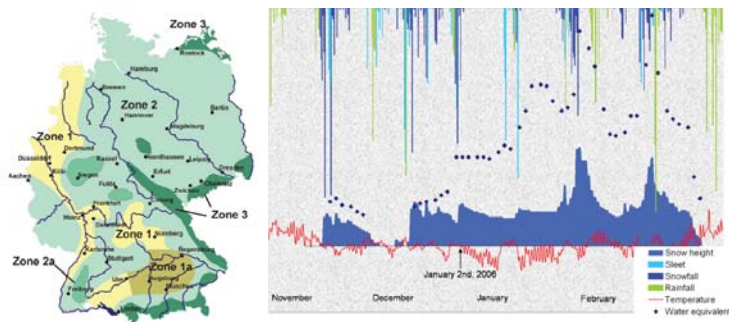


Figure 5.2: Recordings of meteorological variables and ground snow cover from November 2005 to March 2006 at the DWD met office station in Bad Reichenhall (DE) (U. Strasser 2008).



Therefore, the snow load Q varies with time and can be modeled as stochastic process whose statistics will be defined in this section.

Let's assume that snow events occur according to a Poisson Spike Process. In addition the process is considered to be homogeneous (constant rate over time), stationary (same statistic over time whatever time shifting is given), with independent increments and starting from zero.

The Poisson process is suitable to count a number of events occurring in a certain interval of time T . If the set $\{t_n\} = \{t_0, t_n, \infty\}$ is a positive sequence that defines the time occurrences and with $t_0 = 0$, the counting process $N(t)$ can be defined as the process that at each time interval t associates the number of outcomes $n(t)$. Under the hypothesis of stationarity and independent increments the process $N(t)$ is defined Poisson process.

In the Poisson process the occurrences have a Poisson distribution and the probability of having n events in the time interval $[0, T]$ is given in Eq. 5.4.

$$P(N(t) = n) = e^{-\lambda T} \frac{(\lambda T)^n}{n!}. \quad (5.4)$$

In Eq. 5.4 the parameter λ , that represents the mean arrival rate, is always positive and the distribution has both mean value $\mu(t)$ and standard deviation $\sigma(t)$ equal to λt .

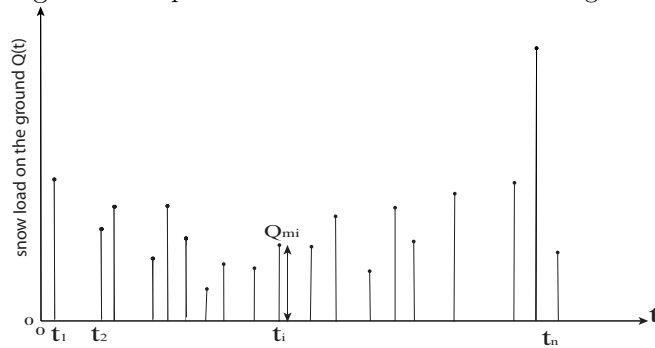
At each occurrence t_i , counted by the counter process $N(t)$, can be assigned an independent realization of the random variable Q_i that is representative of the nature of the event. This realization Q_i is called *jump*. The jumps of the process are assumed here to have instantaneous duration so that each event occur as a spike.

5.2 Snow Load Distribution

Figure 5.3 shows one realization of the snow load process, where t_i are the times of occurrence of the snow events and Q_{mi} is the snow load (spike) at each event.

The assumed mean occurrence rate per year for north Europe is $\lambda = 1.175$

Figure 5.3: Spike train for the snow load on the ground.



[4] over a time interval of 50 years (life time). The maximum snow load in each event Q_m (spike) is modeled by a Gumbel distribution [33] with mean $0.384kN/m^2$ and c.o.v. = 0.4. With this model, the characteristic value of the annual maximum snow load equals $0.8kN/m^2$, which corresponds to snow zone 1 in Germany at an altitude of about 480m above sea level (see [8] for Munich area).

With the model of snow load given above, it is necessary to compute the distribution of the annual maximum snow load Q_m , as described in the following.

Let n be the number of snow events in a year and let Q_n be the maximum snow load in the n snow events. The cumulative probability function (CDF) of Q_n is obtained as a function of the CDF of the maximum snow

load in each event Q_m as in Eq. 5.5, where a and b are the parameters of the Gumbel distribution of Q_i .

$$F_{Q_n}(q|n) = [F_{Q_m}(q)]^n = \left\{ \exp \left[-\exp \left(-\frac{q - b_q}{a_q} \right) \right] \right\}^n. \quad (5.5)$$

The number of snow events per year is a random variable with probability mass function (PMF) $p_N(n)$. The CDF of the annual maximum snow load is therefore given in Eq. 5.6.

$$F_{Q_{max}}(q) = \sum_{n=0}^{\infty} [F_{Q_m}(q|n)]^n \cdot p_N(n). \quad (5.6)$$

In Eq. 5.6 $p_N(n)$ is the Poisson PMF with parameter $\lambda \cdot 1yr$. Combining Eq. 5.5 with Eq. 5.6, the unconditioned CDF of the annual maximum snow load is written in Eq. 5.7, where the parameters of the Gumbel distribution are $a_q = 0.1197$ and $b_q = 0.3147$.

$$F_{Q_{max}}(q) = \sum_{n=0}^{\infty} \left\{ \exp \left[-\exp \left(-\frac{q - b_q}{a_q} \right) \right] \right\}^n \cdot \frac{(\lambda \cdot 1yr)^n}{n!} \cdot \exp(-\lambda \cdot 1yr). \quad (5.7)$$

The expression of the CDF of the snow load on the ground in Eq. 5.7 is not very suitable for the generation of sample needed for the analysis of the system, therefore the expression must be manipulated. Considering

5.2 Snow Load Distribution

that the exponential function is defined as $e^x = \sum_{n=0}^{\infty} \frac{x^n}{n!}$, the expression Eq. 5.7 assumes the form in Eq. 5.2.

$$\begin{aligned}
 F_{Q_{max}}(q) &= \exp(-\lambda \cdot 1yr) \sum_{n=0}^{\infty} \frac{\left\{ \exp \left[-\exp \left(-\frac{q-b_q}{a_q} \right) \right] \cdot (\lambda \cdot 1yr) \right\}^n}{n!} = \\
 &= \exp(-\lambda \cdot 1yr) \exp \left\{ \lambda \cdot 1yr \left[\exp \left(-\exp \left(-\frac{q-b_q}{a_q} \right) \right) \right] \right\} = \\
 &= \exp \{ \lambda \cdot 1yr [\exp(-\exp(-\frac{q-b_q}{a_q}))] - \lambda \cdot 1yr \} = \\
 &= \exp \left\{ \lambda \cdot 1yr \left[\exp \left(-\exp \left(-\frac{q-b_q}{a_q} \right) \right) - 1 \right] \right\}.
 \end{aligned} \tag{5.8}$$

From the CDF of Eq.5.2, it can be defined both the p.d.f. of the snow load on the ground as the derivative of the CDF (Eq.5.9) and the inverse $F^{-1}(Q_{max})$ (Eq.5.10).

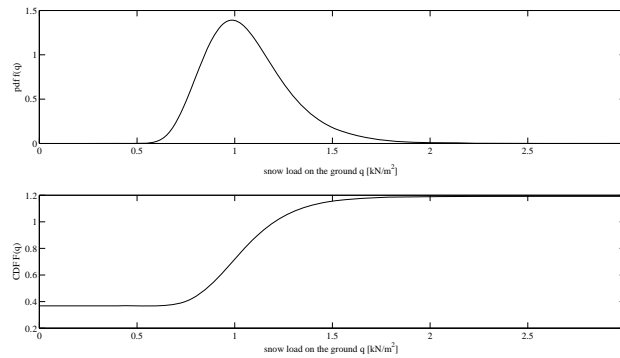
$$\begin{aligned}
 f_{Q_{max}}(q) &= \frac{\lambda \cdot 1yr}{a_q} \exp \left\{ -\exp \left(\frac{b_q - q}{a_q} \right) + \lambda \cdot 1yr [-1 + \right. \\
 &\quad \left. + \exp \left(-\exp \left(\frac{b_q - q}{a_q} \right) \right) \right] + \frac{b_q - q}{a_q} \right\}.
 \end{aligned} \tag{5.9}$$

$$F_{Q_{max}}^{-1}(u) = b_q - a_q \cdot \text{Ln} \left[-\text{Ln} \left(\frac{\text{Ln}(u)}{\lambda \cdot 1yr} + 1 \right) \right]. \tag{5.10}$$

In Eq. 5.10 the variable u is a r.v. uniform distributed between zero and one ($u \sim U(0,1)$). In figure 5.4 the p.d.f. and CDF of snow load on

the ground Q are plotted.

Figure 5.4: Plot of the p.d.f. and CDF for snow load on the ground Q .



The path of the CDF of the snow load on the ground in figure 5.4 shows that the effect of passing from the conditional probability in Eq. 5.5 to the unconditional probability in Eq. 5.6 causes the shifting of the values of the function equal to the quantity $F_{Q_{max}}(q = 0) = 0.38$.

5.3 Shape Factor Distribution

The cumulative distribution given in Eq. 5.2 defines only the snow load on the ground. Due to environmental and geometrical conditions, snow is not spread in uniform way over the roof, but it can accumulate on one side and on localized areas of the pitch. The mass of the drifted snow depends on several factors such as wind velocity and duration of high wind velocity, size of snow grain, snow surface composition, topographic relief and exposure,

5.3 Shape Factor Distribution

temperature and humidity.

According to both [8, 14] this effect of local accumulation of the snow must be taken into account through a *shape factor* that depends on the roof geometry. This factor is defined as a deterministic quantity in the current codes, even if an extensive study was carried out in order to give an appropriate estimation of this factor (see [33]).

In the report of Sanpaolesi [33], data from ten climate regions in Europe were collected and processed according to different statistical approaches to define both combination factors and the snow load shape factor for the Eurocode.

The shape factor ranges values between 0.8 and 1.6 or even higher values according to contour conditions. The data collected showed that the drift due to wind has the same effect in all climatic regions and that the resulting shape coefficient for windy sides are much smaller than the lee side. In addition, also the standard deviation is bigger on windward side.

According to the shape of the roof (for double pitched roofs), the roof shape coefficients were divided in four categories of pitch angle [33]: $0 - 7^\circ$; $8 - 22^\circ$; $23 - 37^\circ$; $38 - 52^\circ$.

Figures 5.6 and 5.7 show the mean and standard deviation for the shape coefficient on windy side (windward side) and sheltered side (lee side) of the reference roof geometry of figure 5.5 as reported in [33].

In this dissertation the *shape factor* C is assumed as Gumbel distributed with parameters computed according to a pitch angle of 10° . For practical reasons, the mean value of the distribution is then taken as mean between the value for lee side and windward side, resulting in a mean value of 0.78,

Figure 5.5: Windward and lee side on a double pitched roof.

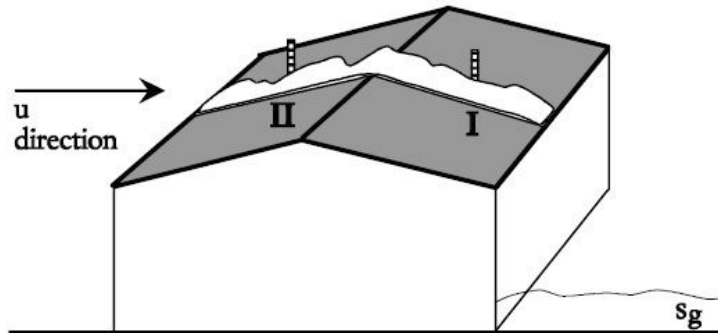
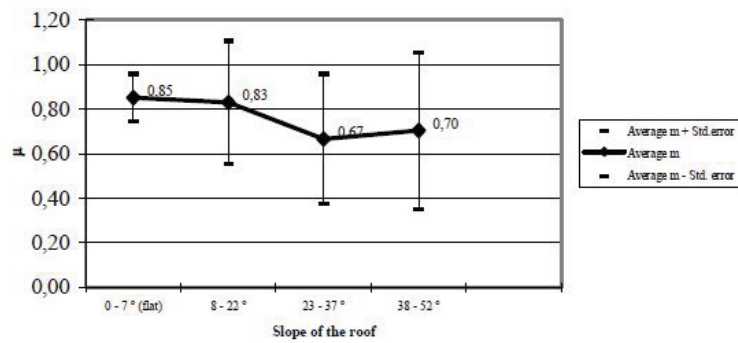


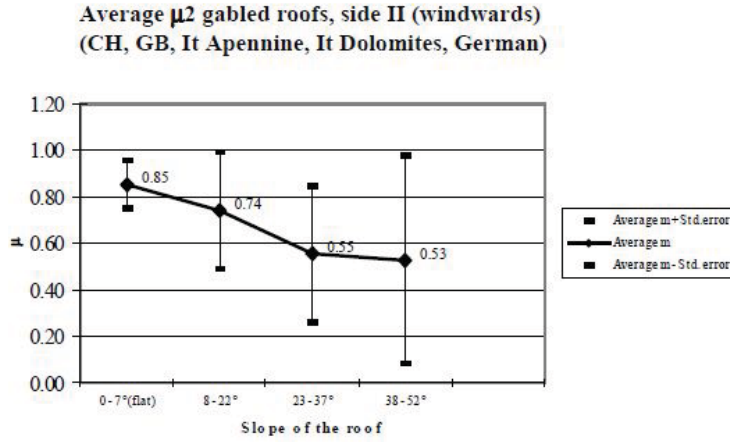
Figure 5.6: Mean and standard deviation of the shape factor for lee side.

Average μ gabled roofs, side I (lee)
(CH, GB, It Apennine, It Dolomites, German)



5.3 Shape Factor Distribution

Figure 5.7: Mean and standard deviation of the shape factor for windward side.



while the standard deviation of windward side is kept. This assumption can be quite severe, but it is motivated by the need of modeling also the accumulation of snow on the roof during the winter season in Germany, when snowfalls are quite near.

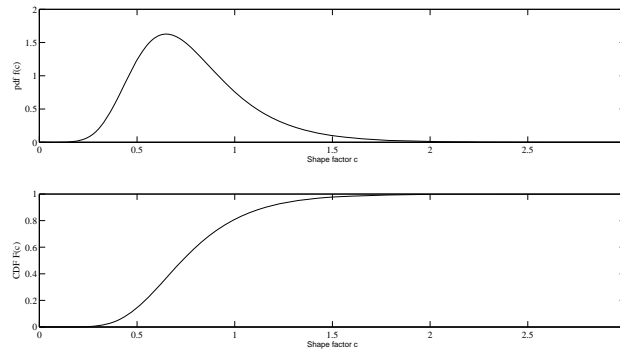
In Eqs. 5.11, 5.12 and 5.13 respectively, the expression of Gumbel CDF, pdf and inverse cumulative distribution for the shape factor C are given. The pdf and CDF are then plotted in Figure . The parameters of the CDF are $a_C = 0.226$ and $b_C = 0.649$.

$$F_C(c) = \exp \left[-\exp \left(-\frac{c - b_C}{a_C} \right) \right]. \quad (5.11)$$

$$f_C(c) = \frac{1}{a_C} \exp \left[-\frac{c - b_C}{a_C} - \exp \left(-\frac{c - b_C}{a_C} \right) \right]. \quad (5.12)$$

$$F_C^{-1}(c) = b_C - a_C \text{Ln} [-\text{Ln}(u)]. \quad (5.13)$$

Figure 5.8: Plot of the pdf and CDF of Shape Factor C .



Finally in Table 5.1 a short review of the load statistics is given.

Load	r.v.	distribution	μ	c.o.v
Permanent load $[kN/m^2]$	P	Normal	0.40	0.10
Snow load $[kN/m^2]$	Q	Gumbel	0.384	0.40
Occurrence $[1/yr]$	T	Poisson	0.175	0.92
Shape Factor	C	Gumbel	0.78	0.35

Table 5.1: Parameters of the load distributions used.

Chapter 6

Application

For the case study described in section 3.1, computations are performed. Hereby, the solution of the probability integral is presented for a simplified case. For the primary and secondary system, Monte Carlo Simulations (MCS) with 10^5 samples are computed. MCS enable the evaluation of the full distribution of the damaged area, $f_{A_F|F}$ as required for the risk and robustness assessment. As an independent check and to assess the sensitivity of the results on the probabilistic model, First-Order Reliability Method (FORM) is used to compute the probability of system failure, $Pr(F)$.

6.1 Purlin's analysis: probability integral for a simplified case

It is useful to compute the solution of the reliability problem computing the reliability integral for a simplified case.

Let's consider a single span simply supported purlin, loaded by snow load Q , permanent load P and self weight W_p and subject to biaxial bending condition as described in section 3.1. Let's also consider the shape factor equal to one and the self weight and permanent load as constant and equal to their mean value, so that their sum is equal to $0.5kN/m$. The statistics of load and bending resistance are fully defined in the previous chapters. Let's assume R and S statistically independent.

The limit state function for the simply supported purlin can be defined directly as vectorial composition of the bending moments along the two main axes. It is a function of the strength R and of the loads S and it is described by Eq. 6.1.

$$g(R, S) = \sqrt{M_{Rx}^2 + M_{Ry}^2} - \sqrt{M_{Sx}^2 + M_{Sy}^2}. \quad (6.1)$$

In Eq. 6.1, M_{Rx} and M_{Ry} are the bending strengths and M_{Sx} and M_{Sy} are the bending demands. At the midspan location, bending strengths and demands are defined below.

$$M_{Sx} = \frac{l_p^2}{8} \cdot [Q + W_p + P] \cos^2 \alpha. \quad (6.2)$$

6.1 Purlin's analysis: probability integral for a simplified case

$$M_{Sy} = \frac{l_p^2}{8} \cdot [Q + W_p + P] \cos\alpha \sin\alpha. \quad (6.3)$$

$$M_{Rx} = \frac{1}{6} \cdot bh^2 \cdot R. \quad (6.4)$$

$$M_{Ry} = \frac{1}{6} \cdot hb^2 \cdot R. \quad (6.5)$$

where b , h are the dimension of the cross section (assumed deterministic), $\alpha = 10$ is the inclination of the roof and l_p is the length of the purlin. It is convenient to arrange the constants of the equations above as follows.

$$C_{load} = \sqrt{\left(\frac{l_p^2}{8} \cos^2\alpha\right)^2 + \left(\frac{l_p^2}{8} \cos\alpha \sin\alpha\right)^2} = 4.43. \quad (6.6)$$

$$C_{res} = \sqrt{\left(\frac{1}{6} \cdot bh^2\right)^2 + \left(\frac{1}{6} \cdot hb^2\right)^2} = 0.745. \quad (6.7)$$

The probability of bending failure for the midspan section is therefore given by Eq.6.8.

$$\begin{aligned} Pr(F) &= Pr(G < 0) = Pr(M_R - M_S < 0) = \\ &= Pr\left(Q > R \frac{C_{res}}{C_{load}} - W_p - P\right) = \\ &= 1 - Pr\left(R \frac{C_{res}}{C_{load}} - W_p - P\right). \end{aligned} \quad (6.8)$$

From Eq. 6.8, it follows that:

$$Pr(F|r) = Pr(Q > R = r) = 1 - F_Q\left(r \frac{C_{res}}{C_{load}} - w - p\right). \quad (6.9)$$

Eq. 6.9 corresponds also to Eq. 6.10 written respect to the bending moments.

$$\begin{aligned} Pr(F|M_R) &= Pr(M_S > M_R = mr) = \\ &= 1 - F_{M_S} \left(\frac{ms}{C_{load}} - w - p \right). \end{aligned} \quad (6.10)$$

Let's compute the distribution of bending moments. Due to the fact that bending strength and demand are given by multiplying R and S by constants, the distribution of the bending strength M_R and demand M_S are the same of R and S . Therefore, M_R has lognormal distribution and M_S has Gumbel-Poisson distribution. It is needed to compute the expectation and variance of the distributions of M_R and M_S as follows.

$$E[M_R] = C_{res} \cdot E[R] = 23.12kNm. \quad (6.11)$$

$$E[M_R^2] = C_{res}^2 \cdot E[R^2] = 12.014(kNm)^2. \quad (6.12)$$

From the values in Eqs. 6.11 and 6.12, the parameters of the lognormal distribution are computed below.

$$\sigma_{\text{Ln}M_R} = \text{Ln} \left[1 + \left(\frac{\sigma_{M_R}}{\mu_{M_R}} \right)^2 \right] = 0.022kNm. \quad (6.13)$$

$$\mu_{\text{Ln}M_R} = \text{Ln}(\mu_{M_R}) - 0.5 \cdot \sigma_{\text{Ln}M_R}^2 = 3.14. \quad (6.14)$$

6.1 Purlin's analysis: probability integral for a simplified case

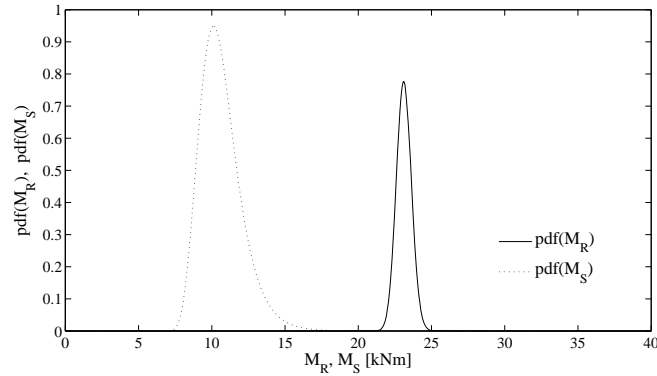
In similar way we compute the parameters of the bending demand.

$$E[M_S] = C_{load} \cdot E[Q + W_p + P] = 3.915 kNm. \quad (6.15)$$

$$E[M_S^2] = C_{load}^2 \cdot E[Q^2] = 0.1045 (kNm)^2. \quad (6.16)$$

From the mean and standard deviation of M_S , the parameters of the Gumbel-Poisson distribution are computed ($a = 0.24$ and $b = 1.68$). The probability density function of M_R and M_S are shown in figure 6.1.

Figure 6.1: Probability density function of M_R and M_S .



According to the *chain rule* and the property of the *convolution integral*, the probability of Eq. 6.9 is given by the integral in Eq. 6.17, where

$$s = \frac{ms}{C_{load}} - w - p.$$

$$Pr(F) = \int_0^{+\infty} \left\{ 1 - \text{Exp} \left[\lambda \left[\text{Exp} \left(-\text{Exp} \left(-\frac{s-b}{a} \right) \right) \right] \right] \right\} \cdot \left\{ \frac{1}{r\sigma_{\text{Ln}M_R}\sqrt{2\pi}} \text{Exp} \left[-\frac{1}{2} \left(\frac{\text{Ln}(r) - \mu_{\text{Ln}M_R}}{\sigma_{\text{Ln}M_R}} \right)^2 \right] \right\}. \quad (6.17)$$

By approximating the integral with the trapezoidal rule, it is easy to compute the probability integral. The Probability of failure computed is reported in table 6.1 together with the corresponding results from Monte carlo sampling. The trapezoidal rule is a too crude approximation of the integral and respect to Monte Carlo, it leads to overestimate the probability of failure.

Computation	$Pr(F)_{1yr}$	$Pr(F)_{50yr}$
Integration	$3.9 \cdot 10^{-6}$	$1.9 \cdot 10^{-4}$
MCS	$2.6 \cdot 10^{-6}$	$1.3 \cdot 10^{-4}$

Table 6.1: Probability of Failure for the middle span of a simply supported purlin.

6.2 Purlin's analysis (FORM, MCS)

6.2.1 First Order Reliability Method formulation for the purlin

The reliability index β and the associated probability of failure are computed by implementing the HLRF algorithm for solving the FORM analysis

6.2 Purlin's analysis (FORM, MCS)

of the purlins series system. As reported in section 2.5, it is necessary to define first the statistics of the variables of the problem and then to compute the transformation function into the Standard Normal space for each of them. The random variables for the formulation of the FORM analysis for the purlins are the bending resistance R_b , the snow load on the ground Q , the roof shape factor C , the self weight of the purlins W_P and the permanent load P . To each of them corresponds a standard normal variable. The transformation function for the snow load on the ground is given in Eq. 6.18.

$$Q^{-1}(u_q) = \begin{cases} 0, & \text{if } u_q < -0.499; \\ b_q - a_q \text{Ln} \left[-\text{Ln} \left(1 + \frac{\text{Ln}(\Phi(u_q))}{\lambda} \right) \right], & \text{else.} \end{cases} \quad (6.18)$$

In Eq. 6.18, the value of $u_q = -0.499$ corresponds to the value of the standard normal variable that has the same probability of the null value of q on the CDF of the snow load on the ground.

The transformation function for the roof shape factor is given in Eq. 6.19.

$$C^{-1}(u_c) = b_c - a_c \cdot \text{Ln} [\text{Ln} (\Phi (u_c))]. \quad (6.19)$$

The transformation function for the self weight is given in Eq. 6.20.

$$W_P^{-1}(u_{wp}) = \mu_{wp} - \sigma_{wp} \cdot u_{wp}. \quad (6.20)$$

The transformation function for the permanent load is given in Eq. 6.21.

$$P^{-1}(u_p) = \mu_p - \sigma_p \cdot u_p. \quad (6.21)$$

The transformation function for the bending resistance is given in Eq. 6.22.

$$R_b^{-1}(u_{r_b}) = \text{Exp} [\mu_{L_n R_b} - \sigma_{L_n R_b} \cdot u_{L_n R_b}]. \quad (6.22)$$

Let's write the equation of the limit state function in the standard normal space, given the vector of the standard normal variables $U = \{u_q, u_c, u_{wp}, u_p, u_{r_b}\}$ corresponding to the variables in the ordinary space. The limit state function G for the purlins in biaxial bending in the standard normal space is given in Eq. 6.23, where the coefficients $C_{load,x}$, $C_{load,y}$, $C_{res,x}$ and $C_{res,y}$ are constants depending respectively on the static configuration of the purlin and on the geometry of the cross section.

$$G(\mathbf{U}) = 1 - \frac{C_{load,x} [Q^{-1}(u_q) \cdot C^{-1}(u_c) + W_P^{-1}(u_g) + P^{-1}(u_p)]}{C_{res,x} \cdot R^{-1}(u_{r_b})} - \frac{C_{load,y} [Q^{-1}(u_q) \cdot C^{-1}(u_c) + W_P^{-1}(u_g) + P^{-1}(u_p)]}{C_{res,y} \cdot R^{-1}(u_{r_b})}. \quad (6.23)$$

Each purlin is modeled as series system of discrete sections, each at distance of 50cm. This means also that each purlin is considered as a series system of equicorrelated elements/components, each of them with its reliability index β and a correlation factor, respect to the other sections, that is constant because the system is loaded by the same external load.

As reported in section 2.5.2, the computation of the components of the gradient is needed. For the case study of the purlins, the components of

6.2 Purlin's analysis (FORM, MCS)

the gradient of the limit state function G are listed below in Eqs. 6.24, 6.25, 6.26, 6.27, 6.28.

$$\begin{aligned} \frac{\partial G}{\partial u_q} &= \left(\frac{C_{load,x}}{C_{res,x}} + \frac{C_{load,y}}{C_{res,y}} \right) \cdot \frac{C^{-1}(u_c)}{\text{Exp}[\mu_{\text{Ln}R_b} + \sigma_{\text{Ln}R_b}]} \\ &\quad \cdot \frac{a_q \left[\frac{1}{\sqrt{2\pi}} \text{Exp} \left(-\frac{1}{2} u_q^2 \right) \right]}{\lambda \Phi(u_q) \cdot \text{Ln} \left(1 + \frac{\text{Ln}(\Phi(u_q))}{\lambda} \right)}. \end{aligned} \quad (6.24)$$

$$\begin{aligned} \frac{\partial G}{\partial u_c} &= \left(\frac{C_{load,x}}{C_{res,x}} + \frac{C_{load,y}}{C_{res,y}} \right) \cdot \frac{Q^{-1}(u_q)}{\text{Exp}[\mu_{\text{Ln}R_b} + \sigma_{\text{Ln}R_b}]} \\ &\quad \cdot \frac{a_c \left[\frac{1}{\sqrt{2\pi}} \text{Exp} \left(-\frac{1}{2} u_c^2 \right) \right]}{\Phi(u_c) \cdot \text{Ln}(\Phi(u_c))}. \end{aligned} \quad (6.25)$$

$$\frac{\partial G}{\partial u_g} = \left(\frac{C_{load,x}}{C_{res,x}} + \frac{C_{load,y}}{C_{res,y}} \right) \cdot \frac{-\sigma_g}{\text{Exp}[\mu_{\text{Ln}R_b} + \sigma_{\text{Ln}R_b}]} \quad (6.26)$$

$$\frac{\partial G}{\partial u_p} = \left(\frac{C_{load,x}}{C_{res,x}} + \frac{C_{load,y}}{C_{res,y}} \right) \cdot \frac{-\sigma_p}{\text{Exp}[\mu_{\text{Ln}R_b} + \sigma_{\text{Ln}R_b}]} \quad (6.27)$$

$$\begin{aligned} \frac{\partial G}{\partial u_r} &= \left(\frac{C_{load,x}}{C_{res,x}} + \frac{C_{load,y}}{C_{res,y}} \right) \cdot \frac{\sigma_{\text{Ln}R_b}}{\text{Exp}[\mu_{\text{Ln}R_b} + \sigma_{\text{Ln}R_b} \cdot u_{r_b}]} \\ &\quad \cdot \left\{ Q^{-1}(u_q) \cdot C^{-1}(u_c) + W_P^{-1}(u_g) + P^{-1}(u_p) \right\}. \end{aligned} \quad (6.28)$$

Results of FORM analysis for the purlins

Table 6.2 summarizes the probability of failure of the critical sections for the three structural configurations, which correspond to the sections that are checked in the deterministic design (highest bending moment section). These calculations assume that there are no systematic errors in the purlins. The results confirm that the design reliability is identical for the three configurations, which is expected since they all were designed to have the same utilization factor. It is furthermore noted that the reliability index is lower than the target value given in Eurocode 0, which is $\beta = 4.7$ for a one-year reference period. The FORM sensitivity factors presented in table 6.3 show that the uncertainty in the snow load Q , the shape factor C and the bending strength R determines the reliability. It is worth to remark that the shape factor C at design point x^* assumes values bigger than one due to the assumed Gumbel distribution to take into account the accumulation of snow. The difference between the calculated reliability indexes and the target value of Eurocode 0 might be explained by the significant uncertainty in the shape factor C .

Configuration	$Pr(F_j(1yr) \bar{D})$	β_j
Simply supported	$7.4 \cdot 10^{-6}$	4.33
Continuous	$7.9 \cdot 10^{-6}$	4.32
Lap-jointed	$7.0 \cdot 10^{-6}$	4.34

Table 6.2: Probability of failure of a critical section j , $Pr(F_j(1yr) | \bar{D})$ and corresponding reliability index β_j .

6.2 Purlin's analysis (FORM, MCS)

Configuration	Q	C	W_P	P	R_b
Simply supported					
α	0.604	0.597	0.0080	0.037	0.526
x^*	1.003	1.77	0.083	0.40	20.12
Continuous					
α	0.604	0.597	0.0078	0.037	0.526
x^*	0.99	1.76	0.084	0.407	20.16
Lap-jointed					
α	0.604	0.597	0.0077	0.037	0.526
x^*	1.05	1.77	0.084	0.406	20.10

Table 6.3: Probability of failure of a critical section j , $Pr(F_j(1yr) | \bar{D})$ and corresponding design point x^* .

Table 6.4 summarizes the probability of failure in 1 year and in 50 years for one purlin with multiple critical sections (one every 50cm), given that there are no systematic errors $Pr(F | \bar{D})$ and for the three purlins configurations. The system of critical sections is modeled as series system with correlation factor $\rho = 0.73$.

Configuration	$Pr(F_j(1yr) \bar{D})$	$Pr(F_j(50yr) \bar{D})$
Simply supported	$1.95 \cdot 10^{-5}$	$9.7 \cdot 10^{-4}$
Continuous	$3.4 \cdot 10^{-5}$	$1.7 \cdot 10^{-3}$
Lap-jointed	$3.4 \cdot 10^{-5}$	$1.7 \cdot 10^{-3}$

Table 6.4: Probability of failure of one purlin.

Table 6.5 summarizes the probability of system failure in 1 year and in 50 years given that there are no systematic errors $Pr(F | \bar{D})$ for the three purlins configurations. The probability of failure is computed with the Kang-Song integral [25]. The reliability of the three secondary systems

is not identical, due to the varying numbers of critical sections. The simply supported configuration has the largest number of critical sections, since it contains more purlins and each purlin has one critical section (in the mid-span). The two static indeterminate configurations have only two critical sections in each line (the outer spans support section). Furthermore, lap-jointed configuration has less purlins than the continuous one, due to the larger possible distance between the purlins. The table 6.5 lists also the Ditlevsen bounds for the probability of failure (see Appendix B).

Configuration	$Pr(F_j(1yr) \overline{D})$	Ditlevsen bounds 1yr
Simply supported	$3.6 \cdot 10^{-4}$	$8.0 \cdot 10^{-5} \div 1.6 \cdot 10^{-3}$
Continuous	$2.9 \cdot 10^{-4}$	$1.5 \cdot 10^{-4} \div 3.1 \cdot 10^{-3}$
Lap-jointed	$2.6 \cdot 10^{-4}$	$1.4 \cdot 10^{-4} \div 2.8 \cdot 10^{-3}$
Configuration	$Pr(F_j(50yr) \overline{D})$	Ditlevsen bounds 50yr
Simply supported	$1.81 \cdot 10^{-2}$	$4.0 \cdot 10^{-3} \div 7.7 \cdot 10^{-2}$
Continuous	$1.45 \cdot 10^{-2}$	$7.7 \cdot 10^{-3} \div 14.5 \cdot 10^{-2}$
Lap-jointed	$1.32 \cdot 10^{-2}$	$7.0 \cdot 10^{-3} \div 13.1 \cdot 10^{-2}$

Table 6.5: Probability of failure of secondary system, $Pr(F_j(1yr) | \overline{D})$ and corresponding Ditlevsen bounds.

6.2.2 Monte Carlo sampling for the analysis of the purlins

Monte Carlo Simulations (MCS) with 10^5 samples are computed. The software used to compute the simulation is implemented in Matlab and it enables the evaluation not only of the probability of failure but also to obtain numerical data to compute the full distribution of the damaged area, $f_{A_F|F}$ as required for the robustness assessment.

6.2 Purlin's analysis (FORM, MCS)

For the system of purlins according to the three static configurations, computations are made both in absence and in presence of systematic weaknesses. This comparison will enable to evaluate the sensitivity of the static configuration to the presence of systematic weaknesses.

The limit state function defined in Eq. 3.4 for purlins in biaxial bending with $K_m = 0.7$ is valid only for rectangular sections. It is worth to compare how this factor changes the probability of failure for the system of purlins.

MCS Results for the purlin system without systematic weaknesses

Table 6.6 lists the probability of biaxial bending failure, with the related statistics and confidence bounds, for the purlin system with $K_m = 1$, while table 6.7 lists the results for $k_m = 0.7$. As expected, the probability of failure in the case of $k_m = 0.7$ is lower, while it seems quite surprising that the probability of failure decreases of 50% only for simply supported and for the lap-jointed configurations. The probability of failure for the continuous configuration does not change with k_m because the effect of the high bending moment on the support is dominant.

Configuration	$Pr(F_j(50yr) \bar{D})$	σ	95% confidence bounds
Simply supported	$4.63 \cdot 10^{-2}$	$6.8 \cdot 10^{-4}$	$4.5 \cdot 10^{-2} \div 4.76 \cdot 10^{-2}$
Continuous	$1.84 \cdot 10^{-2}$	$4.3 \cdot 10^{-4}$	$1.75 \cdot 10^{-2} \div 1.92 \cdot 10^{-2}$
Lap-jointed	$1.46 \cdot 10^{-2}$	$3.8 \cdot 10^{-4}$	$1.39 \cdot 10^{-2} \div 1.54 \cdot 10^{-2}$

Table 6.6: Probability of biaxial bending failure of secondary system for $k_m = 1$.

Despite the three configurations are all designed to achieve the same reli-

Configuration	$Pr(F_j(50yr) \overline{D})$	σ	95% confidence bounds
Simply supported	$2.4 \cdot 10^{-2}$	$4.9 \cdot 10^{-4}$	$2.3 \cdot 10^{-2} \div 2.5 \cdot 10^{-2}$
Continuous	$1.98 \cdot 10^{-2}$	$4.45 \cdot 10^{-4}$	$1.9 \cdot 10^{-2} \div 2.1 \cdot 10^{-2}$
Lap-jointed	$0.7 \cdot 10^{-2}$	$2.6 \cdot 10^{-4}$	$0.65 \cdot 10^{-2} \div 0.75 \cdot 10^{-2}$

Table 6.7: Probability of biaxial bending failure of secondary system for $k_m = 0.7$.

ability at the most critical section, the system reliability of the three configurations is different because of the varying number of elements/components in the series system model.

To assess the robustness criterion and compute the risk, it is needed to organize the data from the MCS with respect to the area failed. Figure 6.2 shows the trend of mean and standard deviation of the area failed for the case $k_m = 1$ and figure 6.3 the trend of mean and standard deviation of the area failed for the case $k_m = 0.7$. The failure rate is approximately constant over the considered service life period (50yr), because the degradation of the timber material has not been considered. In addition, the lap-jointed configuration shows a lower standard deviation for both cases.

The expected value of area failed A_F conditioned to the absence of systematic weaknesses D is listed in table 6.8.

Configuration	$E[A_F F, \overline{D}]$
Simply supported	17.22
Continuous	24.24
Lap-jointed	32.34

Table 6.8: $E[A_F | F, \overline{D}]$ of secondary system for $k_m = 1$.

6.2 Purlin's analysis (FORM, MCS)

Figure 6.2: Mean and Standard Deviation respect to time for $k_m = 1$.

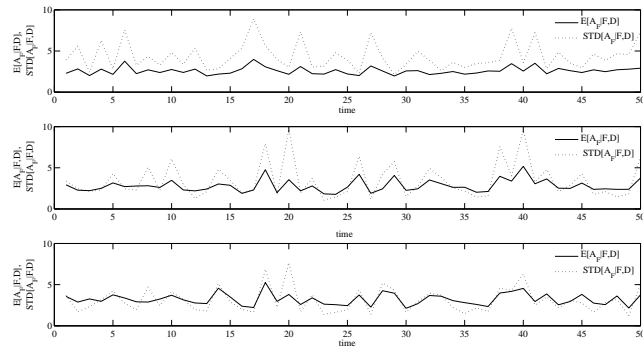
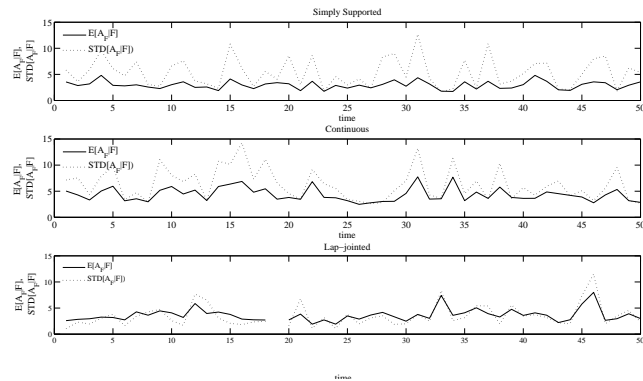


Figure 6.3: Mean and Standard Deviation respect to time for $k_m = 0.7$.



Figures 6.4 and 6.5 show the histograms of the area failed A_F given the events F, \overline{D} for the case $k_m = 1$ and $k_m = 0.7$ respectively. In the case of $k_m = 1$ a higher occurrence of small failures is possible. In addition, for the system of continuous purlins is possible to reach bigger values of area failed upon a failure than the simply supported and lap-jointed configurations.

Figure 6.4: Histogram of A_F given (F, \overline{D}) for $k_m = 1$.

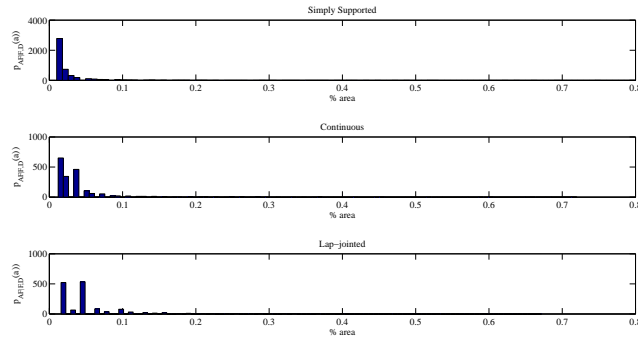
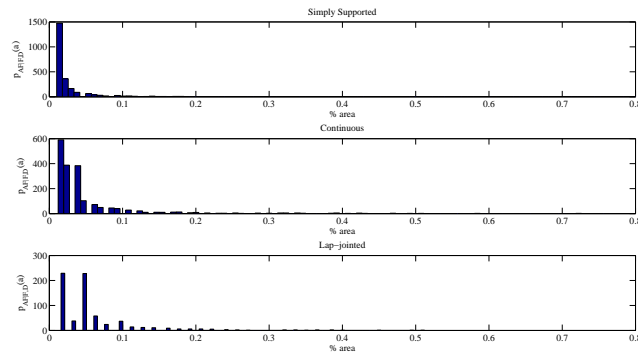


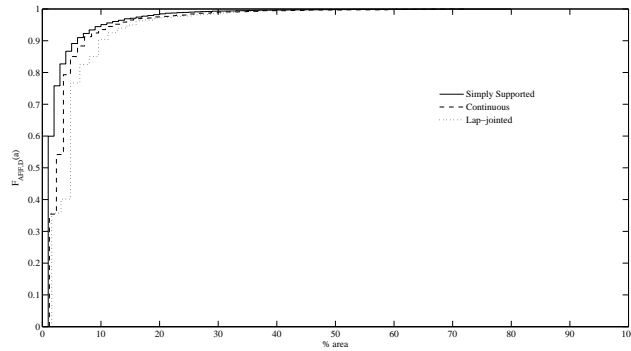
Figure 6.5: Histogram of A_F given (F, \overline{D}) for $k_m = 0.7$.



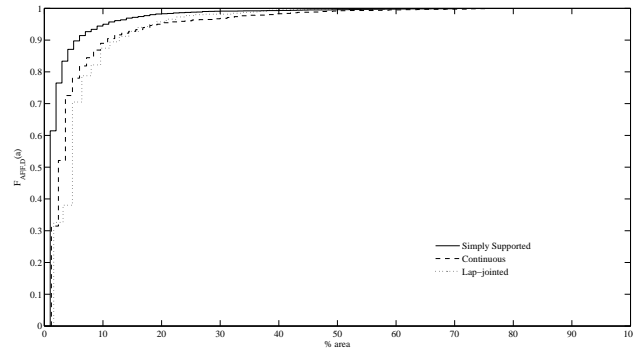
6.2 Purlin's analysis (FORM, MCS)

Figures 6.6 and 6.7 show the cumulative density function of the area failed A_F conditional on the system having failed F and on the absence of systematic errors D for the case $k_m = 1$ and $k_m = 0.7$ respectively. For the case $k_m = 1$ the CDF for the three purlins configurations has a more near trend and shows a better behavior (more stiff trend). This is because a higher number of failure with small area failed correspond to the case $k_m = 1$.

Figure 6.6: CDF of A_F given (F, \overline{D}) for $k_m = 1$.



From figures 6.6 and 6.7, it can be observed that a failure in the structural system with simply supported purlins results in smaller damages than the other configurations. In the simply supported configuration, a smaller number of purlins (and consequently a smaller proportion of the roof area) will fail. In the statically indeterminate configurations, progressive collapse mechanisms lead to a larger number of purlin failed once the first section has failed. Between the static indeterminate configurations, the continuous

Figure 6.7: CDF of A_F given (F, \overline{D}) for $k_m = 0.7$.

purlin behaves better than the lap-jointed purlin. Indeed, in the lap-jointed purlin configuration a bigger number of elements fail at the same time.

MCS Results for the purlin system with systematic weaknesses

As described in section 4.7, systematic weaknesses are introduced in the secondary element system in order to assess which of the three purlin configurations has the best behavior with respect to robustness. Table 6.9 lists the probability of system failure given that there is a systematic weakening of the system, $Pr(F | D)$, for the three structural configurations. As expected, the higher is the process rate p , the bigger is the increase in the probability of system failure, compared to the case of no systematic weakening.

Figures 6.8, 6.9 and 6.10 show the histogram of area failed A_F condi-

6.2 Purlin's analysis (FORM, MCS)

Configuration	$Pr(F_j(50yr) D)$	σ	95% confidence bounds
Simply supported			
p=1%	$4.9 \cdot 10^{-2}$	$7.0 \cdot 10^{-4}$	$4.77 \cdot 10^{-2} \div 5.04 \cdot 10^{-2}$
p=10%	$6.4 \cdot 10^{-2}$	$8.0 \cdot 10^{-4}$	$6.28 \cdot 10^{-2} \div 6.59 \cdot 10^{-2}$
p=30%	$9.4 \cdot 10^{-2}$	$9.7 \cdot 10^{-4}$	$9.19 \cdot 10^{-2} \div 9.57 \cdot 10^{-2}$
Continuous			
p=1%	$1.92 \cdot 10^{-2}$	$4.4 \cdot 10^{-4}$	$1.84 \cdot 10^{-2} \div 2.01 \cdot 10^{-2}$
p=10%	$3.09 \cdot 10^{-2}$	$5.5 \cdot 10^{-4}$	$2.99 \cdot 10^{-2} \div 3.20 \cdot 10^{-2}$
p=30%	$5.36 \cdot 10^{-2}$	$7.3 \cdot 10^{-4}$	$5.21 \cdot 10^{-2} \div 5.50 \cdot 10^{-2}$
Lap-jointed			
p=1%	$1.5 \cdot 10^{-2}$	$3.8 \cdot 10^{-4}$	$1.43 \cdot 10^{-2} \div 1.58 \cdot 10^{-2}$
p=10%	$1.9 \cdot 10^{-2}$	$4.5 \cdot 10^{-4}$	$1.90 \cdot 10^{-2} \div 2.08 \cdot 10^{-2}$
p=30%	$3.0 \cdot 10^{-2}$	$5.5 \cdot 10^{-4}$	$2.94 \cdot 10^{-2} \div 3.15 \cdot 10^{-2}$

Table 6.9: Probability of biaxial bending failure of secondary system for $k_m = 1$ and with systematic weaknesses with rate $p = 1\%$, 10% , 30% .

tioned on failures F and systematic weaknesses D for the $p = 1\%$, 10% , 30% rate of Bernoulli Process.

The expected value of area failed A_F conditioned on the presence of systematic weaknesses D is listed in table 6.10 for $p = 1\%$, 10% , 30% . The average area failed is higher for the static indeterminate purlins system. In addition the average area failed decreases with the weaknesses rate. This is explained by the fact that, the presence of systematic weaknesses increases the uncertainty in the capacity. This means that the capacity has a stronger influence on the behavior of the system. In addition, this leads to a decrease in the statistical dependence among failures of individual sections and, therefore, large numbers of purlin failures become less likely.

Figure 6.8: Histogram of A_F given F, D for $k_m = 1$ and $p = 1\%$.

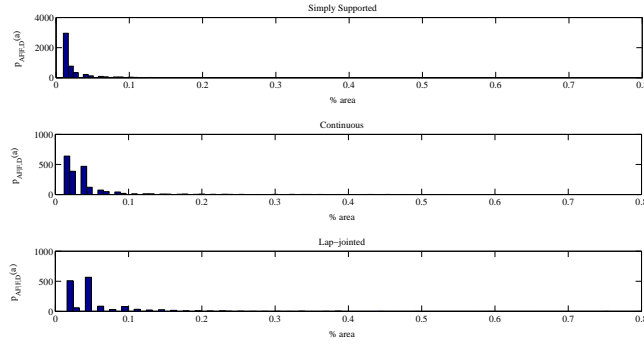
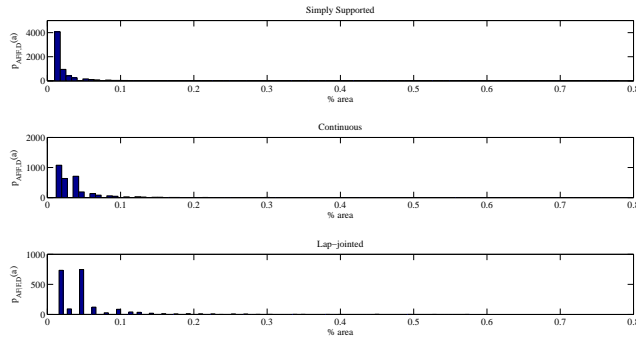


Figure 6.9: Histogram of A_F given F, D for $k_m = 1$ and $p = 10\%$.

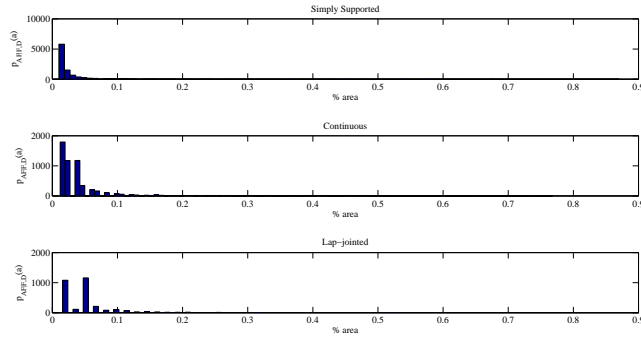


Configuration	$E[A_F F, D]$		
	$p = 1\%$	$p = 10\%$	$p = 30\%$
Simply supported	15.36	14.40	13.62
Continuous	17.52	16.02	16.44
Lap-jointed	20.40	18.30	19.08

Table 6.10: $E[A_F | F, D]$ of secondary system for $k_m = 1$.

6.2 Purlin's analysis (FORM, MCS)

Figure 6.10: Histogram of A_F given F, D for $k_m = 1$ and $p = 30\%$.



Figures 6.11, 6.12 and 6.13 show the computed CDF of the failed area A_F conditional on the system having failed F and on the presence of systematic weakening $F(A_F|F, D)$ with rate $p = 1\%, 10\%, 30\%$.

The three configurations show the same trend as in the case of the system without systematic weakening.

Figure 6.11: CDF of A_F given (F, D) for $k_m = 1$ and $p = 1\%$.

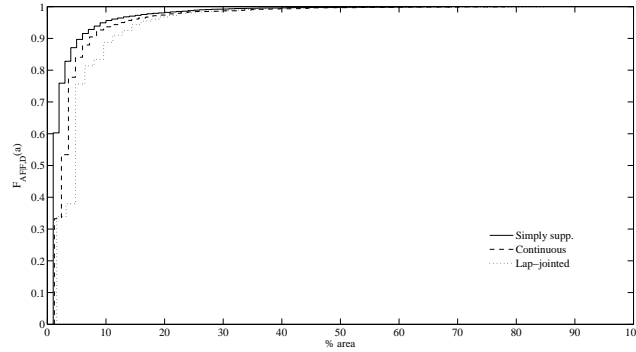


Figure 6.12: CDF of A_F given (F, D) for $k_m = 1$ and $p = 10\%$.

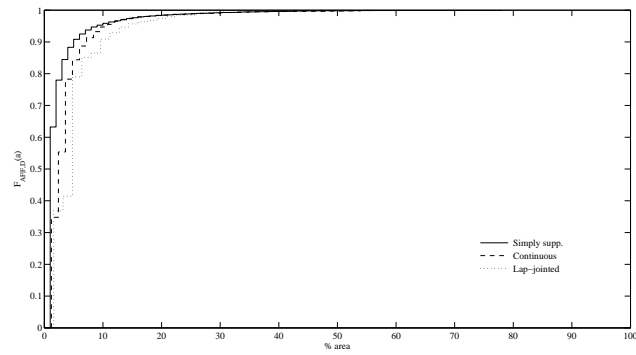
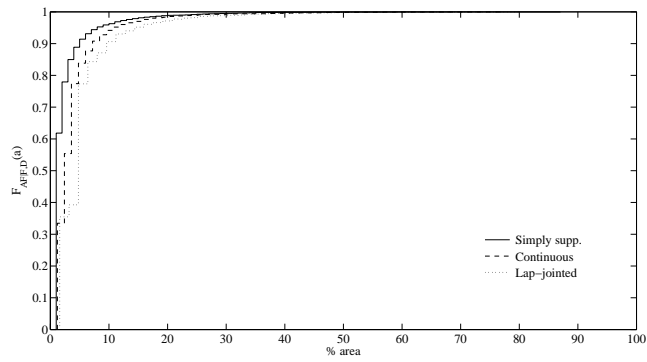


Figure 6.13: CDF of A_F given (F, D) for $k_m = 1$ and $p = 30\%$.



6.2 Purlin's analysis (FORM, MCS)

Comparison for the purlin system with and without systematic weaknesses

Two separate models were employed to compute the pdf and CDF of area failed A_F in absence and in presence of systematic weaknesses: $f_{A_F|\overline{D}}(a)$ and $f_{A_F|D}(a)$. The unconditioned PDF of the failed area is then given by Eq. 6.29.

$$f_{A_F}(a) = f_{A_F|\overline{D}}(a) \cdot Pr(\overline{D}) + f_{A_F|D}(a) \cdot Pr(D). \quad (6.29)$$

where $Pr(D)$ is the probability that a systematic weakening of the structure is present.

It is important to remember that regular design procedures are based on the assumption that systematic errors are prevented by quality control and other measures. This means that it is assumed that $Pr(D) = 0$. Since robustness can be interpreted as the ability of the structure to sustain unforeseen actions, an indicator for robustness is the difference between the total risk, calculated with Eqs. 3.19 and 6.29 and $Pr(D) > 0$, and the risk conditional on no errors, calculated with Eqs. 3.19 and 6.29 and $Pr(D) = 0$. Therefore, we need to compute $F_{A_F|F}$ the distribution of the failed area when it is unknown whether a systematic weakening of the system is present or not by unconditioning on the variable D . This is made by applying the *Total Probability Theorem* and the *Bayes' Rule* as:

$$F_{A_F|F} = A_F | F, \overline{D} \cdot Pr(\overline{D} | F) + A_F | F, D \cdot Pr(D | F). \quad (6.30)$$

The probability $Pr(D | F)$ is computed by Bayes' rule as:

$$Pr(D | F) = Pr(F | D) \cdot \frac{Pr(D)}{Pr(F)}. \quad (6.31)$$

Due to the fact that two separate models were employed to compute the probability of failure in absence and presence of weakening, the probability of failure obtained is conditioned on the variable D . The total probability of failure of the secondary system is computed as:

$$Pr(F) = Pr(F | \overline{D}) \cdot Pr(\overline{D}) + Pr(F | D) \cdot Pr(D). \quad (6.32)$$

The computed values of $Pr(F)$ are listed in table 6.11.

Configuration	$Pr(F)$	
	$Pr(D) = 0.01$	$Pr(D) = 0.10$
Simply supported	0.0468	0.0510
Continuous	0.0188	0.0219
Lap-jointed	0.0148	0.0162

Table 6.11: $Pr(F)$ for the secondary system configurations for $Pr(D) = 1\%, 10\%$ and weakening rate of 30% .

Figures 6.14 and 6.15 show the CDF of the failed area A_F conditional on the system having failed F , when the probability of having systematic errors is assumed as $Pr(D) = 0.01$ and $Pr(D) = 0.10$ respectively and obviously with the $Pr(\overline{D}) = 1 - Pr(D)$. However, it can be observed that the difference between the results obtained with these two values of the $Pr(D)$

6.2 Purlin's analysis (FORM, MCS)

is small. This is because the effect of the weakness on the conditional distribution is low. This can be already seen from comparing figure 6.6 with figures 6.11, 6.12, 6.13.

Figure 6.14: CDF of A_F for $k_m = 1$ and $Pr(D) = 0.01$.

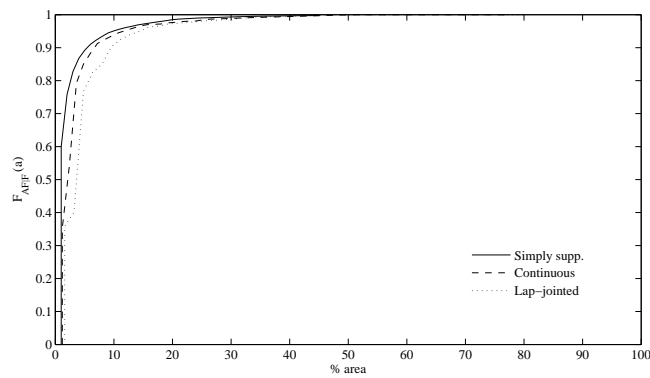
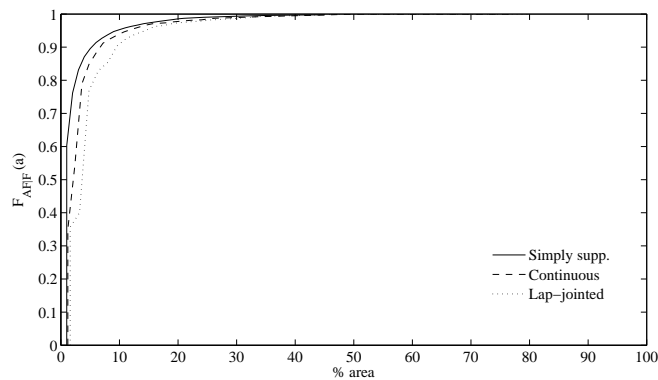


Figure 6.15: CDF of A_F for $k_m = 1$ and $Pr(D) = 0.10$.



To check this "robustness" criterion, the probability that the failed area is less than 15% of the total area given a failure is computed (table 6.12).

Configuration	$Pr(A_F < 0.15 \cdot A_{roof} F)$	
	$Pr(D) = 0.01$	$Pr(D) = 0.10$
Simply supported	0.9711	0.9728
Continuous	0.9690	0.9684
Lap-jointed	0.9561	0.9559

Table 6.12: $Pr(A_F < 0.15 \cdot A_{roof} | F)$ for the secondary system configurations for $Pr(D) = 1\%, 10\%$ and weakening rate of 30%.

With respect to the defined robustness criterion, the roof system configuration with simply supported purlins is the optimal one, because a failure in this configuration leads to the smallest failed area (table 6.8 and 6.10) and it has the lowest probability of not fulfilling the 15% area requirement (table 6.12).

Likewise, the expected value of the area failed upon a failure $E[A_F | F]$ must be computed by unconditioning the average computed above and listed in table 6.10 on the variable D , as shown in Eq. 6.33.

$$\begin{aligned}
 E[A_F | F] &= E[A_F | F, \overline{D}] \cdot Pr(\overline{D} | F) + \\
 &+ E[A_F | F, D] \cdot Pr(D | F).
 \end{aligned} \tag{6.33}$$

The values of $E[A_F | F]$ for the three purlins configurations are listed in table 6.13.

Finally the risk is computed from the $E[A_F | F]$ by unconditioning on the failure event F as $E[A_F | F] \cdot Pr(F)$. The risk computed for the three

6.2 Purlin's analysis (FORM, MCS)

Configuration	E [A _F F]	
	Pr(D) = 0.01	Pr(D) = 0.10
Simply supported	17.16	16.86
Continuous	25.24	24.00
Lap-jointed	32.34	32.22

Table 6.13: Risk as E [A_F] for the secondary system configurations for Pr(D) = 1%, 10% and weakening rate of 30%.

roof systems is given in table 6.14.

Configuration	E [A _F]	
	Pr(D) = 0.01	Pr(D) = 0.10
Simply supported	0.78	0.84
Continuous	0.48	0.54
Lap-jointed	0.48	0.54

Table 6.14: Risk E [A_F] for the secondary system configurations for Pr(D) = 1%, 10% and weakening rate of 30%.

The risk calculated for simply supported configuration is higher than for continuous and lap-jointed configurations. This is due to the fact that the probability of system failure is higher for the system with simply supported purlins, even though the consequences are lower. In addition, the lap-jointed configuration is the cheapest, thus supporting this choice of this configuration from a risk (or rather expected cost) perspective. Therefore, despite the fact that the simply supported configuration is more robust, static indeterminate configurations are more optimal. This points to a general problem in the definition of robustness: *a more robust system might*

often be less optimal from a risk analysis point-of-view. These results are also dependent on the fact that the distances between the purlins were adapted in order to receive the same utilization factor for all three systems, while usually the distances are based on requirements from the roof cladding. If the same distances would be applied to all systems, assuming a consistent utilization factor, the three systems would show a more similar behavior. If continuous and lap-jointed configurations would be modified to have the same distance between purlins than simply supported configuration, they would become slightly more robust but would also have a higher probability of system failure and thus exhibit a higher risk.

6.3 Primary beams analysis (FORM, MCS)

6.3.1 First Order Reliability Method formulation for the primary beam

Also for the system of six primary beams, the reliability index β is computed by implementing the HLRF algorithm to solve the FORM optimization problem. The system is modeled as series system of sections. Differently from the purlins' case, the beams' check is done only at the two most loaded sections and in addition, the random variables for the formulation of FORM for the beams are different according to the limit state chosen.

The ultimate limit state conditions considered for the primary beams are:

- bending failure;
- shear failure;

6.3 Primary beams analysis (FORM, MCS)

- tension perpendicular to the grain.

Differently to the MCS the limit state function for combined tension perpendicular to the grain and shear is not considered, due to the fact that the SIA limit state function is not linear and it has also a point of discontinuity (cusp). Therefore the first order approximation with Taylor series is not possible.

According to the three purlins static configurations chosen, the load is transferred from the purlins to the primary beams in different percentage. For the simply supported purlins configuration each beam is equally loaded, while for the two static indeterminate configurations the distribution of the load among the beams is different.

First Order Reliability Method: primary beam bending failure

The bending limit state function depends on the following random variables: bending resistance R_b , snow load on the ground Q , roof shape factor C , self weight of the beam W_B , self weight of the purlins W_P and permanent load P . To each of them corresponds a standard normal variable.

The transformation functions for the snow load on the ground and roof shape factor are given in Eqs. 6.18 and 5.13, for the purlins self weight and permanent load are given in Eqs. 6.20 and 6.21, for the bending resistance in Eq. 6.22. The expression of transformation functions for the self weight of the primary beam W_B is similar to the expression of W_P .

Let's write the equation of the limit state function in the standard normal space, given the vector $U = \{u_q, u_c, u_{gP}, u_{gB}, u_p, u_{r_b}\}$ of the standard nor-

mal variables corresponding to the variables in the ordinary space.

The limit state function G in the ordinary space is given by the difference between bending strength and bending demand as $g(R, S) = M_R - M_S$.

The limit state function G for the beam for bending failure at the location of maximum effect in the standard normal space is given in Eq. 6.34.

$$\begin{aligned}
 G_b(\mathbf{U}) = & C_{res} \cdot R_b^{-1} - C_{load1} \left[W_B^{-1}(u_{w_b}) + \right. \\
 & + C_{load2} \left(C^{-1}(u_c) \cdot Q^{-1}(u_q) + P^{-1}(u_p) \right) \\
 & \left. + C_{load3} \cdot W_P^{-1}(u_{w_p}) \right]. \tag{6.34}
 \end{aligned}$$

The constants C_{load1} depends on the location of the critical section, while C_{load2} , C_{load3} in Eq. 6.34 depend on the static configuration of the purlins. The constant are listed below.

$$C_{load1} = \frac{1}{2} [1 + \tan(\delta - \alpha)] \cdot (Lz - z^2). \tag{6.35}$$

$$C_{load2} = \frac{l_p}{L} (n_p - 1) \cdot t_i. \tag{6.36}$$

$$C_{load3} = \frac{l_p}{L} n_p \cdot t_i. \tag{6.37}$$

In Eqs. 6.35, 6.36, 6.37 the angle $(\delta - \alpha)$ is the difference between upper and lower inclination of the beam edge, L is the beam length, l_p the purlin length, n_p the number of the purlins according to the static configuration

6.3 Primary beams analysis (FORM, MCS)

chosen and t_i is the factor that corresponds to the load that is carried by the beam. The section of maximum effect of bending moment for the beam is located at a distance equal to $z = \frac{L \cdot h_{apex}}{2 \cdot h_a}$.

For the roof system with simply supported purlins the coefficients are $C_{load1} = 34.44$, $C_{load2} = 5.7$ and $C_{load3} = 6$.

For the roof system with continuous purlins the coefficients are $C_{load1} = 34.44$, $C_{load2} = [2.133, 6.112, 5.254]$ and $C_{load3} = [1.896, 5.433, 4.670]$. For the roof system with continuous purlins the coefficients are $C_{load1} = 34.44$, $C_{load2} = [2.275, 6.520, 5.604]$ and $C_{load3} = [1.422, 4.075, 3.502]$. The coefficients are related to forces in kN and distance in m . The bending strength factor $C_{res,b}$ in Eq. 6.34 is equal to $\frac{b \cdot h_z^2}{6}$, where h_z is the depth of the cross section at location z .

As reported in section 2.5.2, the computation of the components of the gradient is needed. For the bending failure limit state function the components are listed below.

$$\frac{\partial G}{\partial u_q} = C_{load1} \cdot C_{load2} \frac{a_q [b_c - a_c \text{Ln}(-\text{Ln}(\Phi(u_c)))] \cdot \varphi(u_q)}{\lambda \cdot \Phi(u_q) \text{Ln} \left[1 + \frac{\text{Ln}(\Phi(u_q))}{\lambda} \right] \cdot \left[1 + \frac{\text{Ln}(\Phi(u_q))}{\lambda} \right]} \quad (6.38)$$

$$\frac{\partial G}{\partial u_c} = C_{load1} \cdot C_{load2} \frac{a_c [b_q - a_q \text{Ln}(-\text{Ln}(1 + \Phi(u_q)))] \cdot \varphi(u_c)}{\Phi(u_c) \text{Ln}(\Phi(u_c))} \quad (6.39)$$

$$\frac{\partial G}{\partial u_{w_b}} = -C_{load1} \cdot \sigma_{w_b} \quad (6.40)$$

$$\frac{\partial G}{\partial u_{w_p}} = -C_{load1} \cdot C_{load3} \cdot \sigma_{w_p} \quad (6.41)$$

$$\frac{\partial G}{\partial u_p} = -C_{load1} \cdot C_{load2} \cdot \sigma_p. \quad (6.42)$$

$$\frac{\partial G}{\partial u_{r_b}} = C_{res,b} \cdot \sigma_{r_b} \cdot \text{Exp}(\mu_{r_b} + \sigma_{r_b} \cdot u_{r_b}). \quad (6.43)$$

FORM Results for primary beam bending failure

Tables 6.15, 6.17 and 6.19 list the value of reliability index and probability of failure for the most loaded section of the primary beam according to the different location of the beam inside the system. The static configuration of the purlins determines a different distribution of the load on the primary beams. Generally, external beams are less loaded both in the case of simply supported purlins and continuous or lap-jointed purlins (see figure 6.16 for the terminology). Tables 6.16, 6.18 and 6.20 list the α coefficients and the value of the r.v. at optimum.

The results for the beam with the chosen purlins configurations are listed below.

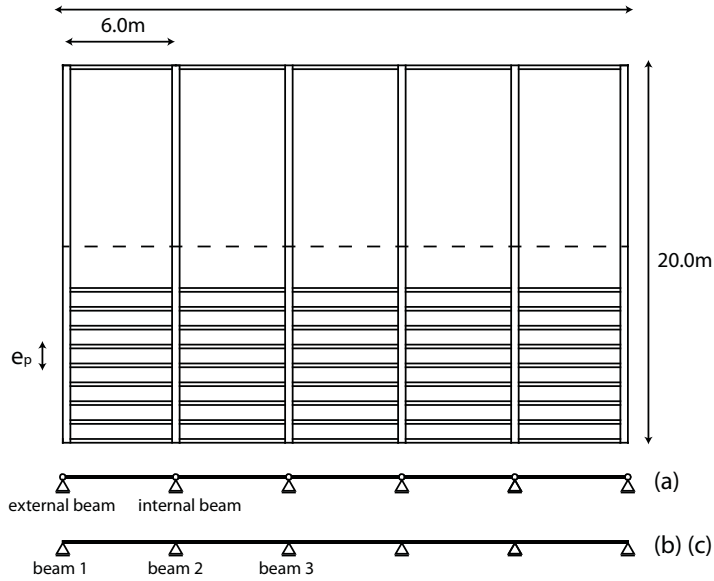
Beam Location	β_j	$Pr(F_j(1yr))$
External beam	7.86	$8.24 \cdot 10^{-16}$
Internal beam	4.67	$1.52 \cdot 10^{-6}$

Table 6.15: Probability of failure of the most loaded section of the primary beam, $Pr(F_j(1yr))$ and corresponding reliability index β_j with the simply supported secondary elements.

Table 6.21 lists the probability of bending failure in 1yr $Pr(F_j(1yr))$ and in 50yr $Pr(F_j(1yr))$ for the most loaded primary beams as series sys-

6.3 Primary beams analysis (FORM, MCS)

Figure 6.16: Roof system configurations.
30.0m



Beam Location	Q	C	W_P	P	W_B	R
External beam						
α coeff.	0.659	0.652	0.0021	0.0099	0.0055	-0.374
x^*	2.3	4.04	0.084	0.403	0.637	19.66
Internal beam						
α coeff.	0.669	0.649	0.0066	0.0316	0.0088	-0.359
x^*	1.17	2.07	0.084	0.406	0.637	23.88

Table 6.16: Importance coefficients and values of the r.v. at design point x^* for the most loaded section of the primary beam with the simply supported secondary elements.

Beam Location	β_j	$Pr(F_j(1yr))$
Beam 1	6.95	$1.868 \cdot 10^{-12}$
Beam 2	4.55	$2.72 \cdot 10^{-6}$
Beam 3	4.89	$4.88 \cdot 10^{-7}$

Table 6.17: Probability of failure of the most loaded section of the primary beam, $Pr(F_j(1yr))$ and corresponding reliability index β_j with the continuous secondary elements.

Beam Location	Q	C	W_P	P	W_B	R
Beam 1						
α coeff.	0.662	0.653	0.0029	0.0137	0.0055	-0.366
x^*	1.89	3.34	0.084	0.404	0.639	20.977
Beam 2						
α coeff.	0.669	0.649	0.007	0.033	0.0086	-0.359
x^*	1.14	2.02	0.084	0.406	0.637	24.04
Beam 3						
α coeff.	0.669	0.651	0.0061	0.0289	0.0087	-0.356
x^*	1.24	2.18	0.084	0.406	0.637	23.65

Table 6.18: Importance coefficients and values of the r.v at design point x^* for the most loaded section of the primary beam with the continuous secondary elements.

Beam Location	β_j	$Pr(F_j(1yr))$
Beam 1	7.00	$1.23 \cdot 10^{-12}$
Beam 2	4.58	$2.29 \cdot 10^{-6}$
Beam 3	4.93	$4.10 \cdot 10^{-7}$

Table 6.19: Probability of failure of the most loaded section of the primary beam, $Pr(F_j(1yr))$ and corresponding reliability index β_j with the lap-jointed secondary elements.

6.3 Primary beams analysis (FORM, MCS)

Beam Location	Q	C	W_P	P	W_B	R
Beam 1						
α coeff.	0.662	0.653	0.0028	0.0135	0.0103	-0.366
x^*	1.92	3.38	0.084	0.404	0.639	20.92
Beam 2						
α coeff.	0.669	0.650	0.0068	0.033	0.0087	-0.356
x^*	1.15	2.03	0.084	0.406	0.637	24.03
Beam 3						
α coeff.	0.669	0.652	0.0059	0.028	0.0088	-0.354
x^*	1.25	2.20	0.084	0.405	0.637	23.65

Table 6.20: Importance coefficients and values of the r.v. at design point x^* for the most loaded section of the primary beam with the lap-jointed secondary elements.

tem of two symmetrical critical sections with correlation factor $\rho = 0.87$.

Purlins configuration	$Pr(F(1yr))$	$Pr(F(50yr))$
Simply supported	$2.74 \cdot 10^{-6}$	$1.37 \cdot 10^{-4}$
Continuous	$4.87 \cdot 10^{-6}$	$2.44 \cdot 10^{-4}$
Lap-Jointed	$4.04 \cdot 10^{-6}$	$2.02 \cdot 10^{-4}$

Table 6.21: Probability of bending failure of the most loaded primary beam respect to the three configurations, $Pr(F(1yr))$ and $Pr(F(50yr))$.

Table 6.22 lists the probability of bending failure in 1yr $Pr(F_j(1yr))$ and in 50yr $Pr(F_j(50yr))$ for the entire system of primary beams as series system of twelve symmetrical critical sections with correlation factor $\rho = 0.87$. As expected the system of six primary beams shows to have a similar reliability respect to the three purlins configurations.

Purlins configuration	$Pr(F(1yr))$	$Pr(F_j(50yr))$
Simply supported	$8.13 \cdot 10^{-6}$	$4.06 \cdot 10^{-4}$
Continuous	$9.18 \cdot 10^{-6}$	$4.59 \cdot 10^{-4}$
Lap-Jointed	$7.74 \cdot 10^{-6}$	$3.87 \cdot 10^{-4}$

Table 6.22: Probability of bending failure of the system of six primary beams respect to the three configurations, $Pr(F(1yr))$ and $Pr(F(50yr))$.

First Order Reliability Method:primary beam shear failure

The random variables for shear limit state function are the shear resistance R_v , the snow load on the ground Q , the roof shape factor C , the self weight of the beam W_B , the self weight of the purlins W_P and the permanent load P . The transformation function for the loads acting on the beam are the same as in the bending failure case. The transformation function for the shear strength has the same law given for the bending resistance, because they both are lognormal distributed random variable. The limit state function for shear failure is written as difference between shear resistance T_R and shear action T_S at the support location, $g(R, S) = T_R - T_S$.

The limit state function in the standard normal space is given in Eq. 6.44. The expression in Eq.6.44 is equivalent to the one in Eq. 6.34 except for the constants and therefore the components of the gradient of the limit state function G_v are the same given for G_b .

6.3 Primary beams analysis (FORM, MCS)

$$\begin{aligned} G_v(\mathbf{U}) = & C_{res,v} \cdot R_v^{-1} - C_{load1} \left[W_B^{-1}(u_{w_b}) + \right. \\ & + C_{load2} \left(C^{-1}(u_c) \cdot Q^{-1}(u_q) + P^{-1}(u_p) \right) + \\ & \left. + C_{load3} W_P^{-1}(u_{w_p}) \right]. \end{aligned} \quad (6.44)$$

In Eq. 6.44, the constants C_{load1} is equal to $\frac{1.5}{2}L$, while the constants C_{load2} and C_{load3} are the same given for the bending limit state function. The coefficient $C_{res,v}$ is equal to $\frac{2}{3}bh$.

FORM Results for primary beam shear failure

Tables 6.23, 6.25 and 6.27 list the value of reliability index and probability of failure for the most loaded section of the primary beam according to the different location of the beam inside the system. Tables 6.24, 6.26 and 6.28 list the α coefficients and the value of the r.v. at optimum.

Table 6.29 lists the probability of shear failure in 1yr $Pr(F(1yr))$ and in 50yr $Pr(F(1yr))$ for the most loaded primary beams as series system of two symmetrical critical sections with correlation factor $\rho = 0.87$.

Table 6.30 lists the probability of bending failure in 1yr $Pr(F_j(1yr))$ and in 50yr $Pr(F_j(1yr))$ for the entire system of primary beams as series system of twelve symmetrical critical sections with correlation factor $\rho = 0.87$. As expected the system of six primary beams shows to have a similar reliability

respect to the three purlins configurations.

Beam Location	β_j	$Pr(F_j(1yr))$
External beam	6.10	$5.35 \cdot 10^{-10}$
Internal beam	4.43	$4.71 \cdot 10^{-6}$

Table 6.23: Probability of shear failure of the most loaded section of the primary beam, $Pr(F_j(1yr))$ and corresponding reliability index β_j with the simply supported secondary elements.

Beam Location	Q	C	W_P	P	W_B	R
External beam						
α coeff.	0.657	0.625	0.0115	0.0549	0.0305	-0.416
x^*	1.59	2.8	0.254	0.404	0.638	3.19
Internal beam						
α coeff.	0.668	0.649	0.0069	0.0328	0.0011	-0.361
x^*	1.10	1.94	0.255	0.406	0.637	3.47

Table 6.24: Importance coefficients and values of the r.v. at design point x^* for the most loaded section of the primary beam with the simply supported secondary elements.

First Order Reliability Method: primary beam tension perpendicular to the grain failure

The random variables for tension perpendicular to the grain limit state function are the tension perpendicular to the grain resistance R_{t90} , the snow load on the ground Q , the roof shape factor C , the self weight of the beam W_B , the self weight of the purlins W_P and the permanent load P . The

6.3 Primary beams analysis (FORM, MCS)

Beam Location	β_j	$Pr(F_j(1yr))$
Beam 1	6.87	$3.45 \cdot 10^{-12}$
Beam 2	4.43	$4.70 \cdot 10^{-6}$
Beam 3	4.78	$8.71 \cdot 10^{-7}$

Table 6.25: Probability of shear failure of the most loaded section of the primary beam, $Pr(F_j(1yr))$ and corresponding reliability index β_j with the continuous secondary elements.

Beam Location	Q	C	W_P	P	W_B	R
Beam 1						
α coeff.	0.663	0.653	0.003	0.0142	0.0105	-0.366
x^*	1.87	3.28	0.084	0.404	0.639	3.07
Beam 2						
α coeff.	0.669	0.648	0.0073	0.035	0.0091	-0.361
x^*	1.11	1.96	0.084	0.406	0.637	3.52
Beam 3						
α coeff.	0.669	0.651	0.0063	0.0303	0.0091	-0.357
x^*	1.2	2.13	0.084	0.406	0.637	3.46

Table 6.26: Importance coefficients and values of the r.v. at design point x^* for the most loaded section of the primary beam with the continuous secondary elements.

Beam Location	β_j	$Pr(F_j(1yr))$
Beam 1	6.91	$2.28 \cdot 10^{-12}$
Beam 2	4.49	$3.43 \cdot 10^{-6}$
Beam 3	4.84	$6.30 \cdot 10^{-7}$

Table 6.27: Probability of shear failure of the most loaded section of the primary beam, $Pr(F_j(1yr))$ and corresponding reliability index β_j with the lap-jointed secondary elements.

Beam Location	Q	C	W_P	P	W_B	R
Beam 1						
α coeff.	0.663	0.653	0.0029	0.014	0.0106	-0.366
x^*	1.89	3.33	0.084	0.404	0.639	3.06
Beam 2						
α coeff.	0.669	0.649	0.0071	0.034	0.0090	-0.358
x^*	1.13	1.99	0.084	0.406	0.637	3.52
Beam 3						
α coeff.	0.669	0.651	0.0062	0.029	0.0091	-0.355
x^*	1.22	2.16	0.084	0.405	0.637	3.46

Table 6.28: Importance coefficients and values of the r.v. at design point x^* for the most loaded section of the primary beam with the lap-jointed secondary elements.

Purlins configuration	$Pr(F(1yr))$	$Pr(F(50yr))$
Simply supported	$8.35 \cdot 10^{-6}$	$4.17 \cdot 10^{-4}$
Continuous	$8.35 \cdot 10^{-6}$	$4.17 \cdot 10^{-4}$
Lap-Jointed	$6.33 \cdot 10^{-6}$	$3.16 \cdot 10^{-4}$

Table 6.29: Probability of shear failure of the most loaded primary beam respect to the three configurations, $Pr(F(1yr))$ and $Pr(F(50yr))$.

Purlins configuration	$Pr(F(1yr))$	$Pr(F(50yr))$
Simply supported	$2.32 \cdot 10^{-5}$	$1.15 \cdot 10^{-3}$
Continuous	$1.52 \cdot 10^{-5}$	$7.59 \cdot 10^{-4}$
Lap-Jointed	$1.16 \cdot 10^{-5}$	$5.78 \cdot 10^{-4}$

Table 6.30: Probability of shear failure of the system of six primary beams respect to the three configurations, $Pr(F(1yr))$ and $Pr(F(50yr))$.

6.3 Primary beams analysis (FORM, MCS)

limit state function in the ordinary space is written as difference between resistance and demand in terms of stresses in direction perpendicular to the grain $g(R, S) = \sigma_{R_{t90}} - \sigma_{S_{t90}}$ and it is related to the middle-span of the beam where the effect of tension perpendicular to the grain is maximum. The resistance in direction perpendicular to the grain takes into account also the volume effect.

The transformation function for the strength perpendicular to the grain is given in Eq. 6.45.

$$R_{t90}^{-1}(u_{r_{t90}}) = a_{t90} [-\text{Ln}(1 - \Phi(u_{t90}))]^{\frac{1}{k_{t90}}} \quad (6.45)$$

The limit state function in the standard normal space is given in Eq. 6.46.

$$\begin{aligned} G_{t90}(\mathbf{U}) = & C_{res,t90} \cdot R_{t90}^{-1} - C_{load1} \left[W_B^{-1}(u_{w_b}) + \right. \\ & + C_{load2} \left(C^{-1}(u_c) \cdot Q^{-1}(u_q) + P^{-1}(u_p) \right) + \\ & \left. + C_{load3} W_P^{-1}(u_{w_p}) \right]. \end{aligned} \quad (6.46)$$

In Eq. 6.46, the load constant C_{load1} is given by Blumer expression at the midspan location and it is equal to 17.412. The constants C_{load2} and C_{load3} are the same given for the bending limit state function. The coefficient $C_{res,v}$ is equal to $k_{dis} \cdot k_{vol} \cdot bh_{apex}$, where $k_{dis} = 1.4$ for curved beams and $k_{vol} = 0.648$ for the used beam geometry. The final value of $C_{res,v}$ is 907.2.

The computation of the components of the gradient is required. The expression in Eq. 6.46 is equivalent to the 6.34 except for the constants and the components of the gradient respect to the strength perpendicular to the grain variable R_{t90} . Therefore, all the components of the gradient are the same given for G_b , except the last component that is given in Eq. 6.47 .

$$\frac{\partial G}{\partial u_{t90}} = a_{t90} \cdot C_{res,t90} \frac{1}{k_{t90}} [-\text{Ln}(1 - \Phi(u_{t90}))]^{\frac{1}{k_{t90}} - 1} \cdot \frac{-1}{1 - \Phi(u_{t90})} \frac{1}{\sqrt{2\pi}} \text{Exp}\left(-\frac{1}{2}u_{t90}^2\right). \quad (6.47)$$

FORM Results for primary beam tension perpendicular to the grain failure

Tables 6.31, 6.33 and 6.35 list the value of reliability index and probability of failure for the most loaded section of the primary beam according to the different location of the beam inside the system. Tables 6.32, 6.34 and 6.36 list the α coefficients and the value of the r.v. at design point x^* .

Beam Location	β_j	$Pr(F_j(1yr))$
External beam	4.41	$5.05 \cdot 10^{-6}$
Internal beam	3.96	$3.73 \cdot 10^{-5}$

Table 6.31: Probability of tension perp. failure of the most loaded section of the primary beam, $Pr(F_j(1yr))$ and corresponding reliability index β_j with the simply supported secondary elements.

6.3 Primary beams analysis (FORM, MCS)

Beam Location	Q	C	W_P	P	W_B	R
External beam						
α coeff.	0.15	0.116	0.007	0.034	0.018	-0.980
x^*	0.45	0.848	0.254	0.405	0.639	0.07
Internal beam						
α coeff.	0.192	0.151	0.0087	0.0415	0.00115	-0.968
x^*	0.484	0.897	0.084	0.406	0.637	0.114

Table 6.32: Importance coefficients and values of the r.v. at design point x^* for the most loaded section of the primary beam with the simply supported secondary elements.

Beam Location	β_j	$Pr(F_j(1yr))$
Beam 1	4.77	$8.83 \cdot 10^{-7}$
Beam 2	3.91	$4.67 \cdot 10^{-5}$
Beam 3	4.05	$2.54 \cdot 10^{-5}$

Table 6.33: Probability of tension perp. failure of the most loaded section of the primary beam, $Pr(F_j(1yr))$ and corresponding reliability index β_j with the continuous secondary elements.

Beam Location	Q	C	W_P	P	W_B	R
Beam 1						
α coeff.	0.136	0.103	0.006	0.031	0.023	-0.984
x^*	0.46	0.866	0.084	0.405	0.641	0.048
Beam 2						
α coeff.	0.198	0.157	0.0089	0.043	0.011	-0.966
x^*	0.487	0.903	0.084	0.406	0.637	0.12
Beam 3						
α coeff.	0.188	0.149	0.0085	0.0407	0.012	-0.969
x^*	0.48	0.899	0.084	0.406	0.638	0.105

Table 6.34: Importance coefficients and values of the r.v. at design point x^* for the most loaded section of the primary beam with the continuous secondary elements.

Beam Location	β_j	$Pr(F_j(1yr))$
Beam 1	4.81	$7.65 \cdot 10^{-7}$
Beam 2	3.94	$4.07 \cdot 10^{-5}$
Beam 3	4.1	$2.14 \cdot 10^{-5}$

Table 6.35: Probability of tension perp. failure of the most loaded section of the primary beam, $Pr(F_j(1yr))$ and corresponding reliability index β_j with the lap-jointed secondary elements.

Beam Location	Q	C	W_P	P	W_B	R
Beam 1						
α coeff.	0.136	0.104	0.0065	0.031	0.0235	-0.984
x^*	0.46	0.868	0.084	0.406	0.642	0.05
Beam 2						
α coeff.	0.200	0.159	0.0089	0.043	0.0113	-0.965
x^*	0.49	0.907	0.0842	0.406	0.637	0.12
Beam 3						
α coeff.	0.190	0.151	0.0086	0.0407	0.0126	-0.969
x^*	0.49	0.09	0.084	0.405	0.638	0.01

Table 6.36: Importance coefficients and values of the r.v. at design point x^* for the most loaded section of the primary beam with the lap-jointed secondary elements.

6.3 Primary beams analysis (FORM, MCS)

Table 6.37 lists the probability of tension perp. failure in 1yr $Pr(F_j(1yr))$ and in 50yr $Pr(F_j(50yr))$ for the entire system of primary beams as series system of twelve symmetrical critical sections with correlation factor $\rho = 0.05$. As expected the system of six primary beams shows to have a similar reliability respect to the three purlins configurations.

Purlins configuration	$Pr(F(1yr))$	$Pr(F(50yr))$
Simply supported	$1.59 \cdot 10^{-4}$	$7.97 \cdot 10^{-3}$
Continuous	$1.46 \cdot 10^{-4}$	$7.29 \cdot 10^{-3}$
Lap-Jointed	$1.26 \cdot 10^{-4}$	$6.27 \cdot 10^{-3}$

Table 6.37: Probability of tension perp. failure of the of the system of six primary beams respect to the three configurations, $Pr(F(1yr))$ and $Pr(F(50yr))$.

6.3.2 Monte Carlo sampling for the analysis of the primary beams

Monte Carlo Simulations (MCS) with 10^5 samples are computed. The software used to compute the simulation is implemented in Matlab and it enables the evaluation not only of the probability of failure but also to obtain numerical data regarding the number of failed primary beams.

As described in section 3.4, only the bending failure leads to a real collapse of the beam, while failure due to tension perpendicular to the grain, shear and combination of shear and tension perpendicular stresses cause a loss of capacity and stiffness. This damage is also taken into account by uploading the resistance of the element, as described in section 3.5.

MCS are computed both for the most loaded primary beam (internal beam for simply supported configuration and beam 2 for static indeterminate configurations in figure 6.16) and for the entire primary system (series system of six primary beams). In the case of primary beams no systematic weaknesses is considered.

Table 6.38 lists the probability of failure for the most loaded primary beam in the roof system, with the corresponding purlin configuration, and for the three independent failure mode considered: bending failure, shear failure, tension perpendicular to the grain failure and combination of tension perpendicular to the grain and shear failure (SIA limit state function).

Bending Failure	$Pr(F(50yr))$	σ	95% confidence bounds
Simply supported	$1.2 \cdot 10^{-3}$	$1.1 \cdot 10^{-4}$	$9.7 \cdot 10^{-4} \div 1.4 \cdot 10^{-3}$
Continuous	$2.1 \cdot 10^{-3}$	$1.4 \cdot 10^{-4}$	$1.8 \cdot 10^{-3} \div 2.3 \cdot 10^{-3}$
Lap-jointed	$1.6 \cdot 10^{-3}$	$2.3 \cdot 10^{-4}$	$1.4 \cdot 10^{-3} \div 1.8 \cdot 10^{-3}$
Shear Failure	$Pr(F(50yr))$	σ	95% confidence bounds
Simply supported	$7.3 \cdot 10^{-4}$	$8.50 \cdot 10^{-5}$	$5.6 \cdot 10^{-4} \div 8.9 \cdot 10^{-4}$
Continuous	$1.1 \cdot 10^{-3}$	$1.05 \cdot 10^{-4}$	$9.0 \cdot 10^{-4} \div 1.3 \cdot 10^{-3}$
Lap-jointed	$9.7 \cdot 10^{-4}$	$7.7 \cdot 10^{-4}$	$7.8 \cdot 10^{-4} \div 1.2 \cdot 10^{-3}$
Tension perp. Failure	$Pr(F(50yr))$	σ	95% confidence bounds
Simply supported	$5.3 \cdot 10^{-3}$	$2.3 \cdot 10^{-4}$	$4.9 \cdot 10^{-3} \div 5.8 \cdot 10^{-3}$
Continuous	$7.5 \cdot 10^{-3}$	$2.7 \cdot 10^{-4}$	$7.0 \cdot 10^{-3} \div 8.1 \cdot 10^{-3}$
Lap-jointed	$6.0 \cdot 10^{-3}$	$2.5 \cdot 10^{-4}$	$5.5 \cdot 10^{-3} \div 6.5 \cdot 10^{-3}$
Shear and Tension perp.	$Pr(F(50yr))$	σ	95% confidence bounds
Simply supported	$4.4 \cdot 10^{-3}$	$2.1 \cdot 10^{-4}$	$4.0 \cdot 10^{-3} \div 4.8 \cdot 10^{-3}$
Continuous	$6.2 \cdot 10^{-3}$	$2.5 \cdot 10^{-4}$	$5.7 \cdot 10^{-3} \div 6.6 \cdot 10^{-3}$
Lap-jointed	$4.7 \cdot 10^{-3}$	$2.2 \cdot 10^{-4}$	$4.2 \cdot 10^{-3} \div 5.1 \cdot 10^{-3}$

Table 6.38: Probability of failure of the most loaded primary beam respect to the chosen limit state.

6.3 Primary beams analysis (FORM, MCS)

Although the bending failure is the only mechanism that leads to the collapse of the beam, the results show that the highest probability corresponds to the failure due to tension perpendicular to the grain direction. As explained in section 3.4, tension perpendicular to the grain failure leads to longitudinal crack development in the curved part across the mid-span. The crack path can develop progressively until the complete splitting of the section in two parts, leading therefore to a loss of capacity and stiffness that must be taken into account in the capacity assessment.

Therefore, a second model that takes into account the reduction of the capacity due to crack development in the curved part when the limit state for tension perpendicular to the grain occurs. The probability of bending failure obtained with this second model is listed in table 6.40 for the three configurations.

Bending Failure	$Pr(F(50yr))$	σ	95% confidence bounds
Simply supported	$1.6 \cdot 10^{-3}$	$1.3 \cdot 10^{-4}$	$1.4 \cdot 10^{-3} \div 1.9 \cdot 10^{-3}$
Continuous	$1.9 \cdot 10^{-3}$	$1.4 \cdot 10^{-4}$	$1.6 \cdot 10^{-3} \div 2.2 \cdot 10^{-3}$
Lap-jointed	$1.4 \cdot 10^{-3}$	$1.2 \cdot 10^{-4}$	$1.2 \cdot 10^{-3} \div 1.7 \cdot 10^{-3}$

Table 6.39: Probability of failure of the most loaded primary beam respect to bending failure when considering the splitting of section due to tension perp.

Comparing the results of table 6.38 and 6.39, it is clear that the mean value of the probability of bending failure for a single beam does not change. A higher value is found only for the beam with simply supported purlins. In order to consider the effect of this cracking on the entire system, it is needed to compare the probability of failure and the extension of the failure

for the entire primary system of six beams.

Table 6.40 lists the results in terms of probability of failure for the primary system (beams) with independent failures.

Comparing the results of the MCS with the FORM results in tables 6.22, 6.30 and 6.37, it can be noted that the probability of failure obtained with Monte Carlo sampling is higher, due to the different number of critical sections (= variables). Indeed, FORM analysis is computed only considering the most loaded sections inside the beams according to the failure mechanism considered (12 variables for bending and shear mechanisms, 6 variables for tension perpendicular to the grain in a series system model). Monte Carlo analysis is computed considering a deterministic discretization of critical sections with one potential critical section every 50cm (i.e. 60 variables for the series system model of six beams). Indeed, the number of variables and the degree of correlation among them is important to the accuracy of the solution in FORM analysis.

Table 6.41 lists the probability of bending failure when the loss of capacity due to failure for tension perpendicular to the grain occurs.

According to the results obtained with Monte Carlo simulations, the probability of bending failure for the system of six primary beams increases of about five times when considering the possibility of having a reduced capacity due to cracking in case a previous failure for tension perpendicular to the grain occur.

Even if degradation of material is here not considered, the results obtained considering a damaged section show the importance of considering the life

6.3 Primary beams analysis (FORM, MCS)

Bending Failure	$Pr(F(50yr))$	σ	95% confidence bounds
Simply supported	$2.5 \cdot 10^{-3}$	$1.6 \cdot 10^{-4}$	$2.2 \cdot 10^{-3} \div 2.8 \cdot 10^{-3}$
Continuous	$2.6 \cdot 10^{-3}$	$1.6 \cdot 10^{-4}$	$2.3 \cdot 10^{-3} \div 2.9 \cdot 10^{-3}$
Lap-jointed	$2.0 \cdot 10^{-3}$	$1.4 \cdot 10^{-4}$	$1.7 \cdot 10^{-3} \div 2.2 \cdot 10^{-3}$
Shear Failure	$Pr(F(50yr))$	σ	95% confidence bounds
Simply supported	$1.5 \cdot 10^{-3}$	$1.22 \cdot 10^{-4}$	$1.2 \cdot 10^{-3} \div 1.2 \cdot 10^{-3}$
Continuous	$1.2 \cdot 10^{-3}$	$1.09 \cdot 10^{-4}$	$9.86 \cdot 10^{-4} \div 1.4 \cdot 10^{-3}$
Lap-jointed	$9.0 \cdot 10^{-4}$	$9.5 \cdot 10^{-5}$	$7.15 \cdot 10^{-4} \div 1.1 \cdot 10^{-3}$
Tension perp. Failure	$Pr(F(50yr))$	σ	95% confidence bounds
Simply supported	$2.7 \cdot 10^{-2}$	$5.3 \cdot 10^{-4}$	$2.64 \cdot 10^{-2} \div 2.85 \cdot 10^{-2}$
Continuous	$1.9 \cdot 10^{-2}$	$4.4 \cdot 10^{-4}$	$1.82 \cdot 10^{-2} \div 1.99 \cdot 10^{-2}$
Lap-jointed	$1.8 \cdot 10^{-2}$	$4.3 \cdot 10^{-4}$	$1.75 \cdot 10^{-2} \div 1.92 \cdot 10^{-2}$
Shear and Tension perp.	$Pr(F(50yr))$	σ	95% confidence bounds
Simply supported	$2.0 \cdot 10^{-2}$	$4.5 \cdot 10^{-4}$	$1.93 \cdot 10^{-2} \div 2.1 \cdot 10^{-2}$
Continuous	$1.43 \cdot 10^{-3}$	$3.8 \cdot 10^{-4}$	$1.36 \cdot 10^{-2} \div 1.51 \cdot 10^{-2}$
Lap-jointed	$1.41 \cdot 10^{-2}$	$3.7 \cdot 10^{-4}$	$1.33 \cdot 10^{-2} \div 1.48 \cdot 10^{-2}$

Table 6.40: Probability of failure of the system of six primary beams respect to the chosen limit state.

Bending Failure	$Pr(F(50yr))$	σ	95% confidence bounds
Simply supported	$1.62 \cdot 10^{-2}$	$4.03 \cdot 10^{-4}$	$1.54 \cdot 10^{-2} \div 1.7 \cdot 10^{-2}$
Continuous	$1.33 \cdot 10^{-2}$	$3.64 \cdot 10^{-4}$	$1.26 \cdot 10^{-2} \div 1.4 \cdot 10^{-2}$
Lap-jointed	$1.17 \cdot 10^{-2}$	$3.42 \cdot 10^{-4}$	$1.11 \cdot 10^{-2} \div 1.24 \cdot 10^{-2}$

Table 6.41: Probability of bending failure for the system of six primary beams upon tension perp. failure.

time managing and inspection planning as a tool to avoid the likelihood of the failure event to increase strongly.

Chapter 7

Structural Interaction

As described in section 3.5, the roof system is modeled as a series system of two subsystems: primary system (beams) and secondary system (purlins). System failure will occur when at least one primary or secondary element fails. Both primary beams and purlins will be considered failed when at least one section is failed in bending.

Hereby, the roof assessment is carried out considering the structural interaction according to the model described in section 3.5. Some assumptions on the capacity and redistribution ability of the connections are made on the basis of data from the Timber Chair of TU-München.

7.1 Numerical results for the roof system (MCS)

Monte Carlo Simulations (MCS) with 10^5 samples are computed. MCS enable the evaluation of the behavior of the roof system under the load

process in 50yr according to the event tree of figure 3.16. This means that according to the element that fails first, between purlins and beams, different path of consequences are taken into account.

As already explained for the assessment of secondary system in section 3.5, when a section inside a purlin fails, the failure does not have any effect for the static determinate purlins, while in case of static indeterminate purlins, the evolution of the static scheme is considered and the purlins checked for the new bending moments until no other section fails.

When a primary beam fails, according to the failure mechanism, the consequences on the roof system are different.

If the beam fails for tension perpendicular to the grain it will exhibit both a loss of capacity and stiffness. The loss of capacity will increase the probability of failure of the beam. The loss of stiffness will cause an additional imposed displacement at the support for the purlins that are supported by the beam. Therefore, additional bending moments are taken into account.

If the beam fails for bending mechanism it will collapse. Before the total collapse, it will be able to redistribute the load to the lateral beam due to the ductility of the connections between purlins and beam, in different percentage according to the purlin configuration as described in section 3.5.

An uncommon but possible event, found during some inspections made on different structures by the research group of the Timber Chair of TU-München, is that the beam is failed in bending due to inadequate capacity, but the high capacity of purlins and ductility reserve of connections can hide this failure, leading to have the beam still hanging to the purlins. The occurrence of this event will be also verified.

7.1 Numerical results for the roof system (MCS)

Table 7.1 lists the probability of bending failure of the roof system and related statistics for the bending failure mechanisms. The results refer to the primary beam system with the simply supported, continuous and lap-jointed purlins and with redistribution factors according to section 3.5. The highest value of the probability of failure (lowest reliability) corresponds to the roof system with continuous purlins.

Tables 7.2, 7.3, 7.4 list the probability of shear failure, tension perpendicular to the grain failure and probability of failure for the combined stress condition of tension perpendicular and shear stresses (SIA limit state) of the primary beam system.

The interaction between primary and secondary system does not change significantly the probability of failure for shear and tension perpendicular to the grain, because they depend only on the capacity of the single beams. On the contrary, the probability of bending failure increases of 30% proportionally to the increasing redistribution factor.

The increasing occurrence of bending failure explains the slight decrease in the shear probability of failure with the increase of redistribution factor.

The results also show a higher value of the probability of failure for all mechanisms for the primary beams' system with continuous purlins, due to the slight higher weight of the secondary system respect to the lap-jointed configuration.

Table 7.5 lists the probability of failure for the secondary system (purlins) for the three configurations chosen when the interaction with the primary system (beams) is considered. As expected, the secondary system with simply supported configuration does not have a big change in the probability

of failure, due to the limited interactions with the primary system. The probability of failure for continuous and lap-jointed purlins increases, due to the effect of the interaction, of 50% and 37% respectively. The difference mostly depends on the fact that continuous purlins are more sensitive to the additional displacement at the support caused by the loss of stiffness of primary beams. Indeed, the higher bending moment on the support caused by the imposed displacement has a lower effect on lap-jointed purlins due to the coupling of the two section across the support.

Beams & Simply Supp. Purlins	$Pr(F_{50yr})$	σ	95% confidence bounds
10% redistribution	$3.00 \cdot 10^{-3}$	$1.72 \cdot 10^{-4}$	$2.6 \cdot 10^{-3} \div 3.3 \cdot 10^{-3}$
20% redistribution	$4.00 \cdot 10^{-3}$	$1.98 \cdot 10^{-4}$	$3.6 \cdot 10^{-2} \div 4.3 \cdot 10^{-2}$
30% redistribution	$5.60 \cdot 10^{-3}$	$2.36 \cdot 10^{-4}$	$5.1 \cdot 10^{-3} \div 6.0 \cdot 10^{-3}$
40% redistribution	$6.60 \cdot 10^{-3}$	$2.60 \cdot 10^{-4}$	$6.1 \cdot 10^{-3} \div 7.1 \cdot 10^{-3}$
Beams& Continuous Purlins	$Pr(F_{50yr})$	σ	95% confidence bounds
40% redistribution	$1.00 \cdot 10^{-2}$	$3.16 \cdot 10^{-4}$	$9.4 \cdot 10^{-3} \div 1.06 \cdot 10^{-2}$
Beams & Lap-Jointed Purlins	$Pr(F_{50yr})$	σ	95% confidence bounds
40% redistribution	$4.7 \cdot 10^{-3}$	$2.12 \cdot 10^{-4}$	$4.35 \cdot 10^{-3} \div 5.1 \cdot 10^{-3}$

Table 7.1: Probability of Bending Failure for the primary beams system.

Figures 7.1 and 7.2, show the trend of mean and standard deviation of the area failed in the 50yr period, computed considering only purlins and only the beams respectively. The area failed follow a constant trend due to the fact that no degradation of materials is considered.

For a redistribution factor of 20% (total redistribution of 40%) and more, the behavior of simply supported purlins does not change both in the mean value and in the standard deviation.

7.1 Numerical results for the roof system (MCS)

Beams & Simply Supp. Purlins	$Pr(F_{50yr})$	σ	95% confidence bounds
10% redistribution	$1.10 \cdot 10^{-3}$	$1.06 \cdot 10^{-4}$	$9.13 \cdot 10^{-3} \div 1.3 \cdot 10^{-3}$
20% redistribution	$1.40 \cdot 10^{-3}$	$1.80 \cdot 10^{-4}$	$1.2 \cdot 10^{-3} \div 1.6 \cdot 10^{-3}$
30% redistribution	$1.20 \cdot 10^{-3}$	$1.10 \cdot 10^{-4}$	$9.8 \cdot 10^{-4} \div 1.4 \cdot 10^{-3}$
40% redistribution	$9.50 \cdot 10^{-4}$	$9.70 \cdot 10^{-5}$	$7.6 \cdot 10^{-4} \div 1.1 \cdot 10^{-3}$
Beams& Continuous Purlins	$Pr(F_{50yr})$	σ	95% confidence bounds
40% redistribution	$2.20 \cdot 10^{-3}$	$1.47 \cdot 10^{-4}$	$1.9 \cdot 10^{-3} \div 2.5 \cdot 10^{-3}$
Beams & Lap-Jointed Purlins	$Pr(F_{50yr})$	σ	95% confidence bounds
40% redistribution	$6.5 \cdot 10^{-4}$	$8.06 \cdot 10^{-5}$	$4.9 \cdot 10^{-4} \div 8.1 \cdot 10^{-4}$

Table 7.2: Probability of Shear Failure for the primary beams system.

Beams & Simply Supp. Purlins	$Pr(F_{50yr})$	σ	95% confidence bounds
10% redistribution	$2.70 \cdot 10^{-2}$	$5.2 \cdot 10^{-4}$	$2.6 \cdot 10^{-2} \div 2.8 \cdot 10^{-2}$
20% redistribution	$2.57 \cdot 10^{-2}$	$5.1 \cdot 10^{-4}$	$2.47 \cdot 10^{-2} \div 2.67 \cdot 10^{-2}$
30% redistribution	$2.74 \cdot 10^{-2}$	$5.2 \cdot 10^{-4}$	$2.63 \cdot 10^{-2} \div 2.84 \cdot 10^{-2}$
40% redistribution	$2.75 \cdot 10^{-2}$	$5.2 \cdot 10^{-4}$	$2.64 \cdot 10^{-2} \div 2.85 \cdot 10^{-2}$
Beams& Continuous Purlins	$Pr(F_{50yr})$	σ	95% confidence bounds
40% redistribution	$2.45 \cdot 10^{-2}$	$4.9 \cdot 10^{-4}$	$2.36 \cdot 10^{-2} \div 2.55 \cdot 10^{-2}$
Beams & Lap-Jointed Purlins	$Pr(F_{50yr})$	σ	95% confidence bounds
40% redistribution	$1.72 \cdot 10^{-2}$	$4.15 \cdot 10^{-4}$	$1.64 \cdot 10^{-2} \div 1.80 \cdot 10^{-2}$

Table 7.3: Probability of Tension perp. Failure for the primary beams system.

Beams & Simply Supp. Purlins	$Pr(F_{50yr})$	σ	95% confidence bounds
10% redistribution	$2.03 \cdot 10^{-2}$	$4.5 \cdot 10^{-4}$	$1.94 \cdot 10^{-2} \div 2.12 \cdot 10^{-2}$
20% redistribution	$1.98 \cdot 10^{-2}$	$4.45 \cdot 10^{-4}$	$1.89 \cdot 10^{-2} \div 2.06 \cdot 10^{-2}$
30% redistribution	$2.07 \cdot 10^{-2}$	$4.5 \cdot 10^{-4}$	$1.98 \cdot 10^{-2} \div 2.16 \cdot 10^{-2}$
40% redistribution	$2.10 \cdot 10^{-2}$	$4.5 \cdot 10^{-4}$	$1.98 \cdot 10^{-2} \div 2.16 \cdot 10^{-2}$
Beams& Continuous Purlins	$Pr(F_{50yr})$	σ	95% confidence bounds
40% redistribution	$1.92 \cdot 10^{-2}$	$4.4 \cdot 10^{-4}$	$1.83 \cdot 10^{-2} \div 2.00 \cdot 10^{-2}$
Beams & Lap-Jointed Purlins	$Pr(F_{50yr})$	σ	95% confidence bounds
40% redistribution	$1.28 \cdot 10^{-2}$	$3.6 \cdot 10^{-4}$	$1.21 \cdot 10^{-2} \div 1.35 \cdot 10^{-2}$

Table 7.4: Probability of Failure for combination of Shear and Tension Perp. for the primary beams system.

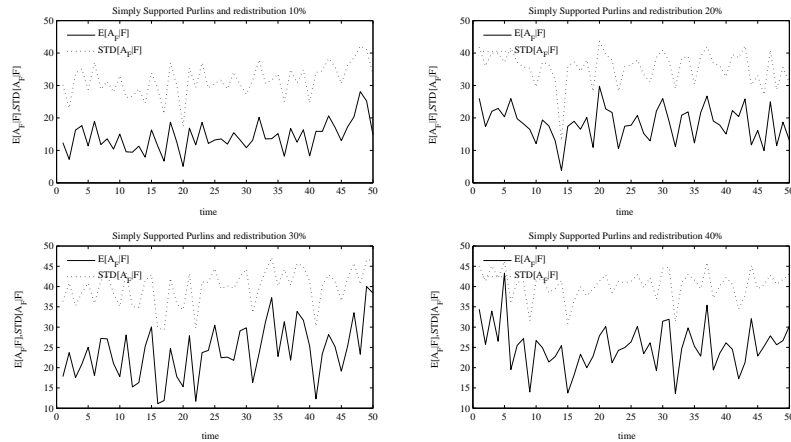
Simply Supp. Purlins	$Pr(F_{50yr})$	σ	95% confidence bounds
10% redistribution	$2.31 \cdot 10^{-2}$	$4.8 \cdot 10^{-4}$	$2.22 \cdot 10^{-2} \div 2.40 \cdot 10^{-2}$
20% redistribution	$2.25 \cdot 10^{-2}$	$4.7 \cdot 10^{-4}$	$2.16 \cdot 10^{-2} \div 2.35 \cdot 10^{-2}$
30% redistribution	$2.35 \cdot 10^{-2}$	$4.8 \cdot 10^{-4}$	$2.26 \cdot 10^{-2} \div 2.45 \cdot 10^{-2}$
40% redistribution	$2.35 \cdot 10^{-2}$	$4.8 \cdot 10^{-4}$	$2.26 \cdot 10^{-2} \div 2.45 \cdot 10^{-2}$
Continuous Purlins	$Pr(F_{50yr})$	σ	95% confidence bounds
40% redistribution	$2.96 \cdot 10^{-2}$	$5.44 \cdot 10^{-4}$	$2.85 \cdot 10^{-2} \div 3.06 \cdot 10^{-2}$
Lap-Jointed Purlins	$Pr(F_{50yr})$	σ	95% confidence bounds
40% redistribution	$9.60 \cdot 10^{-3}$	$3.1 \cdot 10^{-4}$	$9.00 \cdot 10^{-3} \div 1.02 \cdot 10^{-2}$

Table 7.5: Probability of bending Failure for the purlin system.

7.1 Numerical results for the roof system (MCS)

Also for the primary beams (figure 7.2), the value of 20% of the redistribution represents a limit above which the behavior of the system does not change.

Figure 7.1: Mean and Standard deviation of the failed area for the simply supported purlins with redistribution 10%- 20%- 30%- 40%.



Figures 7.3, 7.4 and 7.5, 7.6 show the path of the mean and standard deviation for purlins and beams separately, when the roof is built with continuous and lap-jointed purlin configurations. For both static indeterminate configurations, the behavior is similar with a slight higher mean value of the percentage of area failed for the roof with continuous configuration, due to a slightly higher weight of the roof.

Figures 7.7, 7.8 and 7.9, 7.10 show the histogram of the frequency for the percentage of area failed for the three roof configurations. Results for

Figure 7.2: Mean and Standard deviation of the failed area for the beams with simply supp. purlins with redistribution 10-20-30-40%.

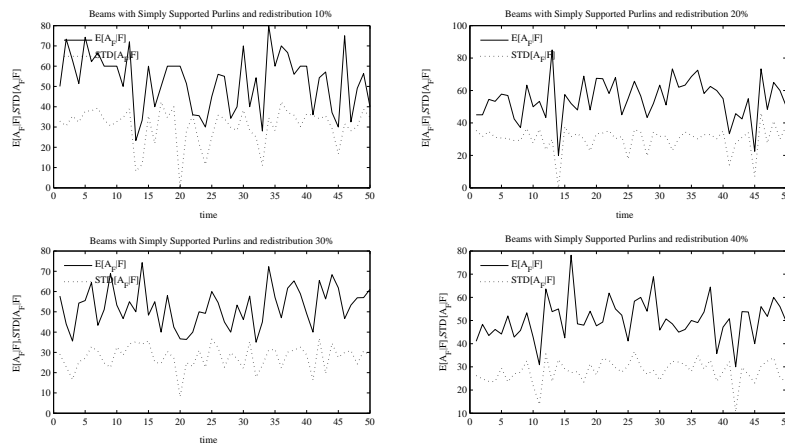
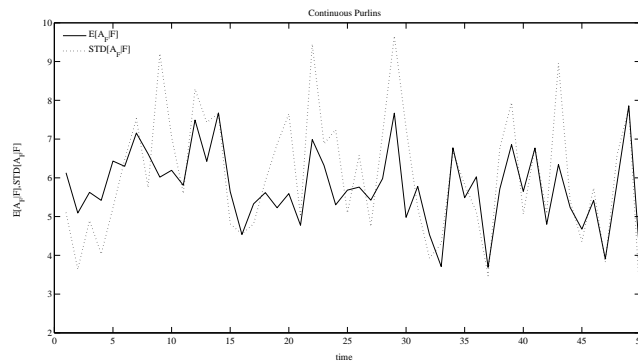


Figure 7.3: Mean and Standard deviation of the failed area for the continuous purlins.



7.1 Numerical results for the roof system (MCS)

Figure 7.4: Mean and Standard deviation of the failed area for the beams with continuous purlins.

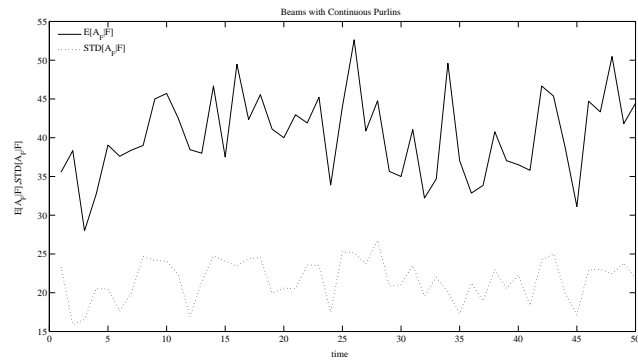


Figure 7.5: Mean and Standard deviation of the failed area for the lap-jointed purlins.

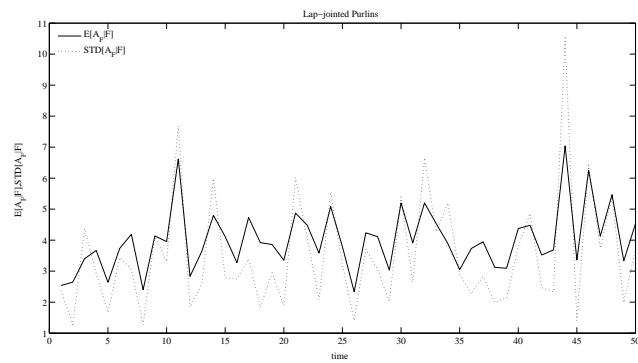
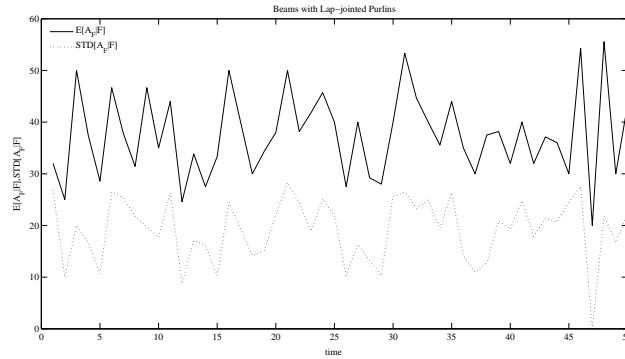


Figure 7.6: Mean and Standard deviation of the failed area for the beams with lap-jointed purlins.



purlins and beams are presented separately. In all cases, the increase in the redistribution factor causes an increase in the frequency of highest values of area failed. For the purlins, the diagrams show a high frequency of small area failed for static indeterminate purlins, while the simply supported purlins show also a not negligible frequency of high values of area failed that increases with the redistribution factor.

The histograms for the primary beams show the highest frequency at the value of 60% of area failed for the roof with simply supported purlins and at the value of 40% for the roof with continuous and lap-jointed purlins.

In figure 7.11 the Cdf of area failed for the simply supported secondary system is reported for the different values of redistribution factor. The path shows that the less is the redistribution ability, the better is the behavior of the secondary system. Indeed, a small redistribution ability together with compartmentalization should contain the extension of the failure. The

7.1 Numerical results for the roof system (MCS)

Figure 7.7: Histograms of the failed area for the simply supported purlins with redistribution 10-20-30-40%.

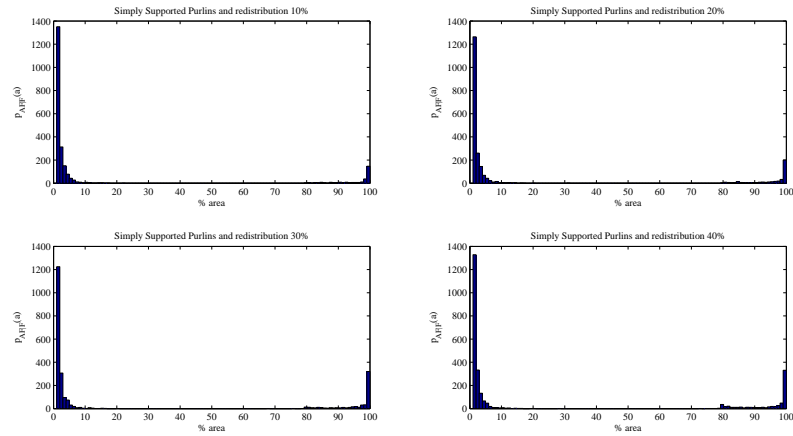


Figure 7.8: Histograms of the failed area for the beams with simply sup. purlins with redistribution 10-20-30-40%.

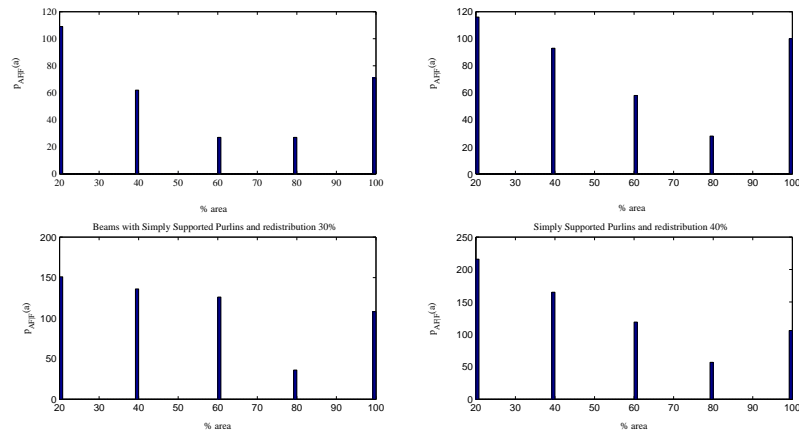


Figure 7.9: Histograms of the failed area for the continuous purlins.

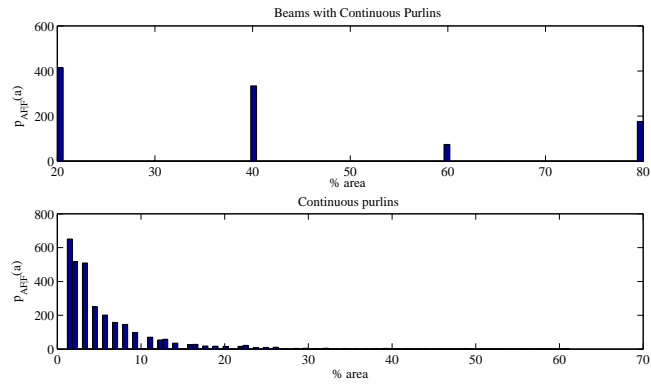
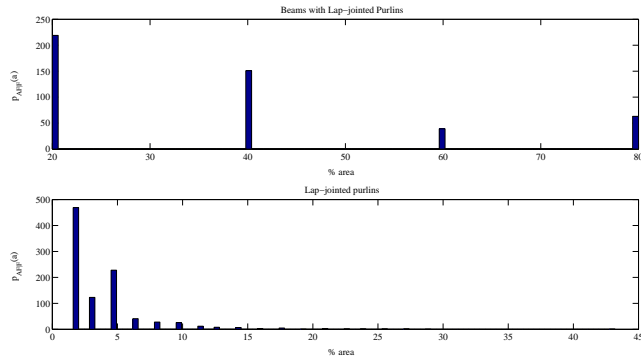


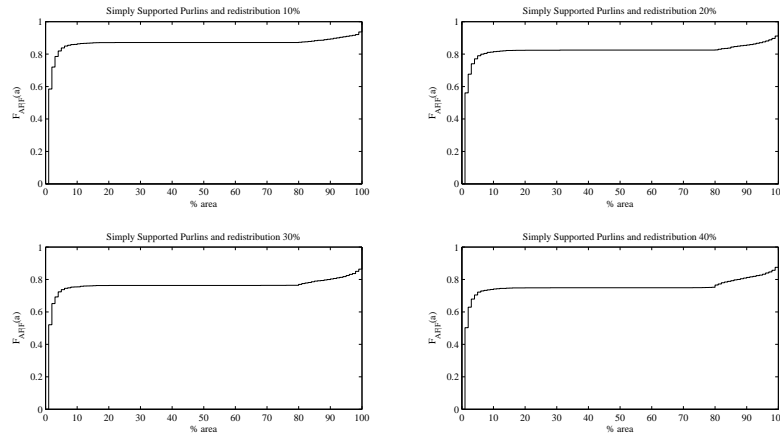
Figure 7.10: Histograms of the failed area for the lap-jointed purlins.



7.1 Numerical results for the roof system (MCS)

primary system with simply supported purlins with low redistribution capacity (see figure 7.12), also behaves better for high values of area failed, because the probability of exceeding the highest values is smaller. In addition, the range 40%-50% of the area failed represents a range of inversion of the behavior for the primary system. This happens because the primary system can withstand small area failed also if a high percentage of the load is redistributed (compartmentalization effect), while for big area failed the system will be already collapsed and no redistribution is possible (compartmentalization becomes inefficient).

Figure 7.11: CDF of the failed area for the simply supported purlins.



In figures 7.13 and 7.14 the CDF of the percentage of area failed for both purlins and beams with static indeterminate purlins is plotted. The CDF for continuous configuration is more stiff. This implies a higher probability to have small values of area failed. The primary system has the same behavior in both cases.

Figure 7.12: CDF of the failed area for beams with simply supported purlins and redistribution 10-20-30-40%.

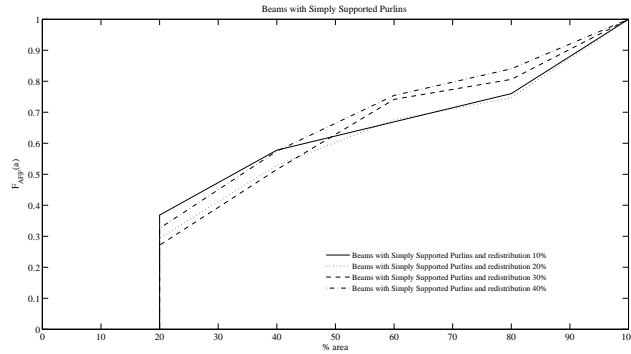


Figure 7.13: CDF of the failed area for the beams and continuous purlins.

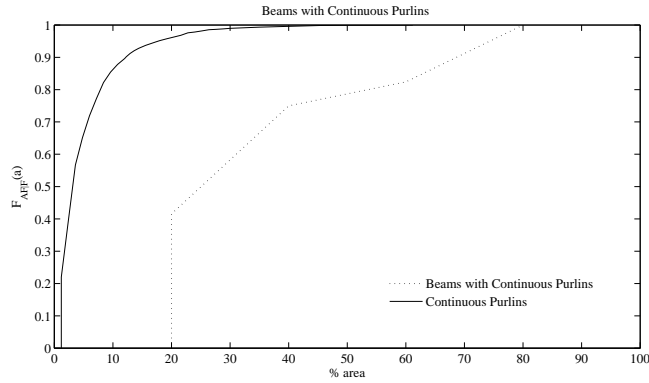
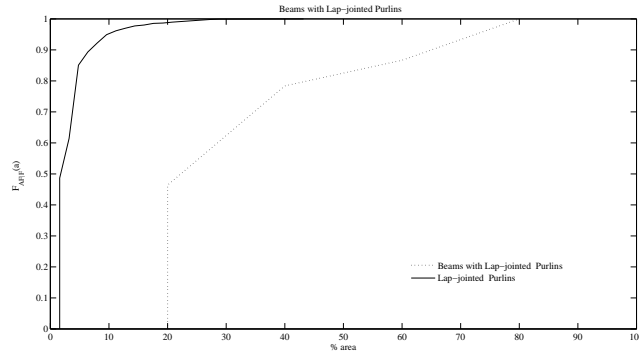


Table 7.6 lists the statistics of the percentage of area failed computed considering only the secondary system.

Table 7.7 lists the statistics of the percentage of area failed computed considering only the primary system.

7.1 Numerical results for the roof system (MCS)

Figure 7.14: CDF of the failed area for the beams and lap-jointed purlins.



Configuration	Secondary System - Purlins					
	min %	max %	$E[A_F F]$	median %	st.dev.	$Pr(F(50yr))$
Simply Supp. 10%	1	100	13.95	1	31.72	$2.31 \cdot 10^{-2}$
Simply Supp. 20%	1	100	18.38	1	35.98	$2.25 \cdot 10^{-2}$
Simply Supp. 30%	1	100	24.16	1	40.37	$2.35 \cdot 10^{-2}$
Simply Supp. 40%	1	100	25.18	1	40.58	$2.64 \cdot 10^{-2}$
Continuous	1.2	61.2	5.8	3.6	6.24	$2.96 \cdot 10^{-2}$
Lap-jointed	1.6	43.2	3.95	3.2	3.89	$0.96 \cdot 10^{-2}$

Table 7.6: Statistics of the percentage of area failed for the secondary system.

Configuration	Primary system - Beams					
	min %	max %	E [$A_F F$]	median %	st.dev.	$Pr(F(50yr))$
Simply Supp. 10%	20	100	52.50	40.0	32.26	$3.0 \cdot 10^{-3}$
Simply Supp. 20%	20	100	55.08	40.0	31.24	$4.0 \cdot 10^{-3}$
Simply Supp. 30%	20	100	53.32	40.0	28.71	$5.6 \cdot 10^{-3}$
Simply Supp. 40%	20	100	50.10	40.0	28.54	$6.6 \cdot 10^{-3}$
Continuous	20	80	40.22	40.0	21.86	$1.0 \cdot 10^{-2}$
Lap-jointed	20	80	37.7	40.0	20.68	$4.7 \cdot 10^{-3}$

Table 7.7: Statistics of the percentage of area failed for the primary system.

Table 7.8 lists the statistics of the percentage of area failed computed considering the entire roof system. The probability of failure in 50yr is quite high because it strongly depends on the probability of failure of the purlins. However, in terms of expected value of area failed, the roof with simply supported purlins behaves better for low value of redistribution ability. Between the two static indeterminate configurations the continuous one behaves better in terms of expected area failed.

Configuration	Roof system					
	min %	max %	E [$A_F F$]	median %	st.dev.	$Pr(F(50yr))$
Simply Supp. 10%	1	100	13.90	1	31.87	$2.61 \cdot 10^{-2}$
Simply Supp. 20%	1	100	18.54	1	36.32	$2.65 \cdot 10^{-2}$
Simply Supp. 30%	1	100	24.30	1	40.58	$2.91 \cdot 10^{-2}$
Simply Supp. 40%	1	100	25.32	1	40.82	$3.30 \cdot 10^{-2}$
Continuous	1.2	80	14.24	4.80	20.06	$3.28 \cdot 10^{-2}$
Lap-jointed	1.6	80	16.25	4.80	21.18	$1.19 \cdot 10^{-2}$

Table 7.8: Statistics of the percentage of area failed for the roof system.

7.1 Numerical results for the roof system (MCS)

Figure 7.15 shows the CDF of the area failed for the entire roof system with simply supported purlins. Again, the roof system with low redistribution ability behaves better (upper path) because high values of area failed have a lower probability to be exceeded.

Figure 7.16 shows the CDF path for the entire roof with the three purlin configurations for the redistribution factor of 40% (total redistribution of 80%). For small area failed, the system with simply supported purlins behaves better, while, for high values of area failed, the roof with static indeterminate purlins shows a better behavior. The value of 20% of area failed represents the value of area failed that corresponds to this change of behavior.

This effect is clearly shown from tables 7.6, 7.7 and 7.8 that lists the expected area failed upon a failure $E[A_F | F]$. The roof with simply supported purlins has an expected area failed that increases with the redistribution factor. However, the two static indeterminate configurations show a lower value of area failed.

Table 7.9 lists the values of the Risk computed according to Eq. 3.19 considering secondary system and primary system separately and then the entire roof. The roof system with the lowest risk is the roof system with lap-jointed purlins, while the roof system with continuous purlins shows the worst behavior. The roof with simply supported purlins has an intermediate behavior with a lower risk, when the secondary system is built with low capacity of redistributing the loads.

Figure 7.15: CDF of the failed area for the roof system with simply supported purlins with redistribution 10%- 20%- 30%- 40%.

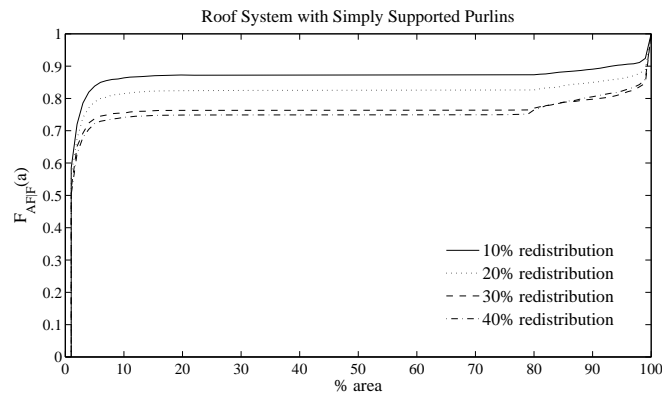
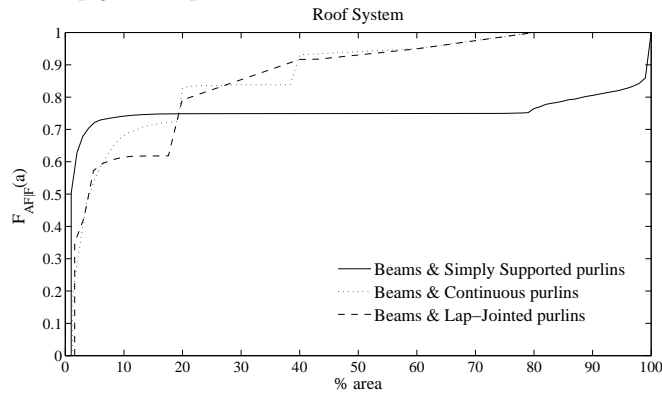


Figure 7.16: CDF of the failed area for the roof system with simply supported continuous and lap-jointed purlins with redistribution 40%.



7.1 Numerical results for the roof system (MCS)

Configuration $Pr(F(50yr))$	E $[A_F]$		
	Purlins	Beams	Roof system
Simply Supp. 10%	193.35	94.50	217.67
Simply Supp. 20%	248.13	132.19	294.78
Simply Supp. 30%	340.65	179.15	424.27
Simply Supp. 40%	398.85	198.39	501.34
Continuous	103.01	241.32	280.24
Lap-jointed	22.75	106.31	116.02

Table 7.9: Risk for the secondary system, primary system and of the timber roof.

Table 7.10 lists the values of the Robustness computed according to Eq. 3.20. It can be noted that the simulations for the roof system with all the interactions give results in terms of robustness of secondary system that are in contrast to the simple model assessed in the previous chapter.

Configuration $Pr(F(50yr))$	$Pr(A_F < 0.15 \cdot A_{roof} F)$		
	Purlins	Beams	Roof system
Simply Supp. 10%	0.869	0.368	0.87
Simply Supp. 20%	0.822	0.294	0.82
Simply Supp. 30%	0.762	0.271	0.76
Simply Supp. 40%	0.747	0.326	0.74
Continuous	0.930	0.415	0.71
Lap-jointed	0.977	0.464	0.61

Table 7.10: Robustness for the secondary system, primary system and the timber roof.

Finally, in table 7.11, an overview of the results in terms of Reliability,

Risk and Robustness of the entire timber roof is presented.

Configuration	$Pr(F(50yr))$	Risk	$Pr(A_F < 0.15 \cdot A_{roof} F)$
Simply Supp. 10%	$2.61 \cdot 10^{-2}$	217.67	0.87
Simply Supp. 20%	$2.65 \cdot 10^{-2}$	294.78	0.82
Simply Supp. 30%	$2.91 \cdot 10^{-2}$	424.27	0.76
Simply Supp. 40%	$3.30 \cdot 10^{-2}$	501.34	0.74
Continuous	$3.28 \cdot 10^{-2}$	280.24	0.71
Lap-jointed	$1.19 \cdot 10^{-2}$	116.02	0.61

Table 7.11: Reliability, Risk and Robustness for the timber roof.

The roof with simply supported purlins has an high probability of failure and a high risk, but also it is the most robust according to the chosen robustness criterion. In addition, risk and likelihood of failure event increase with the redistribution ability and interaction among the components of primary and secondary system. The roof with continuous purlins has the highest probability of failure and therefore a high risk. It is also less robust than the roof with simply supported purlins, with the same redistribution ability. The roof system with lap-jointed purlins has the lowest probability of failure and the lowest risk, but is has the lowest robustness. Indeed, figure 7.16 already shows this different behavior.

It may also be noted, (see figure 7.16), that the chosen threshold of 15% of area failed in the definition of the robustness criterion, compete to the range of area failed in which the compartmentalization effect is still active. This can be seen from the inversion of the path of the CDF at the threshold of 20% of A_F . This inversion means that for wide failures the compartmentalization becomes ineffective, while the redundancy of static indeterminate systems allow to have lower damages (risk), although already a wide area

7.1 Numerical results for the roof system (MCS)

of the roof is collapsed.

In addition, according to the model of section 3.5, for the statically determinate purlins, the failure of the primary beams leads to an additional axial tension force. On the set of simulations it happens in the 98% of the cases that the failure of the beam leads also to the failure of the purlins, instead the primary beam will be hanging only in the 2% of the cases.

Chapter 8

Conclusions

A comparative study of reliability, robustness and risk of large span timber structure is presented. Although reliability and risk analysis are widely studied in the scientific community, robustness is still a tough subject. Indeed, a unique definition of structural robustness still has to be stated and different studies attempt to provide a measure to structural robustness. While structural design rules and existing codes ensure that none of the limit state conditions is violated, providing an acceptable reliability, no rule assure that the system has been designed for robustness. In addition, from a decision-theory point of view, the optimal structural design should minimize the total expected cost (design and maintenance cost plus risk), thus, in order to achieve an optimal solution between additional cost to increase robustness and the reduction of failure consequences, only a probabilistic approach can be used.

In this study, a wide-span timber roof with different configurations of sec-

ondary structures is investigated. All three purlin configurations comply with the code requirements and the critical sections all have the same reliability. However, the system reliability of the three configurations is different because of the varying number of critical section inside each component/element and due to the fact that system failure is defined through a series system model. In terms of reliability of the secondary system, the purlin system with simply supported configuration has the lowest reliability due to the higher number of elements, but it also represents the system with compartmentalization. Between the two static indeterminate purlins configurations (redundancy), the lap-jointed is the most reliable due to a lower number of element.

In terms of robustness of the secondary system, it can be argued the configuration consisting of simply supported purlins with low load redistribution ability, is the optimal one, because a failure in this configuration leads to the smallest failed area and it has the lowest probability of not fulfilling the 15%-area requirement (probability based robustness criterion). These calculations include the possibility of a random but systematic reduction of strength (e.g. due to gross errors) and different redistribution ability. However, the calculated risk for the static determinate configuration is higher than for the statically indeterminate configurations. This is due to the fact that the probability of system failure is higher for simply supported configuration, even though the consequences are lower.

Obviously, the secondary system assessment is not sufficient to state which one is the optimal configuration for secondary structures in wide-span timber structures, because the primary beams were considered intact. A fur-

ther complete investigation of the roof system showed the importance of load redistribution capacity due to connection and residual strength of the elements. The roof system with simply supported purlins shows always the highest risk due to a too high probability of failure (low reliability). For failure events characterized by small area failed, the roof with simply supported purlins has the highest probability of fulfilling the 15%-area requirement, due to the compartmentalization effect. This allows to contain the extension of the failure even for high redistribution ability.

The roof with continuous purlins has very low reliability due to the interaction between beam failure mechanisms and purlins failure mechanism. From the risk and robustness point of view, this configuration has a lower risk but also a lower robustness. The roof configuration with lap-jointed purlins has the lowest probability of failure and risk, even if it has the lowest robustness. However, the roof with simply supported purlins can eventually be subjected to the complete failure of the roof, while the maximum collapsed area for both static indeterminate configurations is 80%. This happens because for small area failed the compartmentalization of simply supported purlins has the effect of contain the failure event, while for failures with big collapsed area, the redundancy effect of static indeterminate configurations is more effective. This is shown by the inversion of the path in the Cumulative Density Function of the area failed, upon a failure, for the entire roof system.

Therefore, it is argued that despite the fact that the secondary system with simply supported purlins is more robust, this study indicates that static indeterminate configurations, and mostly the roof with lap-jointed purlins,

are more optimal. In addition, lap-jointed purlins represent the cheapest configuration, thus supporting the choice of this configuration also from a risk (or rather expected cost) perspective. This points to a general problem in the definition of robustness because a more robust system might often be less optimal from a risk analysis point of view.

These conclusions, are also dependent on the fact that the distances between the purlins were adapted in order to receive the same utilization factor for all systems. In common practice, the distances are based on requirements from the roof cladding. If the same distances would be applied to all systems, assuming a consistent utilization factor, the three systems would show a more similar behavior. If the two static indeterminate configurations would be modified to have the same distance between purlins than simply supported configuration, they would become slightly more robust, but would also have a higher probability of system failure and thus exhibit a higher risk. However, the risk-based approach presented in this study do provide a tool for optimal design of wide-span timber roofs and the results obtained from this study might also hold for other systems. Indeed, this comparative study shows how robustness and risk can be contradictory criteria.

Bibliography

- [1] Baker J.W., Schubert M., Faber M.H.– On the Assessment of robustness– *Structural Safety*, 30, 253-267. (2008).
- [2] Blumer H. – Spannungsberechnungen an anisotropen Kreisbo-genscheiben und Satteltraegern konstanter Dicke – Lecture notes, Lehrstuhl für Ingenieurholzbau und Baukonstruktionen der Univer-sität (TH) Karlsruhe. Karlsruhe, Deutschland. (1972-1979).
- [3] Canisius T.D.G – Structural Robustness design for Practising Engi-neers – *COST Action TU0601. Robustness of Structures.*(2011).
- [4] Cizmar D., Sørensen J.D., Kirkegaard P.H.– Reliability and Robust-ness evaluation of timber structures–*Short Term Scientific Mission, COST E55 Action, DCE Technical Report*, 58. (2009).
- [5] Der Kiureghian A., Liu P.L. – Structural reliability under incomplete probability information – *Journal of Eng. Mech.*. ASCE. 112: pp. 85-104.(1986).

BIBLIOGRAPHY

- [6] Dietlevsen O., Madsen H.O.– Structural Reliability Methods –John Wiley & Sons. England. (1996).
- [7] Dietsch P., Winter S.– Robustness of Secondary Structures in wide-span Timber Structures – *Proceedings WCTE 2010*. Riva del Garda, Italy. (2010).
- [8] DIN EN 1991-1-3/NA National Annex - National determined Parameters - Eurocode 1: Actions on Structures - Part 1-3: General Actions - Snow Loads. DIN Deutsches Institut für Normung e.V., Berlin. (2010).
- [9] DIN EN 338 - Bauholz für tragende Zwecke, Festigkeitsklassen; Deutsche Fassung EN338:2009 - DIN Deutsches Institut für Normung e.V., Berlin. (2010).
- [10] DIN 1052:2008-12 - Design of Timber Structures-General Rules and Rules for Buildings. DIN Deutsches Institut für Normung e.V., Berlin. (2008).
- [11] DIN EN 14080 - Timber structures - Glued laminated timber and glued solid timber - Requirements. DIN Deutsches Institut für Normung e.V., Berlin. (2011).
- [12] Ellingwood B.– Design and Construction error Effects on Structural Reliability –*Journal of Structural Engineering*. 113(2):pp. 409-422. (1987).

BIBLIOGRAPHY

- [13] EN 1991-1-7. Eurocode 1: Actions on structures. Part1-1-7 General actions: Accidental actions, European Committee for Standardization (CEN), Brussels. (2003).
- [14] EN 1995-1-1. Eurocode 5: Design of Timber Structures: Part1-1 General- Common rules and rules for buildings, European Committee for Standardization (CEN), Brussels. (2004).
- [15] Frangopol D.M., Curley J.P.– Effects of damage and redundancy on structural reliability – *Journal of Structural Engineering*. 113(7): pp. 1533-1549.(1987)
- [16] Frühwald E., Serrano E., Toratti T., Emilsson A., Thelandersson S.– Design of safe timber structures-how can we learn from structural failures in concrete, steel and timber?– *Report TVBK-3053*, Div. of Struct. Eng.. Lund University, Sweden. (2007).
- [17] Fu G., Frangopol D.M. – Balancing weight, system reliability and redundancy in a multiobjective optimization framework – *Structural Safety* 7(2-4): pp. 165-175. (1990).
- [18] Genz A. – Numerical Computation of Multivariate Normal Probabilities – *J.Comp.Graph.Stat.*(available on line <http://www.math.wsu.edu/faculty/genz/homepage>). (1992).
- [19] Hansson, M. and Larsen, H. J. – Recent failures in glulam structures and their causes –*Engineering Failure Analysis*. 12(5): pp. 808-818.(2005)

BIBLIOGRAPHY

- [20] Hasofer A.M., Lind N.C. – An Exact and Invariant First Order Reliability Format – *Journal of Engineering Mechanics*. Trans. ASCE, 100(1): pp. 111-121.(1974).
- [21] Ionite O.M., Tarann N., Budescu M., Banu C., Rominu S., Banala R.– Robustness of civil Engineering Structures, a modern approach in structural design – *Technical Report, Intersection*, 6(4). (2009).
- [22] ISO 13824:2009 – Bases for design of structures – General principles on risk assessment of systems involving structures – International Organization for Standardization.(2009).
- [23] Joanni A.E.– Optimizing Design and Maintenance Strategies for Deteriorating Structures based on the Theory of Renewal Processes – *Berichte aus dem konstruktive Ingenieurbau, TU München*. München, Deutschland. (2009).
- [24] JCSS-Joint Committee on Structural Safety. – Probabilistic Model Code, 12th draft– internet version: <http://www.jcss.ethz.ch>.(2008).
- [25] Kang W.H., Song J.– Evaluation of multivariate normal integrals for general systems by sequential compounding – *Structural Safety*. 32:pp.35-41. (2010).
- [26] Kirkegaard P.H.-Sørensen J.D.– A Probabilistic Approach for Robustness Evaluation of Timber Structures – *Technical report*, 55, Aalborg University, Denmark. (2008)

BIBLIOGRAPHY

- [27] Köhler J. – Reliability of Timber Structures – *IBK Bericht N.301*.
ETH Zürich. Schweiz. (2007).
- [28] Melchers R.E.– Structural Reliability Analysis and Prediction – John
Wiley & Sons. England. (1999).
- [29] Miraglia S., Dietsch P., Straub D. – Comparative Risk Assessment of
Secondary Structures in Wide-Span Timber Structures – *Proceedings
of ICASP11*, ETH, Zürich (CH),1-4 August (2011).
- [30] Piazza M., Tomasi R., Modena R. – Strutture in legno, Materiale, cal-
colo e progetto secondo le nuove normative europee – Hoepli. Milan,
Italy.(2005)
- [31] Rackwitz R.– Zuverlässigkeit und Lasten im konstruktiven Ingenieur-
bau – *Lecture Notes, TU München*. München, Deutschland. (1993-
2006).
- [32] Rackwitz R., Friessler B. – Structural Reliability under Combined
Random Load Sequences– *Computers & Structures*. 9: pp. 484-494.
(1978).
- [33] Sanpaolesi L.– Scientific Support Activity in the field of Structural
Stability of Civil Engineering works on Snow Loads– Final Report.
University of Pisa, Italy.(1999).
- [34] SIA 265:2003. Holzbau, Schweizer Norm. Swiss Society of Engineers
and Architects. Zürich, Schweiz. (2003).

BIBLIOGRAPHY

- [35] Sørensen J.D., Dietsch P., Kirkegaard P.H., Köhler J. – Design for robustness of timber structures – *Guideline of COST Action E55-Modelling of the Performance of Timber Structures* Shaker Verlag. Deutschland. (2011).
- [36] Starossek U.– Progressive collapse of Structures – *Proceedings of the Annual conference of the Structural Engineering Committee of the Korean Society of Civil Engineers*. Seoul, Korea. (2006).
- [37] Starossek U.-Haberland M.– Measures of Structural Robustness- Requirements and Applications – *ASCE SEI 2008 Structures Congress- Crossing Borders*. Vancouver, Canada. (2008).
- [38] Starossek U., Haberland M. – Evaluating Measures of Structural Robustness – *ASCE SEI 2009, Structures 2009: Don't Mess with Structural Engineers*. ASCE SEI 2009 Structures Congress. Austin, Texas. (2009).
- [39] Strasser U. – Snow loads in a changing climate: new risks? – *Natural Hazards and Earth System Science*,8,18. (2008).
- [40] Straub D.– Structural Reliability Analysis –*Lecture Notes. TU München*. München, Deutschland. (2010).
- [41] Thelandersson S., Larsen H.J. –Timber Engineering – Wiley & Sons. England. (2003).
- [42] Toratti T., Schnabl S., Turk G. – Reliability Analysis of a glulam beam – *Structural Safety*. 29 :pp. 279-293.(2007).

BIBLIOGRAPHY

- [43] Winter S., Kreuzinger H. – The Bad Reichenhall ice arena collapse and the necessary consequences for wide span timber structures – *Proceedings of WCTE 2008*. Miyazaki, Japan.(2008).

Appendix A

The Fault Tree of the Failure Event

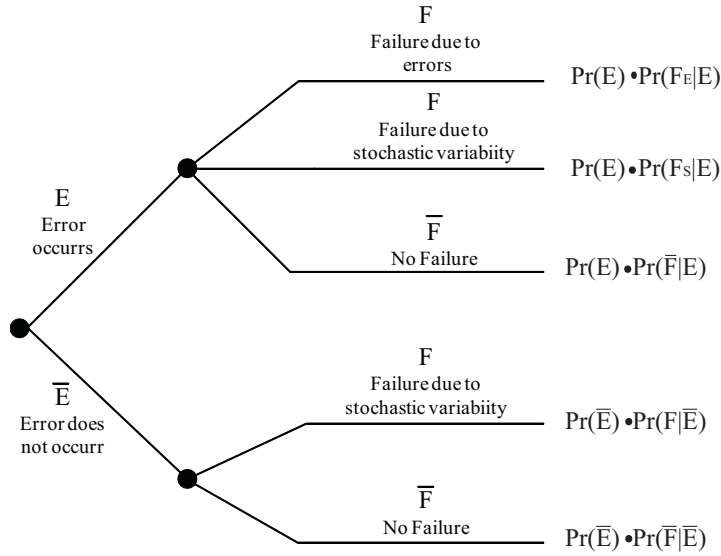
In order to analyze with a logical mathematical approach the failure event with its causes and consequences, not only the occurrences of failures should be considered, but also the possibility that the failure event to be conditioned by errors. The theory of fault tree can be used for this kind of assessment. Fault tree approach allows to consider both probability of failure of the structure (reliability of the structure) and the possible failure scenarios. It is possible to include also the evidence of a monitoring activity according to which the error or the damage can be detected or not.

The simple event tree suggested in Ellingwood [12] is drawn in figure A.1. In figure A.1, F denotes the failure event of the structure (or of a component of the structural system). The failure event can be defined as $F = F_S \cup F_E$, i.e. as union of the failure event F_S related to stochastic variability and

The Fault Tree of the Failure Event

of the failure event F_E related to the presence of errors E . \bar{E} indicates the absence of errors. The event tree shows also that failure due to stochastic variability can occur both in presence and in absence of errors E , but also when an error occur and it is not detected.

Figure A.1: Event-Tree of Failure Event.



For the Total Probability Theorem, the probability of failure $Pr(F)$ can be computed as in Eq. A.1.

$$\begin{aligned}
 Pr(F) = & [Pr(F_E | E) + Pr(F_S | E)] \cdot Pr(E) + \\
 & + Pr(F_S | \bar{E}) \cdot Pr(\bar{E}). \tag{A.1}
 \end{aligned}$$

The $Pr(F_S | E)$ is usually assumed to be zero because it is generally recognized that a structure, in presence of errors, will not fail due to stochastic variability of load and capacity. Under this hypotheses the Eq. A.1 can be written as:

$$Pr(F) = Pr(F_E | E) \cdot Pr(E) + Pr(F_S | \bar{E}) \cdot Pr(\bar{E}). \quad (\text{A.2})$$

Due to the Bayes' Theorem, the following equivalence is stated:

$$Pr(F | E) \cdot Pr(E) = Pr(E | F) \cdot Pr(F) \quad (\text{A.3})$$

Therefore, the Eq. A.2 can be written as:

$$Pr(F) = Pr(F | \bar{E}) \cdot \frac{Pr(\bar{E})}{[1 - Pr(E | F)]}. \quad (\text{A.4})$$

The quantity $\frac{Pr(\bar{E})}{[1 - Pr(E | F)]}$ in Eq. A.4 is also defined in [12] as *human error factor*.

However, the $Pr(F | E)$ is a predominant quantity in the expression of the total probability theorem, while the term $Pr(F | \bar{E})$ represents a base value, according to which load and resistance factor can be chosen, and the term $Pr(F | E)$ is the base value for choosing among different design concepts and construction procedures.

The possibility of different failure scenario can be included in the total probability theorem.

Let's denote with n the number of possible failure scenarios. The failure

event F_E is then defined as union of the failure event F_i caused by an error and within a certain scenario as in Eq. A.5, where O_i is the event that the i -th error occurs and \bar{D}_i is the event that the i -th error is detected and repaired.

$$F_E = \bigcup_{i=1}^n (F \cap \bar{D}_i \cap O_i). \quad (\text{A.5})$$

Due to Eq. A.5, the probability of failure event F_E due to errors becomes:

$$F_E = \sum_{i=1}^n (F | \bar{D}_i, O_i) \cdot Pr(\bar{D}_i | O_i) \cdot Pr(O_i). \quad (\text{A.6})$$

According to Eq. A.6, the effect of design and construction errors on the probability of failure can be reduced either by reducing their incidence or by reducing their impact on the structural performance, while it is useless to increase the safety factors.

Appendix B

Computation of Ditlevsen bounds for a series system

As reported in section 2.6.1, the upper and lower bound of the probability of failure of a series system can be defined with the Ditlevsen Bounds.

The upper and lower bounds of probability of failure $Pr(F)$ for a series system of n_p components are defined in Eqs. B.1 and B.2 respectively.

$$Pr(F) \geq P(F_1) + \sum_{i=2}^{n_p} \max \left[0, Pr(F_i) - \sum_{j=1}^{i-1} Pr(F_i \cap F_j) \right]. \quad (\text{B.1})$$

$$Pr(F) \leq \sum_{i=1}^{n_p} \left[P(F_i) - \sum_{i=2}^{n_p} \max_{j < i} Pr(F_i \cap F_j) \right]. \quad (\text{B.2})$$

In Eqs. B.1 and B.2, the probability of failure of the component i and the joint probability of the pair of cut set ij can be computed knowing the reliability index β_i of each component and the correlation coefficient ρ_{ij} of

the pair of cut set (see Eqs. B.3 and B.4).

$$Pr(F_i) = \Phi(-\beta_i). \quad (\text{B.3})$$

$$Pr(F_i \cap F_j) = \Phi_2(-\beta_i, -\beta_j, \rho_{ij}), \quad j = 1, \dots, n_p. \quad (\text{B.4})$$

By writing the Eq. B.1 in explicit form, the following expression for the lower bound can be derived.

$$\begin{aligned} Pr(F) \geq & Pr(F_1) + 0 + \max\{0, Pr(F_2) - Pr(F_2 \cap F_1)\} + \\ & + \max\{0, Pr(F_3) - [Pr(F_3 \cap F_2) + Pr(F_2 \cap F_1)]\} + \\ & + \max\{0, Pr(F_4) - [Pr(F_4 \cap F_3) + Pr(F_3 \cap F_2) + Pr(F_2 \cap F_1)]\} + \\ & + \dots + \max\{0, Pr(F_{n_p}) - [Pr(F_{n_p} \cap F_{n_p-1}) + \dots + Pr(F_2 \cap F_1)]\}. \end{aligned} \quad (\text{B.5})$$

By writing the Eq. B.2 in explicit form, the following expression for the upper bound can be derived.

$$\begin{aligned} Pr(F) \leq & Pr(F_1) - 0 + Pr(F_2) - Pr(F_2 \cap F_1) + \\ & Pr(F_3) - [\max\{Pr(F_3 \cap F_2), Pr(F_2 \cap F_1)\}] + \\ & + Pr(F_4) - [\max\{Pr(F_4 \cap F_3), Pr(F_3 \cap F_2), Pr(F_2 \cap F_1)\}] + \dots + \\ & Pr(F_{n_p}) - [\max\{Pr(F_{n_p} \cap F_{n_p-1}), \dots, Pr(F_2 \cap F_1)\}]. \end{aligned} \quad (\text{B.6})$$

If the components of the series system have all the same reliability and the system is equicorrelated with number of components $n_p \geq 5$ and correlation factor ρ_{ij} near to 1, the joint probabilities of the pairs of cut set have negligible values. Therefore, the expression in Eq. B.5 assumes the simple form of Eq. B.7 and expression in Eq. B.6 assumes the form of Eq. B.8.

$$Pr(F) \geq 5 \cdot \Phi(-\beta) - 10 \cdot \Phi_2(-\beta, -\beta, \rho). \quad (\text{B.7})$$

$$Pr(F) \leq n_p \cdot \Phi(-\beta) - (n_p - 1) \cdot \Phi_2(-\beta, -\beta, \rho). \quad (\text{B.8})$$

In addition, the probability of failure of the component i and the joint probability in B.7 and B.8 are simply computed as follows.

$$Pr(F_1) = Pr(F_2) = \dots = Pr(F_{n_p}) = \Phi(-\beta). \quad (\text{B.9})$$

$$\begin{aligned} Pr(F_2 \cap F_1) &= Pr(F_3 \cap F_2) = Pr(F_4 \cap F_3) = \\ &= \dots = Pr(F_{n_p} \cap F_{n_p-1}) = \dots = \Phi_2(-\beta, -\beta, \mathbf{R}). \end{aligned} \quad (\text{B.10})$$

where the correlation matrix of the bivariate-normal distribution $\mathbf{R} = [\rho, 1; 1, \rho]$.